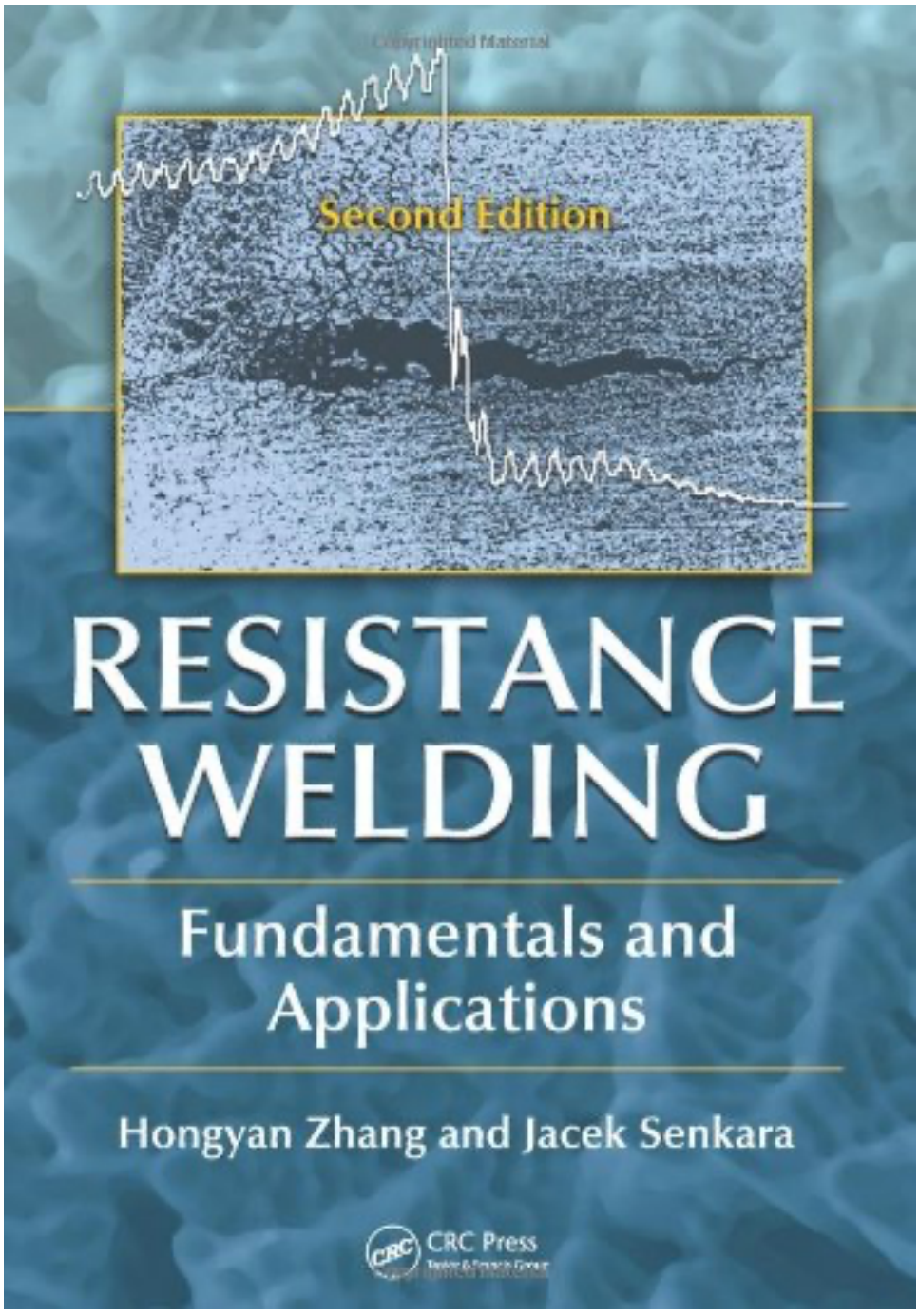

A portion of the book is freely available in internet for marketing purpose.

Second Edition

RESISTANCE WELDING

Fundamentals and Applications

Second Edition

RESISTANCE WELDING

Fundamentals and Applications

Hongyan Zhang and Jacek Senkara

CRC Press
Taylor & Francis Group
Boca Raton London New York

CRC Press is an imprint of the
Taylor & Francis Group, an **informa** business

CRC Press
Taylor & Francis Group
6000 Broken Sound Parkway NW, Suite 300
Boca Raton, FL 33487-2742

Version Date: 20120222

International Standard Book Number-13: 978-1-4665-5641-6 (eBook - PDF)

To

Kevin, Jackie, and Qun

Ela, Agatha, Anna, and Christina

Contents

Preface

Resistance welding, largely represented by and referred to as resistance spot welding, is a complex, yet exciting subject for both research and engineering practice. The multi-process nature of resistance welding and its wide range of industrial applications have attracted sufficient attention from researchers around the world, and a huge number of publications have been devoted to this topic. However, because of the complexity of resistance welding processes, research papers and books generally take two drastically different approaches: they either focus on a specific topic, or they cover most of the multiple facets of a welding process in a handbook style. In order to obtain a general knowledge of resistance welding of necessary depth, one must rake through a large quantity of research works on resistance welding as well as many related essential subjects, such as statistical analysis. This book is intended to provide the reader a systematic view of the fundamentals and applications in resistance welding, which may benefit both students and researchers in academia and welding practitioners in the sheet metal industry.

Resistance welding is quite different from other well-cultivated subjects, such as plasticity or dynamics, in which one may start with a number of reasonable assumptions, derive a set of equations based on these assumptions, and solve them. In welding, however, the engineering sense, which is largely qualitative rather than quantitative, is more important in understanding the process, solving problems, and drawing valid conclusions. For instance, the electrical current, an important process parameter for resistance welding, is not determined through solving a set of equations, although some commercial software packages claim that they can do so through numerical calculation alone. The actual value of an electric current is almost always determined experimentally, often with the guidance from handbooks or computer programs. The difficulties in both teaching and research in welding lie in dealing with the complicated multi-physical processes involved in welding, especially resistance spot welding. It is very hard, if not impossible, to extract "*a*" dominant process even for a particular aspect of resistance welding. Two or more coupled simultaneous processes, such as electrical and metallurgical processes, in welding make quantitative analyses impractical, as evidenced by the fact that there are no commercially available programs that are capable of treating the main physical processes in a fully coupled manner.

As a result, resistance welding is often treated as an "art" rather than a "science." Based on the state-of-the-art research results, this book presents the fundamental aspects of the important processes in resistance welding and discusses their implications on real-world welding applications in a systematic manner. As educators and researchers in welding, the authors have extensive interaction with the sheet metal manufacturing industry. The experiences they gained over the years and the desire to have suitable textbooks for their teaching provoked the inception of writing this book.

Welding metallurgy is presented first because of its obviously important role in resistance welding. Phase transformations in resistance spot welding, including melting, solidification, and solid-state phase transformations in a heat-affected zone, determine the quality of a weldment. They are introduced in Chapter 1 and emphasized in other chapters whenever an application requires such a consideration. Another largely metallurgy-dependent process also presented in the chapter is cracking in either the nugget or the heat-affected zone. This subject deserves more attention, and a more in-depth discussion can be found

in Chapter 3. Significant changes and additions are made in the current edition to reflect advances in the past few years in adopting magnesium alloys in the automobile industry, whereas the previous (first) edition of the book dealt with steels and aluminum alloys only. In Chapter 2, the basics of welding schedule selection based on the fundamental thermo-electrical consideration are presented. The electrode life is discussed in the chapter, considering both the thermo-electrical and metallurgical effects. Although the quality of a weld refers to a number of performance characteristics of the weld and is measured in various ways, mechanical testing is the most common means to test its quality because of its simplicity and consistency. The commonly conducted mechanical tests are presented in Chapter 4, and a more general definition of weld quality together with its measures, either obtained in a destructive or non-destructive manner, is covered in Chapter 6. The monitoring and control of a welding process are essential in ensuring weld quality, and they are presented in Chapter 5.

The mechanisms of expulsion, an important process in resistance welding largely responsible for defect formation and other unwanted features, are thoroughly analyzed in Chapter 7. This edition also presents a different type of expulsion observed in welding magnesium AZ91D that is not covered by previous expulsion models. The metallurgical, electrical, and thermo-mechanical influences are discussed, and the methods to predict and suppress expulsion are proposed and experimentally verified. The influence of the mechanical aspects of welding machines, which is often overlooked in resistance welding-related research, is presented in Chapter 8. Chapter 9 presents the procedure for numerically simulating a resistance welding process. Although it is not as mature as people have hoped, simulation proves a significant help in understanding the welding process, as it provides an insight to the process that is impossible to obtain otherwise. The last chapter of the book has been devoted to statistical design and analysis that is a method especially suitable for welding-related applications. This chapter explains the procedure of statistical analysis using welding research as an example. The research results by the authors have shown that a statistical analysis can indeed provide useful information of a welding process. This chapter provides an accurate yet convenient step-by-step procedure to apply statistical approaches to welding research. Overall, this book places its emphasis on establishing a relationship among welding parameters, characteristics of welded joints, and their performance. We have tried our best to provide, based on the available resources, a thorough review of the state-of-the-art results in resistance welding research and a solid foundation for solving practical problems in a scientific and systematic manner to the reader.

This book would not be possible without the encouragement and collaboration of our colleagues, friends, families, and the staff at CRC/Taylor & Francis over a span of more than 14 years. Although it is impossible to list everybody who has helped at various stages in the course of preparing this book, the authors feel obliged to acknowledge those based on their best recollections. While omission cannot be avoided, it is certainly not intentional as the planning and writing of this book have stretched over such a long period of time. The authors are extremely grateful for Mr. John C. Bohr and Prof. C.-L. Tsai whose encouragement was the determinant factor for the authors to undertake this exciting task. Many of our colleagues in Advanced Technology Program, Intelligent Resistance Welding (IRW), have provided various support in a span of 5 years, which formed the basis of this book. Drs. S. J. Hu, X. Wu, W. Li, H. Peng, M. Zhou, W.-K. Hou, and H. Tang, Mr. J. Grasse, Drs. M. V. Li, X. Sun, and Z. Feng, Mr. M. Kimchi, Mr. M. Fleming, Mr. D. Androvich, Mr. D. Boomer, Mr. J. W. Dolfi, Mr. T. Mackie, Mr. T. Morrissett, Mr. A. M. Turley, and Dr. W. Trojanowski, all contributed in some way to the first edition of this book. Special thanks

go to Dr. S.-W. Cheng who helped in writing the chapter on statistical analysis, Mr. P. Deshpande who helped in writing the chapter on numerical simulation, and Dr. S. Babu who generously allowed the authors to use many of his illustrations in this book. Dr. J. Jakubowski helped in preparing several photos used in the book. The help from the current and former students of the authors, Dr. A. Shayan, Ms. H. Zheng, Mr. N. Ari, Mr. G. Karve, Mr. S. Agashe, Mr. V. Vaddadi, Ms. X. Su, and Mr. K. Yadav, is highly appreciated. The authors have benefited tremendously from their professional interaction with welding practitioners in the US automobile industry. In particular, the biannual Sheet Metal Welding Conferences chaired by J. Bohr, M. Karagoulis, M. Palko, and M. Gugel have inspired the authors in many ways.

Revising this book was proposed by our editor at CRC Press/Taylor & Francis, Allison Shatkin, senior editor of materials science and chemical engineering, and the planning was critiqued and perfected by our peers at the universities and the sheet metal industry, including Drs. W. Li, M. D. Tumuluru, X. Wu, D. L. Chen, and S. Ramasamy.

A high standard of professionalism has been demonstrated in the course of publishing the first edition by CRC/Taylor & Francis Group, LLC, through its staff members including S. Kronzek and C. R. Carelli (acquisitions editors), T. Delforn (project coordinator), and K. L. Nazzaro (project editor). The significant improvement of the new edition would not have been possible without the detailed guidance, constant encouragement, and extraordinary patience of A. Shatkin (senior editor), K. A. Budyk (senior project coordinator), E. Curtis (project editor), A. Dale (editorial assistant), and A. Nanas (project manager). It has been a rewarding process working with such a group of knowledgeable, friendly, and enthusiastic individuals.

Finally, the authors express their gratitude toward their respective families for their unconditional support, love, understanding, and belief in their husbands and fathers in the course of writing this book.

Hongyan Zhang
The University of Toledo, Toledo, Ohio

Jacek Senkara
Warsaw University of Technology, Warsaw, Poland

Authors

Dr. Hongyan Zhang is an Associate Professor at the Department of Mechanical, Industrial, and Manufacturing Engineering (MIME), University of Toledo. He holds a BS in Applied Mathematics, an MS in Metal Physics, and a PhD in Materials Science. Among many of his research and teaching interests are materials, forming, welding, and mechanical fastening; manufacturing process monitoring and control; failure analysis; and hybrid propulsion systems. He has published over 70 peer-reviewed journal and conference papers and contributed to a number of American Welding Society Standards. Dr. Zhang has served as a principal reviewer for *Welding Journal* and as a reviewer for several other journals.

Dr. Zhang has extensive experience working with the automotive industry. He has been active in a number of AWS/SAE technical committees, and he has served as an organizer for several conferences such as Sheet Metal Welding Conferences and ASME annual meetings.

Dr. Jacek Senkara is a Professor of the Production Engineering Faculty at Warsaw University of Technology in Poland. He holds an MS in Metallurgy, a PhD in Materials Science, and a DSc in Welding Engineering. His research interests include fundamental research in welding such as materials aspects of welding and welding-related processes, along with surface modification of materials.

Dr. Senkara is the author of about 100 scientific and technical papers published in professional journals and conference proceedings. He has served as a principal investigator for a number of government, industry, and university-supported research projects. He has been teaching courses of Fundamentals of Welding and Welding Metallurgy for undergraduate, MS, and PhD students. From 1995 to 1999, while on leave from his parent university, he worked as a visiting scientist at the University of Michigan at Ann Arbor.

Dr. Senkara's service to professional organizations includes active involvement in the State Committee for Scientific Research, Polish Welding Society, and Polish Vacuum Society.

1

Welding Metallurgy

Welding is a metallurgical process—all aspects of a welding process can be, more or less, related to the metallurgy of the materials involved in welding, either the base metal or the electrodes. There are a number of books dedicated specifically to welding metallurgy.[1–7] Although most of them are on fusion welding, the general metallurgical principles are applicable to resistance spot welding (RSW). In this chapter, the metallurgical principles governing the various aspects of RSW are discussed. They are critical in understanding the formation of the structures of an RSW-welded joint, the mechanisms of defect formation, and their impact on a weld's strength. This chapter is categorized according to the materials most relevant to RSW as workpieces and electrodes. The metallurgical characteristics of steels, aluminum alloys, and magnesium alloys that affect welding processes and weld quality are discussed. In addition to "conventional" materials used in RSW such as steels, magnesium alloys are also included because of their increasing presence in automobile construction for significant weight reduction. The impact of electrode material on resistance welding has been widely recognized by the resistance welding community, yet little can be found from the public domain that directly aids the understanding and control of the RSW process. In fact, many processes in RSW are electrode dependent. For instance, resistance heating at the electrode–workpiece interface introduces unwanted changes such as alloying and others, affecting the life and performance characteristics of the electrodes, and the integrity of the weld. Therefore, Cu is included in this chapter as it is the most common material for electrodes. Finally, the metallurgical aspect of cracking is presented. For additional information regarding the metallurgy in resistance spot welding these materials, the reader is referred to the recommended reading listed at the end of this chapter.

1.1 Solidification in Resistance Spot Welding

The cast structure of ingots in the sheet materials used in RSW, such as steels, is deliberately modified by hot or cold working, such as rolling and heat treatment operations. In the process, grains are refined through cold working and recovery/recrystallization, and structures are homogenized through solution annealing or quenching and tempering. However, such operations are difficult to perform in welding, especially in RSW, as melting and solidification occur between two sheets in a short period. Welding parameters, such as hold time and post-heating, may alter the microstructure to a certain extent. However, because of the steep temperature gradient in a weldment, the extremely high cooling rate, and the very short time elapsed in welding, such a treatment is not comparable to the controlled heat treatment processes of the parent sheets. Therefore, the microstructures and properties of a weldment are generally not as optimized as in the base metal.

During welding, solidification of a liquid nugget is similar to that in a metal casting. It consists of two steps: nucleation of solid phases and subsequent crystal growth, same

as solidification in an ingot mold. The crystallization process is controlled by the heat dissipation into the base metal and the electrodes. The direction and rate of cooling, in addition to the alloy's composition, decisively affect the type, size, and orientation of the crystals formed. During solidification of a liquid nugget, a change in alloy composition takes place in the crystals being precipitated, compared to the original composition of the alloy. In the case of a very rapid cooling of a spot weldment, the insufficient diffusion in the precipitated solid crystals and the remaining liquid, and the difference in solubility of certain elements in solid and liquid, produce a sharp gradient in the composition distribution through microsegregation. The difference in composition between the core and outer layer of a crystal increases with increasing distance between the liquidus and solidus lines in a phase diagram, and decreases with increasing diffusion rate and the time span for solidification. In addition to microsegregation, which occurs in the scale of crystals, segregation also takes place as the solid–liquid interface advances into the liquid, as solidification proceeds, and results in enrichment in concentration in the remaining melt of alloying elements. Some of the elements form eutectics of lower melting temperature that exist in the liquid state, mainly around the central portion of a nugget after it is cooled to a temperature below the solidus of the alloy but above the eutectic temperature. Examples of such eutectics are Al–Cu, Al–Mg, and Al–Mg–Si in aluminum alloys, and certain compounds such as sulfur and phosphorous eutectics in steels. Because of their lower melting temperatures, they are the last bits of liquid to solidify, mainly at grain boundaries, as they are rejected from the solidified crystals due to reduced solubility during cooling. Grains surrounded by such liquid at the boundaries can be torn apart as the liquid has no strength when they are stretched, either by external loading or thermal stresses in the same way as in the case of fusion welding. However, such cracking rarely occurs in RSW as it may be suppressed by the pressure from the electrodes during cooling if proper electrodes and welding schedule are used. After solidification, solid-phase transformation may occur and it may alter a weld's microstructure, which may be drastically different from the just solidified structure. For instance, martensitic transformation may occur in certain steel welds which may result in a significantly more complex structure than the austenite solidified from the liquid.

The formation of various crystals, such as dendrites, globular, and cellular crystals, is controlled by the composition and heat transfer through the liquid–solid interface. Solidification occurs when the liquid nugget reaches the liquidus temperature of the alloy and there is a net heat loss in the liquid; that is, the heat dissipated from the liquid is greater than that into the liquid. Under proper welding conditions, the water-cooled electrodes may act as a large heat sink during welding. The parent sheet metal also absorbs heat from the periphery of the liquid nugget. A possible scenario of solidification during RSW can be constructed based on understanding the metallurgical and thermal changes that may occur in welding. Solid grains in the partially molten or mushy zone at the nugget–HAZ (heat-affected zone) borders may serve as nuclei for crystal growth, and solidification starts in this region. Further cooling results in columnar grains in directions approximately normal to the fusion line, and the solid–liquid interface advances toward the center of the nugget. The remaining molten metal in the central portion of the nugget solidifies last and forms equiaxed grains when the liquid volume is small after much of its surrounding is solidified. Shrinkage cracks or voids, if created, tend to be located in the nugget center that is last solidified. The actual structures formed in a weld nugget depend strongly on welding schedules and other conditions. A carefully created spot weld on a TRIP (TRansformation Induced Plasticity) steel is shown in Figure 1.1, with a clearly defined HAZ and columnar structure in the weld nugget.

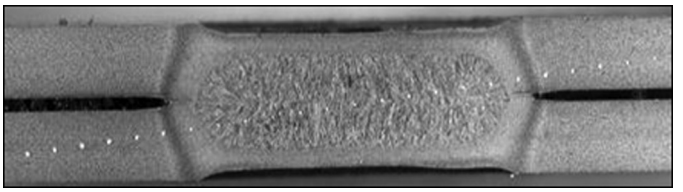

FIGURE 1.1
A spot weld made on 780-MPa TRIP steel.[8] Equally spaced white dots are indentation marks formed during microhardness testing.

During solidification of the last bit of liquid, usually at a location close to the original faying surface of the sheets, a deficit of volume can easily create cracks or voids. In general, a volume deficit of liquid metal during solidification may result from insufficient pressure exerted onto the weldment, insufficient molten metal volume, and excessive cooling rate. A large electrode force can effectively compensate the volume shrinkage of a weldment during cooling, and can suppress the formation of voids or cracks. Insufficient heating, such as that generated by low welding current and/or short welding time, can result in a small volume of molten metal and a high cooling rate. Under a small electrode force, such insufficient melting can easily form voids and cracks. One such example is shown in Figure 1.2, where the fracture surface of a weldment failed in interfacial fracture mode, revealing a macroscale shrinkage void with a clear evidence of freely solidified surface.[9] The fracture surface along the original faying interface is shown in Figure 1.2a. There is a clear evidence of fusion and fracture of fused metals in the nugget area. The central part of the nugget,

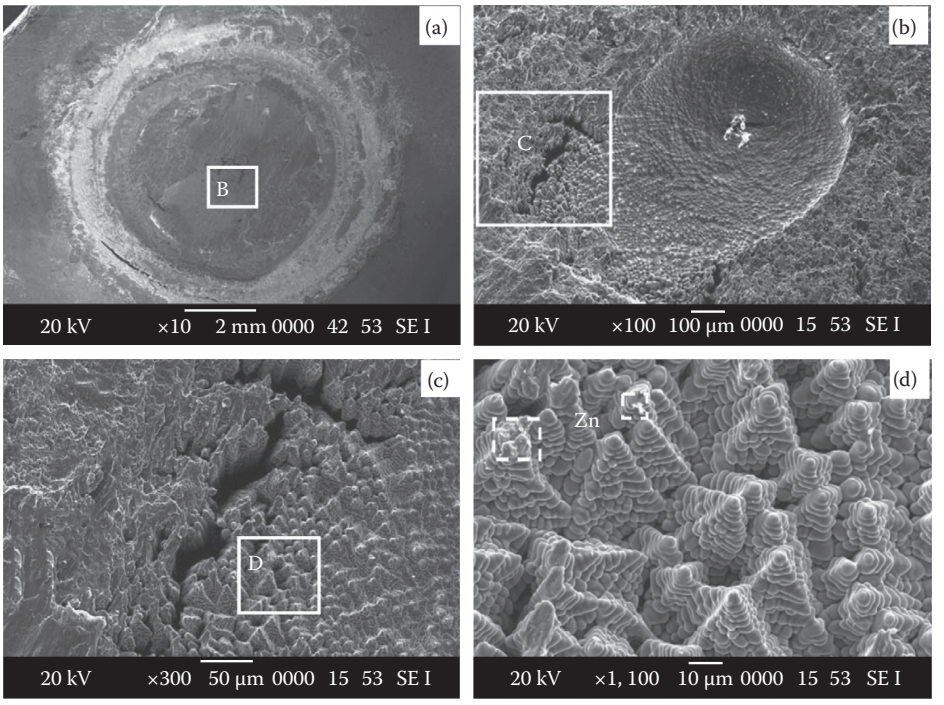

FIGURE 1.2
Microstructure of interfacial fracture surface in DP600 steel weld.[9]

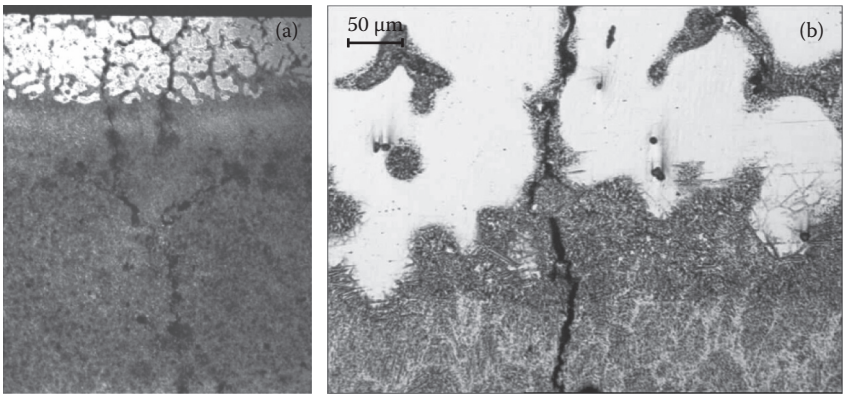

FIGURE 1.3
Morphologies of cracked sections of AZ91D weld: (a) shrinkage cracks extended from nugget, through HAZ, to surface; (b) a closer look at cracks near fusion line.[10]

marked as Box B, is enlarged in Figure 1.2b. There is a void of about 600 μm in diameter. The dendrites observed on the surface of the large void consumed the last liquid during cooling and remained intact. The opening in Figure 1.2c which corresponds to Box C in Figure 1.2b, near the border of the void could result from mechanical loading the cracks created due to volume deficit during solidification of the weld. A closer look of the structure marked by Box D in the figure is shown in Figure 1.2d. It possesses the characteristics of free solidification structure. The white boxes in the figure show the dendrites enriched in zinc, from the hot-dipped zinc coating of the DP steel. This is an evidence of insufficient melting of the nugget.

When cooling from electrodes is impeded, for instance, when the actual electrode–sheet contact area is small due to electrode misalignment or electrode wear, most of the heat is conducted out through the sheet metal. Therefore, the last bit of liquid solidifies around the center of the nugget in the thickness direction. Because of the small volume of such a liquid and the often accompanied volume deficit, cracks and porosity are often formed around the center of the nugget along the electrode direction. As these discontinuities are far from the HAZ at the faying interfaces, they should have a small effect on strength. However, such cracks very often propagate from the center to the edges of the nugget in the form of branching out. This is discussed in more detail in Chapter 3. An example of solidification cracking along the nugget thickness direction is shown in Figure 1.3. In welding a magnesium alloy AZ91D, it was found that cracks were formed around the center of a spot weld, extending from the faying surface, across the fusion line, to the electrode–sheet interface.[10]

1.2 Metallurgical Characteristics of Metals

The welding-related metallurgical characteristics of commonly used structural materials, such as steels, aluminum alloys, and magnesium alloys, are presented in this section. Copper alloys are also discussed since they are the most common material for electrodes.

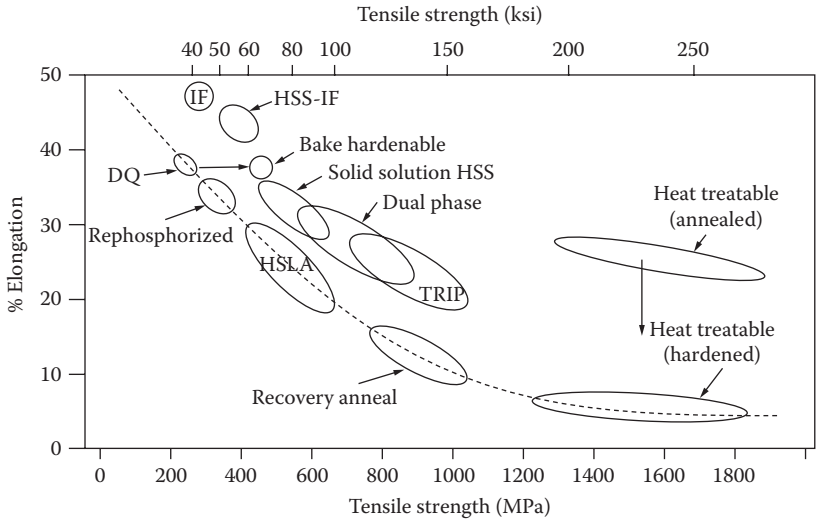

FIGURE 1.4
Mechanical property diagram of various steels. (Courtesy of Auto-Steel Partnership.)

1.2.1 Steels

Properties of the parent sheets and those of the weld metals are determined by both the chemical composition of the alloys and the fabrication conditions, such as heat treatment and hot and cold working. The property map of various steels, shown in Figure 1.4, illustrates the influence of chemistry and processing. In general, low-carbon steels have low tensile strength and high ductility, whereas ductility diminishes as strength rises. The figure shows that by altering the chemical composition and controlling phase transformations, desirable properties of an alloy can be achieved. However, for a weld nugget and the heat-affected zone in RSW, there is only a limited control on transformations and processing. Therefore, the sheet strength obtained through sophisticated metallurgical and mechanical processes during fabrication may disappear in a weld metal.

1.2.1.1 Solid Transformations in Steels

The upper-left corner of the equilibrium iron–carbon phase diagram is shown in Figure 1.5. Consider a steel with a carbon content lower than the eutectoid composition (0.77 wt.% C) cooled from a temperature above the A3 temperature, such as in the case of cooling a solidified nugget or the HAZ. Face-centered cubic austenite is the stable phase at this temperature. When it is slowly cooled to below A3 temperature, the body-centered cubic (BCC) ferrite phase is produced, containing a smaller amount of dissolved carbon. The volume fraction of austenite grains decreases, yet they are progressively enriched in carbon. At the eutectoid temperature (727°C), the residual austenite transforms into a laminated eutectoid mixture of ferrite and cementite (Fe_3C), called pearlite. Therefore, the resultant steel has a structure of ferrite and pearlite mixture. Cementite is not *stable*; rather, it is termed *metastable*, as it decomposes to iron and graphite if held at an elevated temperature for a long period. Same phase transformations occur when cooling at a higher rate,

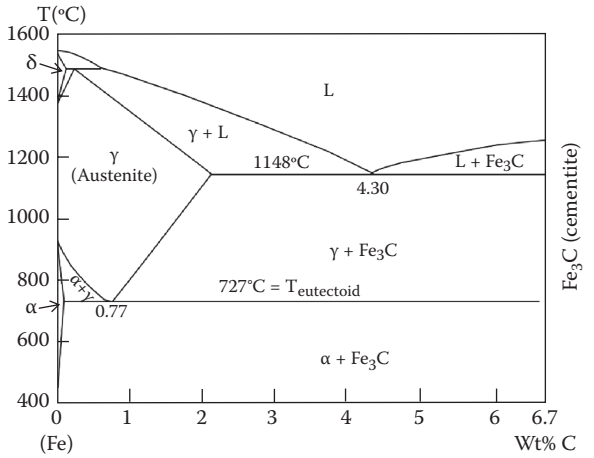

FIGURE 1.5
Fe–C phase diagram. (Adapted from Callister, W.D., Jr., *Materials Science and Engineering: An Introduction*, 6th edition, John Wiley & Sons, Inc., New York, 2003.)

but usually at temperatures lower than those marked on the equilibrium phase diagram. Although a mixture of soft ferrite and hard cementite is the typical structure for low-carbon steels, the morphology of the phases is a strong function of cooling rate, and the mixture can be either pearlite or bainite depending on the cooling rate.

Isothermal phase transformation, or sometimes called time–temperature transformation (TTT) diagram, is an important tool in understanding the microstructures that may occur upon cooling. A TTT diagram is developed isothermally by quenching samples into molten salt baths of fixed temperatures and keeping them for predetermined periods, then quenching quickly in an ice–salt brine. These diagrams show how metals transform with time at given temperatures. Figure 1.6 is a TTT diagram for an iron–carbon alloy. A typical TTT diagram of a plain carbon steel shows the starts and completions of pearlite formation, bainite formation, and martensite formation.

Such diagrams are generated under equilibrium conditions that are rarely met in practice. Especially in an RSW process, the heating and cooling rates are extremely high and transformations are far from equilibrium. Because most industrial heat treatment processes use controlled cooling rather than isothermal transformation, continuous-cooling transformation (CCT) diagrams are more representative of actual transformations than TTT diagrams. Cooling of a weldment of RSW is also far from isothermal; therefore, CCT diagrams are more applicable to understanding the microstructures of a weldment. CCT diagrams are similar to TTT diagrams except that in CCT diagrams, transformations occur over a range of temperatures. A typical CCT diagram of a mild steel is shown in Figure 1.7. A continuous cooling with a slow cooling rate results in a mixture of ferrite and pearlite; an intermediate cooling tends to produce a mixture of ferrite, bainite, and martensite; and a rapid cooling (above the critical cooling rate) creates a structure of all martensite. Although some techniques such as CCT diagrams take into account the dynamic nature or kinetics of phase transformations, they are usually material dependent, and there is a serious lack of information on transformations occurring at such a high cooling rate as in RSW. Therefore, most phase diagrams are not adequate when used in a quantitative manner. Nevertheless, information of possible transformations and reactions during welding can be obtained from the phase diagrams.

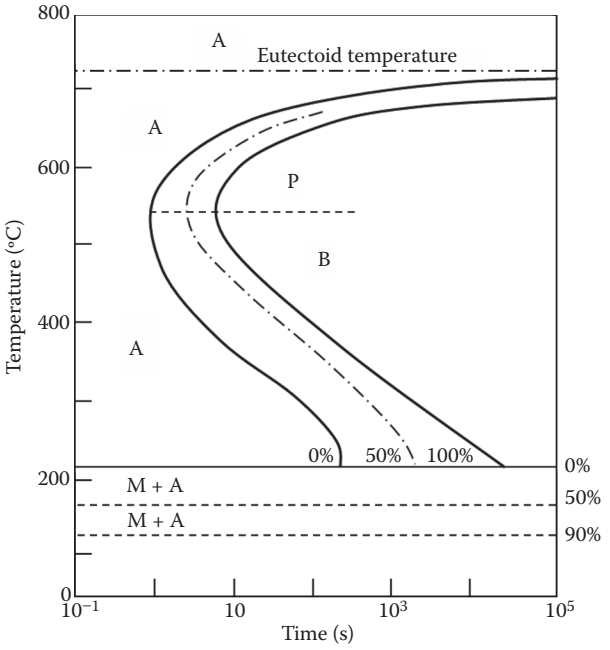

FIGURE 1.6
A TTT diagram for an iron–carbon alloy of eutectoid composition: A, austenite; B, bainite; M, martensite; P, pearlite. (Adapted from Callister, W.D., Jr., *Materials Science and Engineering: An Introduction*, 6th edition, John Wiley & Sons, Inc., New York, 2003.)

Under certain conditions, such as when the carbon (or carbon equivalence) content is sufficiently high, a very high cooling rate, as what often occurs during RSW, may result in martensitic transformation. The rapid cooling makes equilibrium phase transformations impossible, and it tends to depress the transformation temperatures. At low temperature, the nucleation rate is high, whereas the growth rate is low. The resultant structure (ferrite

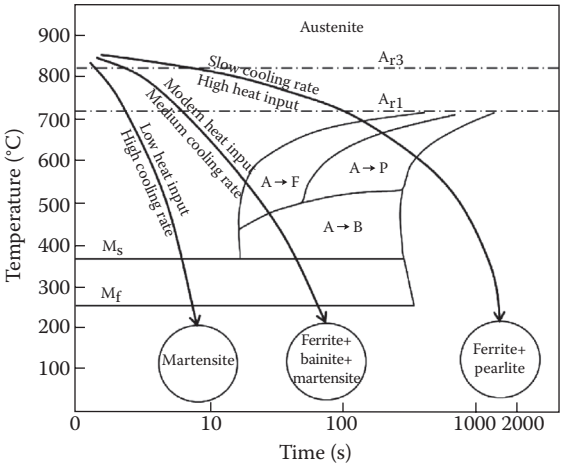

FIGURE 1.7
Typical CCT diagram of a mild steel: A, austenite; F, ferrite; P, pearlite; B, bainite; M, martensite.

+ cementite) appears in the form of fine needles rather than thick laminar plates. Further depression of the transformation by a higher cooling rate may result in the transformation of austenite to martensite. In general, a higher cooling rate results in a lower transformation temperature and a harder structure. Alloying elements are commonly added to control the phases produced in steel making, and they have significant effects on the temperatures as well as the shape and location of the C-shaped curves in the phase diagrams. Elements such as titanium, molybdenum, chromium, and tungsten lower the eutectoid carbon content and raise the transformation temperature and, therefore, they are called ferrite stabilizers. The existence of such elements raises the pearlite nose and moves it to the right side. Other elements such as nickel and manganese lower the eutectoid carbon content and lower the transformation temperature, so they are austenite stabilizers. Their effect is demonstrated on the TTT and CCT diagrams by lowering the pearlite nose and moving it to the right side. In fact, all metals except cobalt increase the hardenability of steels, a measure of how rapid a quench is necessary to form martensite. That is, they move the nose of the pearlite curve to the right, allowing martensite to form with less rapid quenching.

Martensite is responsible for the high strength of most steels. It has a distorted BCC lattice structure. The amount of distortion and, therefore, the properties of martensite are a strong function of carbon content. For low-carbon steels (less than 0.2 wt.%), the lattice structure of the martensite is very close to BCC and it is a little brittle. On the other hand, for higher-carbon steels, martensite is body-centered tetragonal (BCT) and is brittle. High carbon content promotes the formation of martensite and increases its hardness. Because the martensitic transformation is diffusionless and instantaneous, the start and finish of this transformation are represented by horizontal lines. More horizontal lines as in Figure 1.6 are used to indicate the percentage of completion of the austenite-to-martensite transformation. The influence of alloying elements on the effectiveness of carbon in martensitic formation is measured by the so-called "carbon equivalent," and it is discussed in Section 1.2.1.3.

1.2.1.2 Transformations in HAZ of a Steel Weld

The heat-affected zone of a resistance spot weld experiences thermal cycles and its microstructure is determined accordingly. Upon heating a steel through its upper critical temperature, the stable austenite forms and grows. The austenite grain growth is very sensitive to temperature, and aluminum and other elements are added to steel in order to produce fine grains by impeding the growth of austenite grains during various thermal cycles. Lancaster[4] divided an HAZ into three zones from a metallurgical viewpoint: supercritical, intercritical, and subcritical:

- The supercritical region is divided into two parts: grain growth region and grain refinement region. A thermal cycle during welding above the grain-coarsening temperature promotes grain growth, and it refines the grain structure below that temperature. This region is located near the fusion line, next to the weld nugget. Different steels contain different grain growth inhibitors, and they have different grain-coarsening temperatures.
- In the intercritical region, the peak temperature is lower than that in the supercritical region and, therefore, partial phase transformation is experienced in this region. New phases that do not exist in the original base metal may form in this region, and such transformation depends on the duration of the metal exposed to the peak temperature and on the cooling rate.

- The subcritical region does not normally undergo any observable microstructural changes as the temperature is generally low. It is usually difficult to distinguish this region from the base metal. In some cases, very fine precipitates may appear in the region.

Nonmetallic inclusions such as sulfides and oxides may have an effect on the hardenability of the HAZ. They produce a lower hardness by nucleating ferrite within the transforming austenite grains and reducing the amount of austenite for transforming to martensite or bainite. In some cases, a low hardenability is preferred in the HAZ in order to minimize the risk of stress corrosion cracking.

The microstructure of a nugget is determined by the composition of the base alloy and the thermal history, and it can be predicted using the relevant phase and transformation diagrams. Therefore, it is critical to obtain the temperature distribution as a function of welding time in a weldment. However, it is difficult to obtain the temperature profile of a weldment during resistance welding, as directly and accurately measuring temperature is impossible. Using sensors such as thermal couples may interfere with the welding process and result in invalid temperature readings. Numerical simulation such as finite element modeling can provide an approximation, yet its lack of ability to fully couple the electrical–thermal–mechanical effects and a lack of temperature-dependent material property data make accurate prediction impossible. Nevertheless, the temperature profile can be estimated based on the structures and sizes of various zones in a weldment revealed by metallographic examination, and the temperature ranges of the structures for the alloy determined on a phase diagram.

Figure 1.8 shows an approximated relation between the phase diagram and microstructures linked by the possible temperature distribution in a steel weldment at the peak of heating. The regions of various structures indicate the possible phase transformations experienced at such locations upon heating and cooling. These structural changes are closely associated with the heights of the phase regions in the phase diagram, which outline the temperature limits for phase transformations. The peak temperature in the melt can be approximated as a few hundred degrees above the liquidus, and its value does not drastically affect the temperature distribution. By drawing such lines from the phase diagram and the cross section of a weldment, the possible temperature distribution can be established by the intersections of the lines. In Figure 1.8, an HSLA steel weld shows regions of various structures. These structures are different from the base metal as they were modified during welding by the heating and cooling cycles. In the nugget region, a clear casting structure indicates melting and solidification, and, therefore, the peak temperature in this region has to be over the melting point of the alloy. Next to this region is the partial melting zone, as it is filled partially by columnar grains. This region corresponds to the temperature limits between the liquidus and solidus in the phase diagram. Beyond this region, no melting occurred during welding, but changes in structures, such as grain shape and size, can be clearly observed in the solid structures. They have experienced solid-phase transformations. The temperature range in the Fe–C phase diagram for this region is fairly wide, yet the region is narrow, resulting in a large temperature drop in the temperature distribution. When determining the possible temperature ranges from the phase diagram, it is reasonable to assume that the temperature distribution is continuous in the weldment at any instance during welding. From the figure, it can be seen that the temperature gradient in the molten nugget is not large, and it increases dramatically in the HAZ. It again drops near the base metal. In the region next to the partial melting zone, a supercritical region exists. In the overheated zone, as marked in the figure, grain growth is evident; therefore,

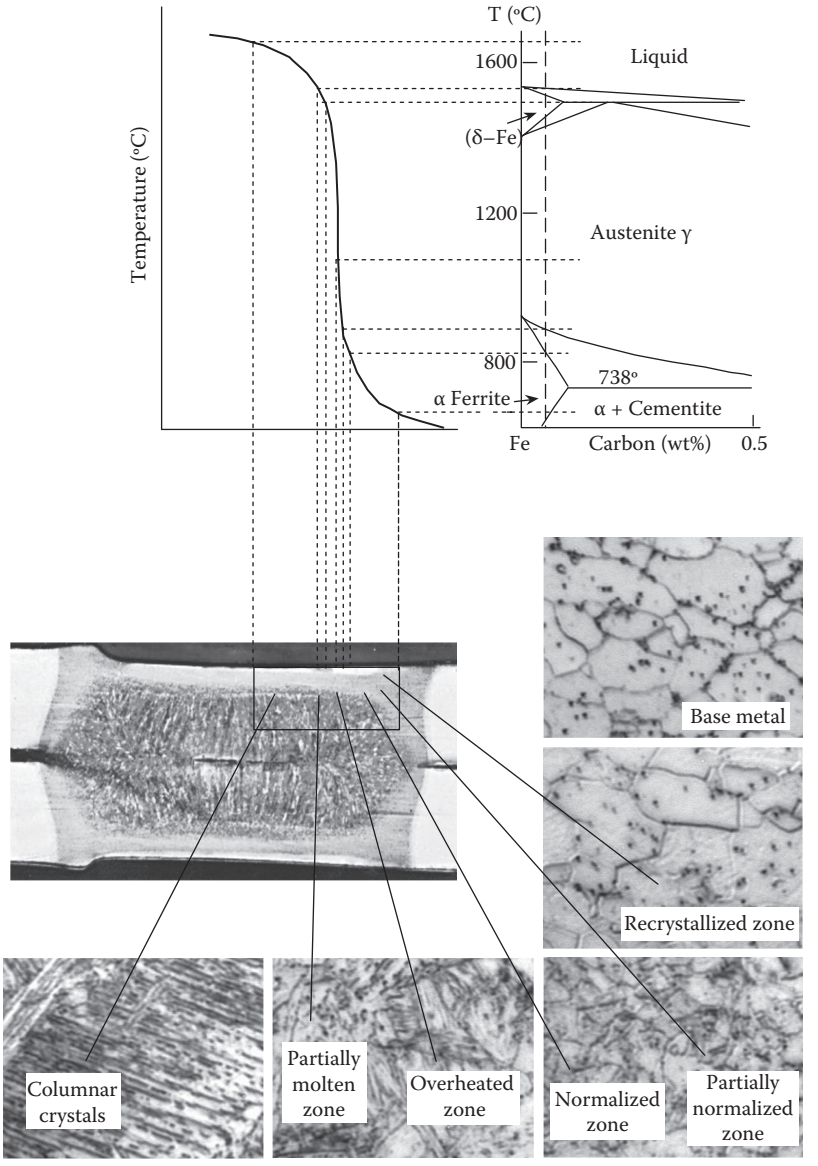

FIGURE 1.8
Structure of high-strength, low-alloy steel (HSLA) steel weldment against temperature gradient and basic Fe–C phase diagram.[12]

the peak temperature of this region exceeded the grain-coarsening temperature. Such an overheated region may be embrittled and have a coarse intergranular fracture when impact loaded. The embrittlement is mainly due to the solution of inclusions such as sulfides and aluminum nitride at high temperature, and their reprecipitation at grain boundaries on cooling. Next to the grain-coarsening region is the grain-refined region of the supercritical zone. The refinement is mainly due to a process similar to that of normalization.

Next to this region, there is a recrystallized structure, which is the so-called intercritical region. This region basically retains the original structure with parts of the grains showing

a slight sign of recrystallization and grain growth. The figure does not show a subcritical region, as its difference from the base metal may be invisible under the magnification.

The microstructure of a weldment, including the base metal, the HAZ, and the fusion zone are dictated by the chemical composition of the weld metal as well as the welding process. The microstructure shown in Figure 1.9 for a DP600 steel weld[9] is significantly different from that of the HSLA steel weld in Figure 1.8. In Figure 1.9, a significant change in microstructure is observed from the original, unaltered base metal to the molten and then solidified weld center, through the HAZ. Each of the regions consists of the two typical phases, α-ferrite (BCC) and martensite (BCT), but with different amount and morphology. In the base metal, the martensite is evenly distributed in a matrix of ferrite. More martensite is observed in the HAZ, and the volume fraction of martensite increases rapidly from the base metal to the fusion line. Finer constituents of martensite and ferrite are observed in the HAZ. According to the authors, the fine structure in the HAZ results from the repeated rapid heating–cooling cycles and the restricted grain growth in the region. Because of the rapid heating and then cooling, austenitizating is not complete and austenite grain growth is interrupted by the rapid cooling that results in martensite transformation. Other phases, such as retained austenite and lower bainite, are also observed in the region. It is filled with martensite due to the presence of high carbon and manganese contents in DP600, and the rapid cooling during RSW, which is estimated at a few thousands of degrees Celsius per second.

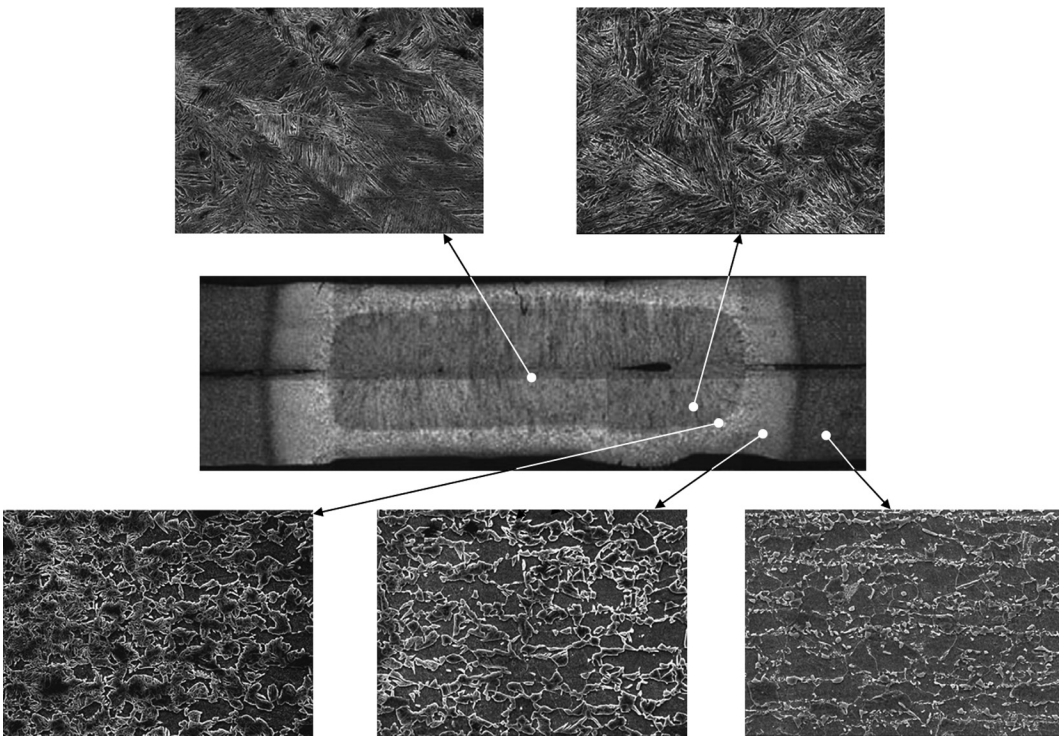

FIGURE 1.9
Microstructure of various zones in DP600 steel weld.[9]

1.2.1.3 Effect of Carbon Content

The ability to form hard (often brittle and hydrogen cracking-prone) metallurgical constituents, such as martensite, bainite, carbide, and other hard phases in a ferrous alloy, either steel or cast iron, depends on the content of carbon and other alloying elements, and the cooling rate. In RSW, it directly affects the integrity as well as the strength of a weldment.

Although carbon and many other alloying elements such as manganese, chromium, silicon, molybdenum, vanadium, copper, and nickel can all raise the hardness of a steel, their mechanisms and contributions are different. Carbon content in the parent austenite phase is directly responsible for, and has the largest effect on the formation of martensite. For instance, the plate martensite formed with a high carbon content has a higher hardness than the lath martensite formed with a low carbon content. As summarized by Krauss[13] on the hardness data from the literature for Fe–C alloys and steels in Figure 1.10, the hardness increases monotonically with carbon content in most of the carbon range of steels.

The effects of other alloying elements, however, are different from that of carbon. They raise the hardness of steels through alteration of the metallurgical process, micro-alloying, and precipitation of hard particles. Cr, Ni, Mo, Si, and Mn may help in retaining austenite by retarding the eutectoid transformation $\gamma \rightarrow \alpha + Fe_3C$ and, therefore, promote martensite formation. The addition of small amount of vanadium can significantly increase the strength of steels through refinement of the ferrite grain size and the formation of hard vanadium carbides. In addition, alloying elements such as vanadium, niobium, and titanium may react preferentially with carbon and/or nitrogen, to form fine dispersion of precipitated hard particles in the steel matrix. All carbide formers are also nitride formers, and the tendency of several alloying elements to form hard nitrides and, therefore, to increase the hardness of a steel by precipitation hardening is shown in Figure 1.11. In general, carbon is the most significant alloying element affecting the hardness of steel and, therefore, the influence of other alloying elements is accounted for in the form of equivalent carbon content (CE), or carbon equivalence.

Equivalent carbon content, or carbon equivalence [or carbon equivalent (CE)], is an empirical value in weight percent, relating the combined hardening effect of different

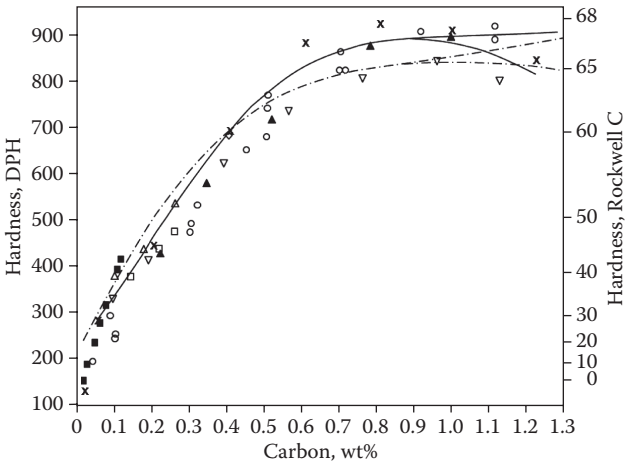

FIGURE 1.10
Summary of hardness data from literature for Fe–C alloys and steels by Krauss.[13] Symbols on the curves indicate the sources of the data.

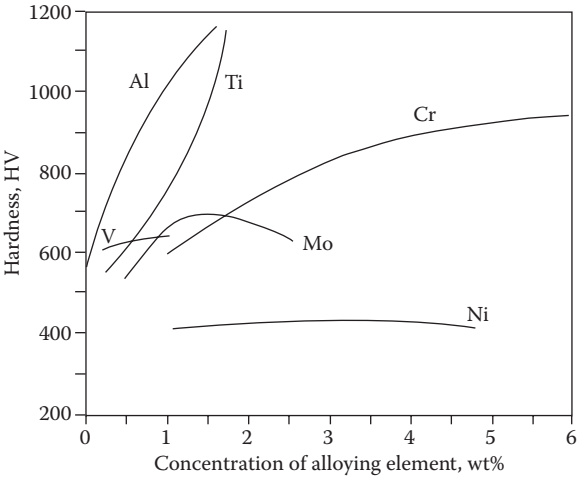

FIGURE 1.11
Effect of alloying element additions on hardness after nitriding. Base composition: 0.25% C, 0.30% Si, 0.70% Mn.[14]

alloying elements used in the making of carbon steels to an equivalent amount of carbon. It is usually expressed in the form of a simple mathematical summation of weighted contributions of various alloying elements, and the weighting factors are obtained through a systematic experimentation. A first-order model containing only the contents of the alloying elements is usually used for simplicity. As a simplified "equivalency" of alloying elements to carbon may not account for the nonlinear effect of alloying elements on hardness, as seen in Figure 1.11, and the interactions among the alloying elements and with material processing, etc., carbon equivalence should be used with discernment. The application of such a model should be limited to the specific class of steels on which the model is developed. There are a number of commonly used CE formulas for particular material systems. For instance, a well-known carbon equivalent formula developed by Dearden and O'Neill[15] based on carbon–manganese steels and later modified by the International Institute of Welding, works well for high-carbon, low-alloy steels:

$$\mathrm{CE} = C + \frac{\mathrm{Mn}}{6} + \frac{\mathrm{Cr} + \mathrm{Mo} + \mathrm{V}}{5} + \frac{\mathrm{Cu} + \mathrm{Ni}}{15} \tag{1.1}$$

A different formula was developed for low-carbon steels or micro-alloy steels:

$$\mathrm{CE} = C + \frac{\mathrm{Si}}{25} + \frac{\mathrm{Mn} + \mathrm{Cr}}{16} + \frac{\mathrm{Cr} + \mathrm{Ni} + \mathrm{Mo}}{20} + \frac{\mathrm{V}}{15} \tag{1.2}$$

Another formula, the Ito–Bessho carbon equivalent, is often used for low-carbon (with C between 0.07% and 0.22%) and micro-alloyed steels[16]:

$$\mathrm{CE} = C + \frac{\mathrm{Si}}{30} + \frac{\mathrm{Mn} + \mathrm{Cu} + \mathrm{Cr}}{20} + \frac{\mathrm{Ni}}{60} + \frac{\mathrm{Mo}}{15} + \frac{\mathrm{V}}{10} + 5\mathrm{B} \tag{1.3}$$

For steels with a carbon content between 0.02% and 0.26%, the Yurioka[17] formula can be used to calculate the CE:

$$\mathrm{CE} = C + A(C) * \left(5B + \frac{\mathrm{Si}}{24} + \frac{\mathrm{Mn}}{6} + \frac{\mathrm{Cu}}{15} + \frac{\mathrm{Ni}}{20} + \frac{\mathrm{Cr}}{5} + \frac{\mathrm{Mo}}{5} + \frac{\mathrm{Nb}}{5} + \frac{\mathrm{V}}{5}\right) \tag{1.4}$$

where $A(C) = 0.75 + 0.25 * \tanh[20(C - 0.12)]$.

If the contents of some alloying elements are not available, the following formula is sometimes used:

$$\mathrm{CE} = C + \frac{\mathrm{Mn}}{6} + 0.05 \tag{1.5}$$

In addition to being used as an indicator of the hardness of steel, CE is more applied directly to describing the processing and predicting performance of steels. By varying the amount of carbon and other alloying elements, the desired strength levels can be achieved through proper heat treatment. Other properties such as weldability and low-temperature toughness can also be controlled or predicted by altering CE. The American Welding Society states that for an equivalent carbon content above 0.40%, calculated based on Equation 1.1, there is a potential for cracking in the HAZ on flame-cut edges and welds.[18] The following carbon equivalent formula was used to determine the weldability of spot welding high-strength, low-alloy steels with excessive hardenability[19]:

$$\mathrm{CE} = C + \frac{\mathrm{Mn}}{30} + \frac{\mathrm{Cr} + \mathrm{Mo} + \mathrm{Zr}}{10} + \frac{\mathrm{Ti}}{2} + \frac{\mathrm{Cb}}{3} + \frac{\mathrm{V}}{7} + \frac{\mathrm{UTS}}{900} + \frac{h}{20} \tag{1.6}$$

where UTS is the ultimate tensile strength in ksi and h is the sheet thickness in inches. Note that the formula contains the mechanical strength and sheet thickness, in addition to the alloying element contents. Therefore, it can be used to describe the failure mode of a spot weld.

In a study on a DP600 steel with a nominal chemical composition of 0.08 C, 1.91 Mn, 0.04 Si, 0.018 P, 0.006 S, 0.035 Al, and 0.005 N (in wt.%), Ma et al.[9] studied the effect of alloying elements on the hardness profile in a spot weld, and established a relationship between the CE value and fracture mode. Because of the high content of the alloying elements in steel and high cooling rate during welding, a significant increase in hardness is observed in a typical DP600 steel weld, from the base metal to the center of the weld due to the formation of martensite (Figure 1.12).

A large proportion of the welds tested exhibit interfacial fracture failure mode in their study. Using the Nippon Steel CE formula and a variation of Equation 1.5 as in the following,[20,21]

$$\mathrm{CE} = C + \frac{\mathrm{Si}}{30} + \frac{\mathrm{Mn}}{20} + 2\mathrm{P} + 4\mathrm{S} \tag{1.7}$$

$$\mathrm{CE} = C + \frac{\mathrm{Mn}}{6} \tag{1.8}$$

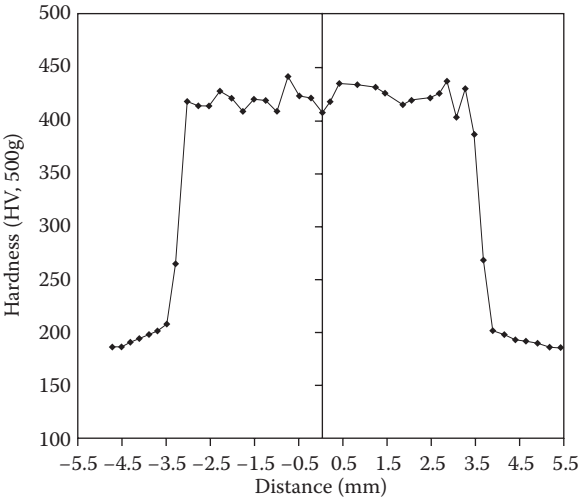

FIGURE. 1.12
Microhardness profile of a typical DP600 steel spot weld. Welding current = 8.26 kA, electrode force = 3.34 kN, and welding time = 300 ms. (From Ma, C. et al., *Mater. Sci. Eng. A*, 485, 334–346, 2008. With permission.)

CE values of 0.242 and 0.367, respectively, were obtained. Both formulas yield a CE value larger than 0.24, which is considered as the threshold of interfacial failure of spot welds.[20]

In another study by Khan et al.,[22] experiments were conducted on welding dissimilar material combination of HSLA350/DP600 steels. The fusion zone of such a spot weld was found to be predominantly martensitic with some bainite. The hardness of such a dissimilar material spot weld is different from that of the similar ones in each of the HSLA350 and DP600 steels, and tests revealed that the DP600 weld properties played a dominating role in the microstructure and tensile properties of the dissimilar material spot welds.

In their study, spot welds of 7.5 mm diameter were made using various material combinations: DP600/DP600, HSLA350/HSLA350, and HSLA350/DP600. Their microhardness profiles are shown in Figure 1.13. The DP600 weld has the highest hardness, whereas that of HSLA is the lowest. It is interesting to see that the hardness of the dissimilar material weld lies between those of the same material combinations. Using the same material combination (HSLA350/DP600), the 5.5-mm weld has a higher hardness than that of the 7.5-mm nugget, possibly due to the more martensitic microstructure resulting from the faster cooling it experienced because of a smaller weld diameter. The CE values were calculated according to the formula in Equation 1.3, and 0.208 and 0.141 were obtained for the DP600 steel and the HSLA350 steel, respectively, using the data listed in Table 1.1. The higher CE of the DP600 steel corresponds to a more martensitic and harder microstructure as compared to the HSLA350 steel. Combining these two steels produces a CE in the weld nugget lying between those of these two materials, as well as a hardness as seen in Figure 1.13. The difference in the peak hardness values of the HAZ of the HSLA350/DP600 nugget is an indication of the difference in hardenability between the base metals, similar to the observations by Marya and Gayden[20] for the TRIP/HSLA combination.

1.2.2 Aluminum Alloys

As an important structural material, aluminum alloys are often the material of choice because of their balanced overall quality of strength, weight, corrosion resistance,

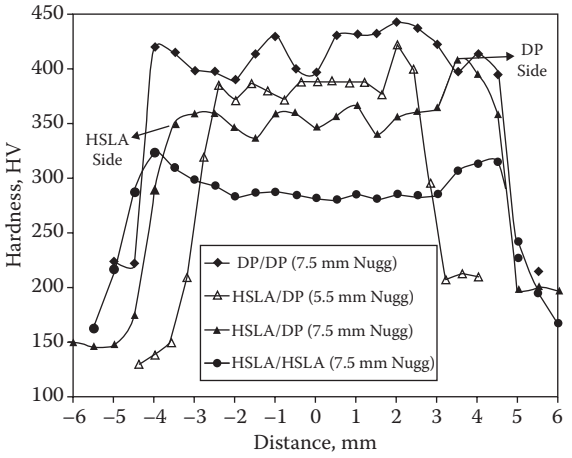

FIGURE 1.13
Microhardness profiles of DP/DP, HSLA/DP, and HSLA/HSLA spot welds. (From Khan, M.S. et al., *Sci. Technol. Welding Joining*, 14(7), 616–625, 2009. With permission.)

manufacturability, and cost. Pure aluminum is rarely used as engineering material, and various alloying elements are used in order to achieve a wide range of engineering properties. Aluminum alloys are made either as casting alloys or wrought alloys. Because of Al alloys' light weight and high specific strength, they are widely used in the aerospace industry. Over the past two decades, they have been introduced to the automobile industry mainly for weight reduction. Significant knowledge has been accumulated in manufacturing such as welding Al alloys.

1.2.2.1 Classifications and Properties

Aluminum alloys are classified as casting alloys and wrought alloys, and both are further divided as heat-treatable and non–heat-treatable alloys. More specific classifications are made by a number system by the American National Standards Institute, or by names indicating their main alloying elements (as by the German Institute for Standardization and International Organization for Standardization), and others. Wrought alloys are identified with a four-digit number indicating the alloying elements. Casting alloys use a four- to five-digit number with a decimal point, which is used for the form of casting (cast shape or ingot). Table 1.2 lists the major alloying elements in the aluminum alloy series, as well as the main hardening mechanisms of these alloys. As resistance welding is usually performed on sheet materials, only wrought aluminum alloys are discussed in this section.

TABLE 1.1
Chemical Composition of Test Materials (wt.%)[22]

C	Mn	Si	Ni	Cr	V	Mo	Ti	P	S	Cu	Nb
Hot-dip galvannealed HSLA350 steel											
0.05	0.6	0.05	0.01	0.04	0.003	0.004	0.001	0.03	0.004	0.043	0.01
Hot-dip galvannealed DP600 steel											
0.10	1.5	0.19	0.01	0.18	0.005	0.24	0.02	0.009	0.002	0.02	0.007

TABLE 1.2

Designation and Hardening Mechanisms for Alloyed Wrought Aluminum Alloys

Major Alloying Element	Designation	Work-Hardened	Solution Heat-Treated/ Age-Hardened
None (99% + Aluminum)	1XXX	Yes	
Copper	2XXX		Yes
Manganese	3XXX	Yes	
Silicon	4XXX		Yes
Magnesium	5XXX	Yes	
Magnesium + Silicon	6XXX		Yes
Zinc	7XXX		Yes
Lithium	8XXX		Yes

The typical alloying elements for aluminum alloys are copper, magnesium, manganese, silicon, zinc, and lithium. Small quantities of chromium, titanium, zirconium, lead, bismuth, and nickel are also added, and the presence of iron in small quantities is invariable. The taxonomy of aluminum alloys reflects the composition, hardening mechanism, processing, and strength of the alloys. In addition to the digits for the major alloying elements, designations are also made to specify the work-hardening or heat-treatment conditions.

The 1000, 3000, and 5000 series aluminum alloys are work hardened by cold work such as cold rolling. Their properties are determined by the degree of cold work and heat treatment following the cold work. The nomenclature used to describe these conditions is presented in Table 1.3. On the other hand, the designation, as listed in Table 1.4, is different for the solution heat-treated and age-hardened aluminum alloys, that is, the 2000, 4000, 6000, 7000, and 8000 series alloys. The large number of possible combinations of composition, solution heat treatment temperature and duration, quench rate, shaping, and other factors make it possible to tailor the alloys' properties in a wide range.

TABLE 1.3

Standard Nomenclature for the Heat Treatment of Work-Hardened Aluminum Alloys

Symbol	Description
O	Annealed, full soft
F	As fabricated
H12	Work hardened, without thermal treatment, 1/4 hard
H14	Work hardened, without thermal treatment, 1/2 hard
H16	Work hardened, without thermal treatment, 3/4 hard
H18	Work hardened, without thermal treatment, fully hard
H22	Work hardened, partially annealed, 1/4 hard
H24	Work hardened, partially annealed, 1/2 hard
H26	Work hardened, partially annealed, 3/4 hard
H28	Work hardened, partially annealed, fully hard
H32	Work hardened, stabilized, 1/4 hard
H34	Work hardened, stabilized, 1/2 hard
H36	Work hardened, stabilized, 3/4 hard
H38	Work hardened, stabilized, fully hard

TABLE 1.4

Heat Treatment Designation for Aluminum Alloys

Symbol	Description
T1	Cooled from hot working and naturally aged (at room temperature)
T2	Cooled from hot working, cold worked, and naturally aged
T3	Solution heat-treated, cold worked, and naturally aged
T4	Solution heat treated and naturally aged
T5	Cooled from hot working and artificially aged (at elevated temperature)
T6	Solution heat treated and then artificially aged
T7	Solution heat treated and overaged/stabilized
T8	Solution heat treated, cold worked, and artificially aged
T9	Solution heat treated, artificially aged, and cold worked
T10	Cooled from hot working, cold worked, and artificially aged
W	Solution heat treated only

When welding an aluminum alloy, it is important to consider the influence of its metallurgical characteristics on welding process and weld quality. For instance, the structure of the HAZ in an alloy 6111 may be quite different from that of a 5754 alloy, because the former is heat treatable. Another metallurgical factor, the high affinity of aluminum for oxygen, makes aluminum easily oxidized when exposed to air. Therefore, there is always a clear, protective layer of aluminum oxide on the surface of aluminum alloys. Such an oxide layer has a significant implication in the electrical contact resistance and, therefore, affects a welding process.

1.2.2.2 Resistance Welding Aluminum Alloys

Welding aluminum alloys is significantly different from welding other metals such as steels due largely to their unique metallurgical properties. For instance, aluminum welding is more prone to expulsion and cracking. The wide solidus–liquidus gap in the Al–Mg phase diagram (Figure 1.14) indicates the existence of a partial melting zone for a relatively long period of time during heating and cooling an alloy with Mg as the major alloying element. The presence of low-melting-point eutectics and impurities also weakens the HAZ in a weldment. A typical microstructure of the region in the HAZ close to the nugget is presented in Figure 1.15 for aluminum alloy 5754. Precipitates inside the grains and at grain boundaries (intergranular precipitates), where they form chains or even continuous layers, are visible. Energy-dispersive x-ray (EDX) and wavelength dispersive x-ray analyses revealed an increased amount of Mg in such regions. This is most probably due to an Al_3Mg_2 secondary phase (the presence of which should be about 6% in the Al–Mg 3.5% alloy, according to the Al–Mg equilibrium phase diagram), which exists in the alloy before welding and serves as the source of liquid at elevated temperature. This was confirmed by an x-ray diffraction examination. More discussion of the effect of low-melting eutectics on cracking of aluminum alloys can be found in Chapter 3. In addition to cracking, resistance welding aluminum alloys has other unique characteristics associated with their metallurgical properties, such as massive shrinkage voids/porosity, rapid electrode wear. They will be discussed in detail in other chapters specifically dealing with these subjects.

The microstructures of an aluminum weldment can be linked to the metallurgical characteristics of aluminum alloys through a possible thermal history during resistance welding. Such a relation for an aluminum AA5754 weldment is shown in Figure 1.16. The

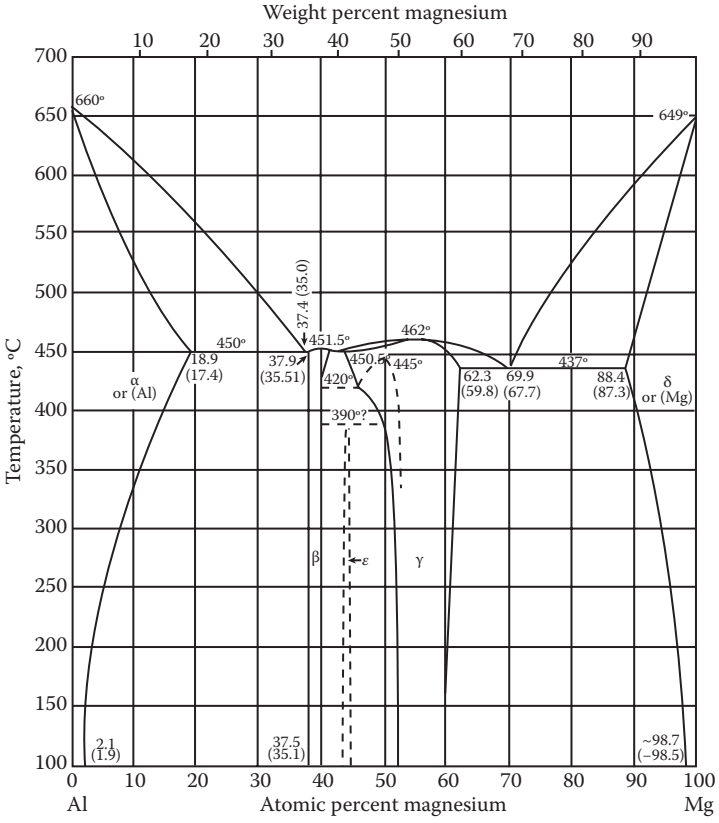

FIGURE 1.14
Al–Mg binary phase diagram. (From Hansen, M., Anderko, K., *Constitution of Binary Alloys*, 1958, 106. With permission.)

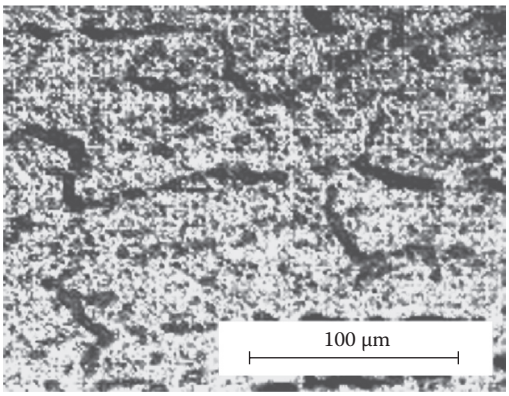

FIGURE 1.15
Precipitation zone in HAZ.

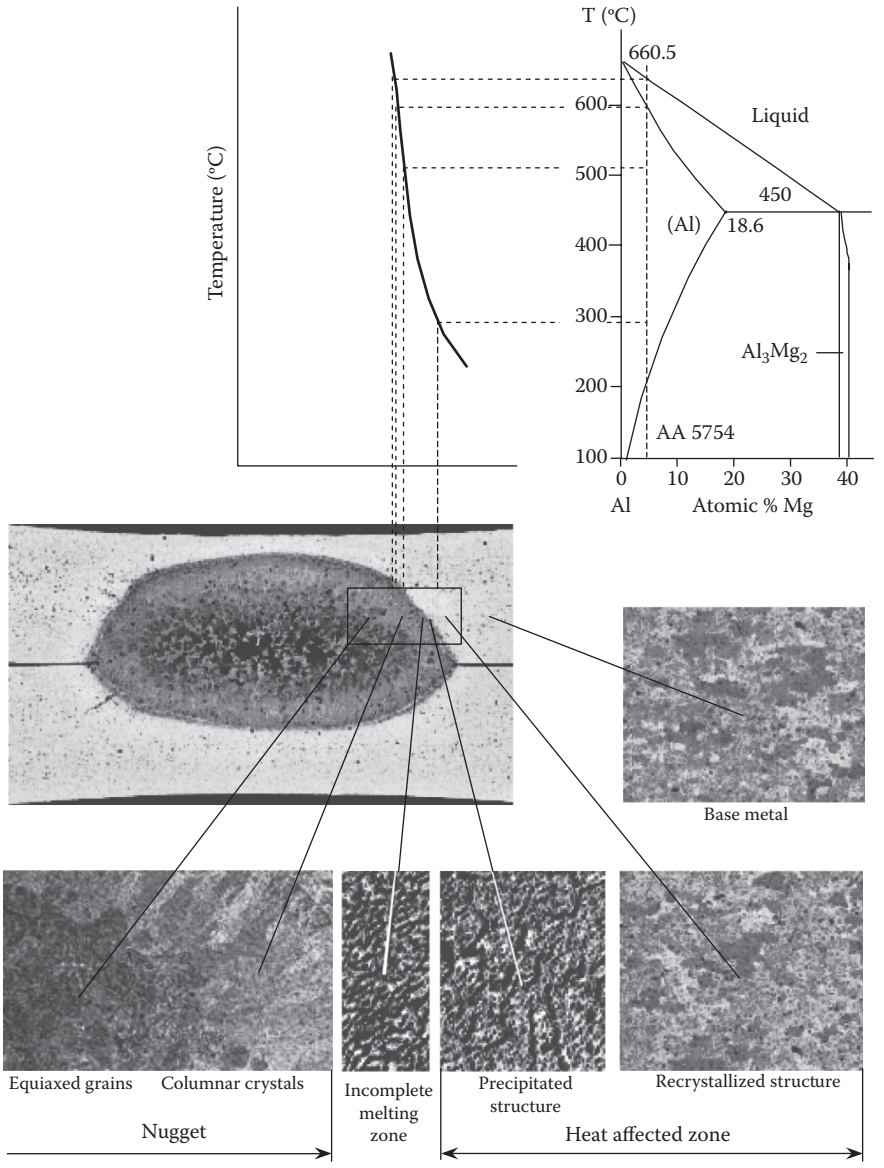

FIGURE 1.16
Weldment structure of a 5754 aluminum alloy against temperature gradient and basic Al–Mg phase diagram.[12]

structures of aluminum welds are usually not as clearly distinguishable as in steel welds, and the HAZ is significantly narrower for an aluminum weld. These make the identification of various zones difficult. The Al–Mg phase diagram used for this alloy indicates precipitation at temperatures just below the solidus, and under that there is a recrystallization temperature range. The temperature gradient is very high in the HAZ, indicating a possible large thermal stress development in the region.

1.2.3 Magnesium Alloys

Magnesium alloys are an attractive alternative to steels and even Al alloys for auto components due to their low density, high specific strength, excellent recyclability, and many other advantages. In order to achieve substantial vehicle weight reduction and improving fuel efficiency, a vehicle's average magnesium content is expected to increase to as much as 350 lb by the year 2020, replacing heavier components, as stated in *Magnesium Vision 2020*.[24] A crucial issue in large-scale application of Mg alloys is an industrial joining means of Mg components, such as RSW for joining sheet materials. Because of the relatively small volume of Mg used in sheet metal industry, limited knowledge is accumulated in joining Mg alloys, and the knowledge on resistance welding steels and Al alloys cannot be directly applied to welding Mg.

1.2.3.1 Properties and Applications of Mg Alloys

Among the lightest of all the metals, magnesium is principally used as an alloying element for aluminum, lead, zinc, and other nonferrous alloys. When magnesium is used as a structural material, however, it is usually used in the form of alloys, as pure magnesium has too low a strength for any engineering application. The strength of magnesium alloys containing small amounts of aluminum, manganese, zinc, zirconium, etc., is similar to that of mild steels. Commercially available magnesium alloys can be classified into three groups:

1. Mg–Mn alloys. Because of their good weldability, they are often used for sheet metal fabrications.
2. Mg–Al–Zn alloys. These alloys can be heat treated by solution treatment and precipitation hardening, and can be processed through die casting, sand casting, extrusion, and forging.
3. Mg alloyed with rare earths. This group also includes zirconium as alloying element. They are used in both cast and wrought form.

Magnesium alloys are coded differently by different organizations. ASTM and SAE use two letters, indicating the two major alloying elements, followed by two digits for the nominal percentage contents of these two elements. The letters usually used are A for aluminum, B for bismuth, C for copper, D for cadmium, E for rare earth, F for iron, H for thorium, K for zirconium, M for manganese, and Z for zinc. There are other coding systems such as the Unified Numbering System and the British Standard for magnesium alloys.

Magnesium alloys are an ideal material for weight reduction mainly because of their high specific strength. They have a wide range of other mechanical properties, depending on the composition, condition (whether cast or wrought), fabrication process, heat treatment, and other factors. In addition, magnesium alloys have higher damping capacities than cast iron (up to about 3 times) and aluminum (about 30 times), which make them ideal for automobile applications. Their high electrical and thermal conductivities make them preferred for certain applications such as heat sink for heat dissipation. Because of their high chemical reactivity, magnesium alloys usually have a protective film on their surface to protect against corrosion. However, it is not as dense as the oxide layer on an aluminum alloy, and it is easily corroded by chlorides, sulfates, and other chemicals. Therefore, magnesium is often anodized for corrosion protection.

Both casting and wrought magnesium alloys are used in automobile applications. In sheet metal fabrication, however, wrought alloys are prevalent. As the mechanical properties of such alloys are determined by the fabrication and they are usually anisotropic,

attention is needed in identifying the direction dependence of the material properties. The inference of such anisotropy in properties on welding can be a subject of study. For rolled sheets, the longitudinal properties are normally a little lower than the transverse properties, and the tensile properties of sheets are usually determined on specimens cut parallel to the direction of rolling. The yield strengths of wrought magnesium alloys normally vary with the direction of metal flow. The modulus of elasticity of commercial magnesium alloys in tension and compression is about 45 GPa, the shear modulus is about 16 GPa, and Poisson's ratio is 0.35. The modulus of elasticity decreases with temperature. It was found that cyclic cold loading beyond the yield strength in both tension and compression reduces the modulus of elasticity of magnesium alloys. A number of low-melting eutectics between Mg and other elements may form during material processing, and they play an important role in the behavior of Mg alloys. For instance, wetting of grain boundaries by low-melting eutectics was considered responsible for the super-plastic deformation of these alloys.[25] They may affect the weldability by promoting hot cracking during welding.

Magnesium alloys have found a wide range of applications in automobile, electronics, aerospace, and other industries because of their advantages over other structural materials, and the abundance of Mg resources. In automobile construction, for instance, magnesium alloys have been used as structural components, chassis system support, and interior components. Their unique contributions to vehicle weight reduction, fuel economy, emission reduction, noise reduction, safety, recyclability, and many others make them a focus in automobile material and processing research. Because of the limitations in fabricating rolled products and in material joining techniques, a large portion of magnesium products are in the form of castings.

1.2.3.2 Welding Mg Alloys

Welding magnesium alloys is not as robust as welding steels or aluminum alloys. The difficulties in welding Mg alloys arise from their intrinsic physical properties. Nevertheless, extensive research work has been carried out in fusion welding Mg alloys, and a number of important findings have been made. Some of them are summarized in the following[26,27]:

1. Excessive grain growth in the fusion zone. A high heat input rate is necessary in welding Mg alloys because of their high thermal conductivity. In addition, the melting temperatures of the alloys and, therefore, the recrystallization temperatures are fairly low. As a result, coarse grains are usually observed in the fused and solidified area, accompanied by large segregation of alloying elements. These severely affect the strength of a welded joint.
2. Excessive thermal stresses and distortion. The large coefficient of thermal expansion (CTE) and rapid heat input during welding Mg alloys produce significant deformation, distortion, and thermal stress in the weldment during welding.
3. Cracking. Mg may form a number of eutectics with other alloying elements having much lower melting temperatures than the Mg matrix. Therefore, there is a partial melting zone in which the melting of eutectics weakens the material and makes it prone to cracking, with the aid of thermal stresses.
4. Void formation. Hydrogen from various sources such as moisture and coating compound may dissolve in the molten metal. As the solubility of hydrogen in Mg drops drastically during cooling, gas bubbles may form during solidification.

The aluminum content in the Mg–Al–Zn alloys, such as AZ31B, AZ80A, AZ91, and AZ92A, generally promotes weldability, as it helps refine the grain structure. Zinc of more than 1% makes the material prone to hot cracking. Therefore, Mg alloys of high zinc content (ZH62A, ZK51A, ZK60A, and ZK61A) have poor weldability. The weldability of these alloys can be improved by adding a small amount of thorium.

Because of the difficulties in welding Mg alloys, alternative means of joining such as mechanical fastening and adhesive bonding have been explored. However, the automobile industry still prefers RSW because of its robustness proven in the practice of joining other metals over a few decades, and the high comfort level of the operators.

1.2.3.3 Resistance Welding Mg Alloys

There is very limited information available on resistance spot welding Mg alloys in the public domain. In a study on welding AZ31B alloys,[28,29] it was found that the center of a weld nugget consists of fine equiaxed grains, decorated with β-$Mg_{17}Al_{12}$ precipitated from α-Mg. Cracking was speculated to initiate in the welds during solidification, and electrode deterioration and expulsion were found to be the most common defects in welding Mg alloys. In another work of welding AZ91D and AM50, low-melting phases at the grain boundaries in the base metal, possibly formed by segregation, melted during heating (below the melting temperature of the alloy), and solidified during cooling.[30]

Because of the similarities between Al and Mg in electrical, thermal, and metallurgical properties, knowledge of welding Al alloys can be utilized as guidance for welding Mg alloys. In welding both alloys, care must be taken to avoid expulsion, cracking, and premature electrode failure. However, one has to recognize that welding Mg alloys is different from welding Al alloys in several aspects. For instance, experiments have found that Mg alloys are more prone to both surface and interfacial expulsion, as discussed in more detail in Chapter 7. In general, resistance welding Mg alloys has the following characteristics:

1. High electric current. The low electrical resistivity of Mg and its alloys warrants a high electric current to be applied, in order to generate sufficient heat through the Joule process.
2. Short welding time. The resistance heating has to be done in a short period of time, as the high thermal conductivity of the alloys makes the heat dissipate rapidly.
3. Large electrode force. This serves two purposes: reducing the contact resistance by breaking up the oxide layer and creating sufficient electric contact at the electrode–sheet interface, and confining the expansion of the weldment, which is critical for containing expulsion and reducing defect formation. These alloys have a fairly large CTE and, therefore, a large electrode force is needed.
4. High expulsion tendency. Both surface and interfacial expulsion are prevalent in welding Mg alloys, and the expulsion mechanisms are different in welding different alloys.
5. Short electrode life. The electrode life can be significantly shorter than in welding Al alloys, as a result of surface expulsion and alloying between the sheet and electrode.
6. Defect formation. Both cracks and voids are common in Mg welds, due to the large expansion of the alloys, and volume deficit created by expulsion.

In a study on the characteristics of resistance welding Mg alloys AZ31B and AZ91D, Luo et al.[31] studied cracking and expulsion during resistance welding. Some of the phases in the base metal and the weldment can be found from a binary Mg–Al phase diagram in Figure 1.17. As seen from a typical microstructure of the AZ91D casting shown in Figure 1.18a, in addition to small voids possibly formed during casting, a large amount of β phase ($Mg_{17}Al_{12}$) exists at the grain boundaries. The structures and properties of different phases are drastically different, and the difference exists even after the material is heat-treated for tempering and homogenization. The rolled AZ31B sheets have a significantly different morphology of microstructure with much finer grain boundaries, possibly due to the smaller amount of alloying elements and a different fabrication process (Figure 1.18b).

Due to the different metallurgical characteristics of AZ31B and AZ91D, these two alloys behaved quite differently in welding. Expulsion is observed in welding AZ31B, at both surface and interface. Expulsion is also prevalent in welding AZ91D. However, the liquid metal is ejected both from the faying interface and through a liquid network consisting of low-melting eutectics.

Unlike in welding most metals such as steels, columnar dendritic grains are not common in the fusion zone of Mg welds. In welding AZ31, it was found that the edge of a weld tends to have a cellular dendritic structure, whereas the nugget center has an equiaxed dendritic structure (Figure 1.19).[32] These structures are similar to those revealed from the opened crack surfaces in the same work, as shown in Figure 1.6a and b, respectively. The epitaxial growth of cellular dendritic crystals is believed to be driven by the supercooling created by the rapid heat dissipation during cooling, which is possible through the solid portion of the weldment as a result of the high thermal conductivity of Mg alloys. The temperature gradient decreases as the solid–liquid interface advances toward the weld center; and the Al and Zn concentrations increase due to segregation, which creates a large constitutional supercooling. Both conditions favor the equiaxed dendritic crystal growth

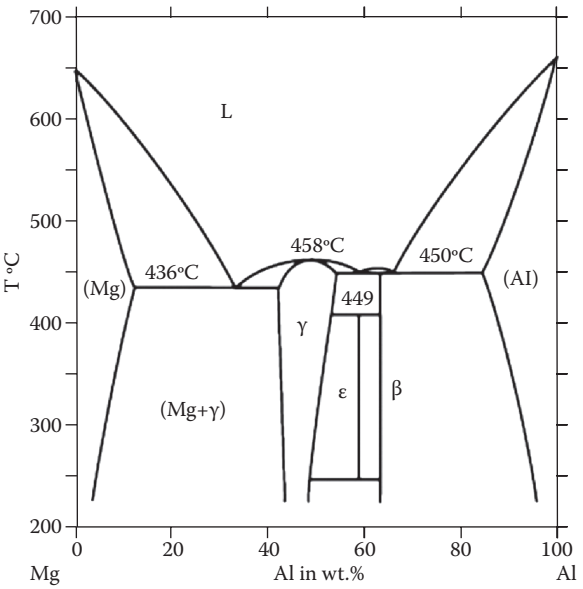

FIGURE 1.17
Mg–Al phase diagram.

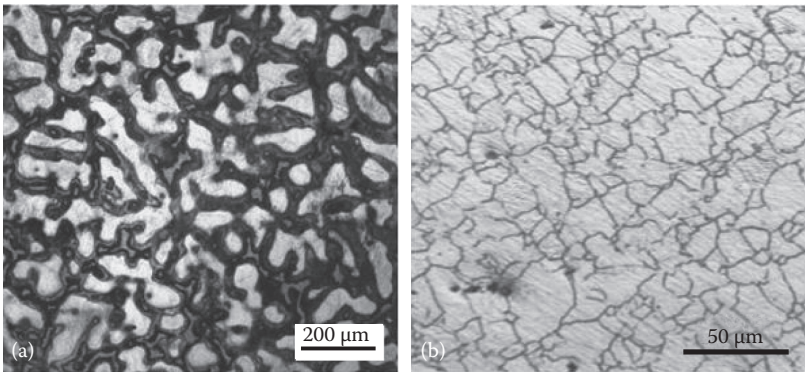

FIGURE 1.18
Microstructures of (a) AZ91D and (b) AZ31B sheets.

at the weld center. Another study on AZ31 confirmed the equiaxed dendritic structure in the weld nugget.[29]

The microstructure of a Mg weld also depends on the heating/cooling process, or welding parameters. In a study on welding AZ31B,[10] it was found that the welds usually consist of cellular dendritic structure in the nugget near the fusion line, and equiaxed dendrites away from the fusion line (Figure 1.20a and b), same as observed by other researchers. Cellular dendrites may also form at the interior of a weld, as shown in Figure 1.20c under certain heating/cooling conditions. Similar structures are observed in an AZ91D weld (Figure 1.21).[10]

The existence of low-melting eutectics in Mg alloys has a significant effect on the structure and defect formation in Mg welds. Because these eutectics are generally rich in alloying element, they are concentrated around grain boundaries, largely resulting from segregation. They may be created during fabrication of the material, as shown in Figure 1.18a in the AZ91D casting, or they may be formed during solidification in the fusion zone. Grain boundary melting of such eutectics in the HAZ may weaken the structure, and cracking may occur under tensile loading. Figure 1.22a shows a crack in the HAZ near the base metal. Its intergranular nature is an indirect evidence of grain boundary melting. Similar cracking is observed inside of a weld, as seen in Figure 1.22b, which shows

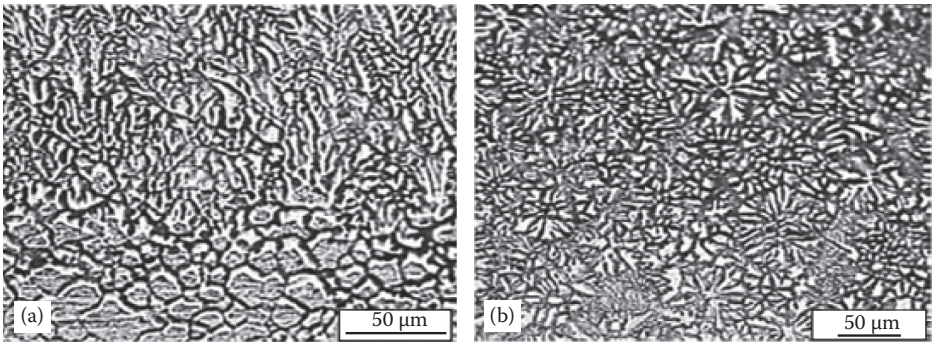

FIGURE 1.19
Microstructure of AZ31 weld nugget: (a) cellular dendritic structure near fusion line, and (b) equiaxed dendritic structure at center. (From Sun, D.Q. et al., *Mater. Sci. Eng. A*, 460, 461, 494–498, 2007. With permission.)

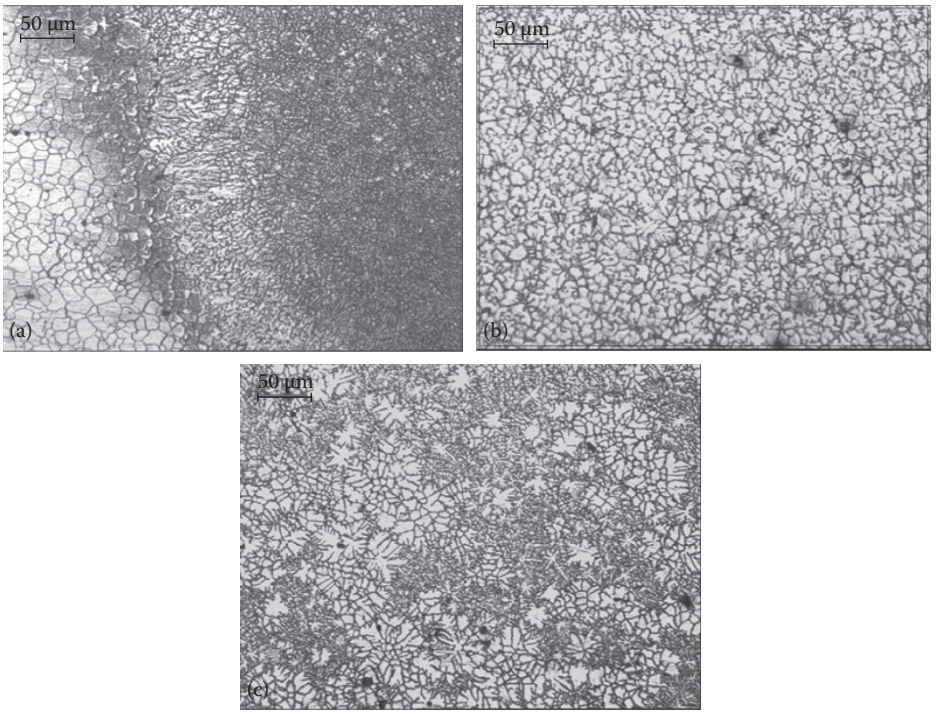

FIGURE 1.20
Microstructures of AZ31B welds. Those of the HAZ and nugget near the fusion line (a), and at a distance from the fusion line (b). The interior of an AZ31B weld created under a different welding condition is shown in (c). (From Luo, H., New joining techniques for magnesium alloy sheets, MS thesis, Institute of Metal Research, Chinese Academy of Sciences, May 2008. With permission.)

both cracks and voids. The formation of these defects is driven by the liquid eutectics that remain as liquid until all their surroundings are solidified, the volume deficit created by the irreversible thermal expansion and expulsion, and the thermal stress developed during cooling. The structures shown in Figure 1.23 from crack surfaces are the result of free solidification that occurred in such a process.

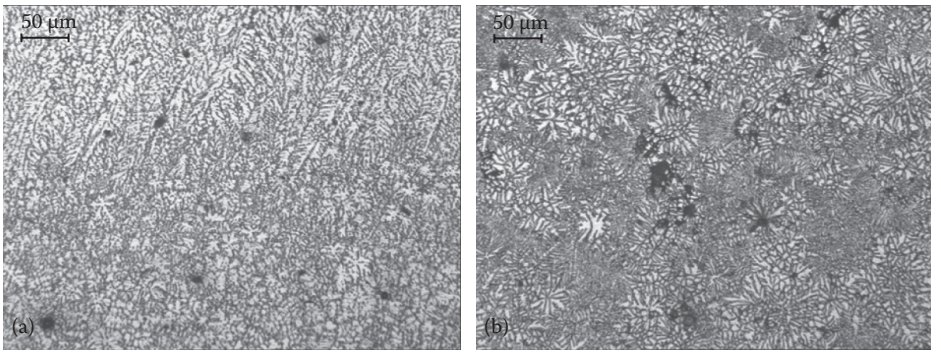

FIGURE 1.21
Weld microstructure of AZ91D weld. (From Luo, H., New joining techniques for magnesium alloy sheets, MS thesis, Institute of Metal Research, Chinese Academy of Sciences, May 2008. With permission.)

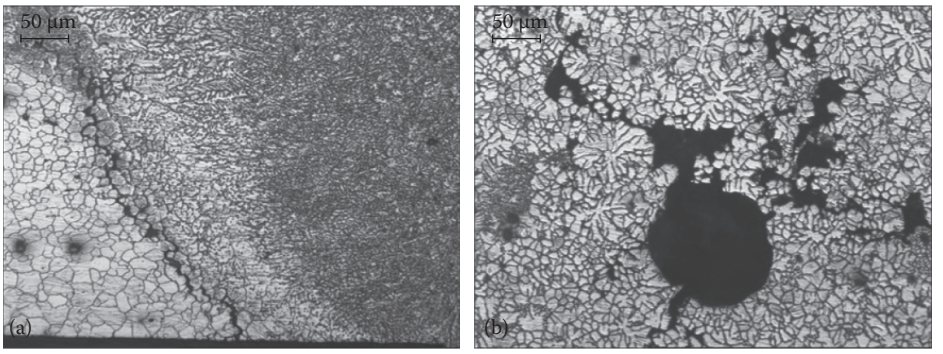

FIGURE 1.22
Microstructure near HAZ (a) and inside (b) of an AZ31B weld. (From Luo, H., New joining techniques for magnesium alloy sheets, MS thesis, Institute of Metal Research, Chinese Academy of Sciences, May 2008. With permission.)

1.2.4 Copper Alloys

Copper is the base metal normally used for resistance welding tongs and tips. The major functions of the electrodes are to conduct the welding current, to apply pressure to the weld joint, and to transfer heat from the workpiece. Copper is an industrial metal that is widely used in both pure and alloyed forms, mainly because of its unique characteristics of high electrical conductivity, high thermal conductivity, high corrosion resistance, good ductility and malleability, and reasonable mechanical strength. Pure copper is the ideal material for electric current conductors, but the electrodes for resistance welding require a strength that exceeds the level attainable with pure copper. Therefore, the use of copper alloys becomes necessary. The most common Cu alloys used as electrode materials are:

1. Cu–Cr
2. Cu–Cr–Zr
3. Cu–Zr
4. Dispersion-strengthened copper (DSC)

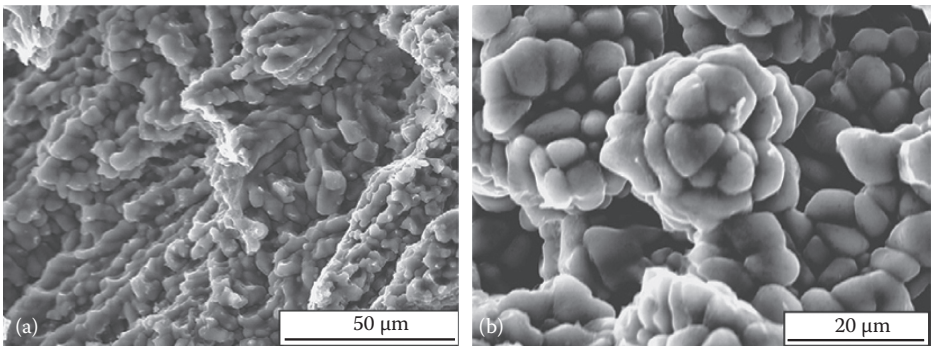

FIGURE 1.23
Morphology of opened crack surface: (a) cellular dendrites, and (b) equiaxed dendrites. (From Sun, D.Q. et al., *Mater. Sci. Eng. A*, 460, 461, 494–498, 2007. With permission.)

Cu–Cr and Cu–Cr–Zr are the original materials used to weld bare steels. Cu–Zr and DSC were introduced to deal with coated steels when sticking became a major production issue.[33] In general, copper alloys used as electrode materials must exhibit high electrical and thermal conductivities, combined with high strength, at elevated temperatures.

1.2.4.1 Strengthening of Cu Alloys

The difficulty in developing a suitable material for electrodes lies in achieving a balance between mechanical strength and electrical conductivity, and resistance to softening at elevated temperatures. Significant research efforts have been put forward in order to raise the mechanical strength while maintaining the high electrical and thermal conductivities of copper. Over the years, a large variety of high-copper alloys with reasonable strength has been developed through solid solution hardening and precipitation hardening, and often aided by cold work.

Copper lattice is able to dissolve a certain amount of atoms of other metals to form a solid solution. In such a solid solution, the lattice in the vicinity of the impurity atoms is distorted because of the difference in size of the impurities from that of copper. Such distortion creates local stress fields that impede dislocation motion and, therefore, strengthens the metal. This is called solid solution strengthening. Solid solution strengthening is often accompanied by a certain degree of cold work to further increase the strength. However, a tradeoff for the increase in strength is the decrease in electrical conductivity, resulting from the lattice distortion caused by alloying atoms. In general, all dissolved additions to copper reduce electrical conductivity, and the extent of this effect varies widely from element to element. Cadmium additions, for example, affect conductivity the least, whereas others, such as phosphorus, tin, and zinc, are more detrimental. In order to minimize the drop in electrical conductivity, solid solution-hardened high copper alloys with low content of alloyed elements have been developed for applications such as resistance welding electrodes. Among them, Cu–Cr alloys have a favorable combination of mechanical properties and electrical conductivity, and are commonly used as electrode materials for resistance welding of low-carbon steels.[34]

There is a limit, called solubility limit, as to how much a particular impurity can be dissolved in a metal. It in general increases with temperature. A different phase may start to form if a solid solution is cooled down and the solubility limit is undershot. The second phase, usually an intermetallic, is in the form of fine (often lower than 100 nm in size) and hard particles, and it strengthens the material. This is precipitation strengthening. In addition to the strength, this process also affects the electrical conductivity of the metal. As the impurity atoms leave the lattice, the lattice distortion is undone and the electric conductivity of the material is restored to a certain extent. The solubility of Cr in Cu is fairly low: no more than 0.7 wt.% Cr could be dissolved into solid solution at a safe solution treatment temperature. An addition of a very small amount of Zr (less than 0.1 wt.%) improves hardness and electrical conductivity of the Cu–Cr alloy due to the very low solubility of Zr in Cu matrix at room temperature. Zr in the alloys adjusts the orientation relationship between Cr and the matrix, and tends to increase the conductivity of aged Cu–Cr–Zr alloys after deformation. In the Cu–Cr–Zr alloys, the precipitated phases are characterized as Cr, $Cu_{51}Zr_{14}$, and Cu_5Zr,[35] as well as the Hesuler phase $CrCu_2Zr$.[36] The plastic deformation during fabrication of electrodes involves cold work, which increases the hardness but reduces the conductivity. Such cold work after the solution annealing but before the age annealing promotes the formation of fine and homogeneously distributed precipitates. An important characteristic of precipitation-hardened alloys is their high relaxation resistance. This is critical for resistance welding electrodes as they are exposed to fairly high temperature and pressure during

welding. Solid solution-hardened alloys generally have insufficient relaxation resistance at elevated temperatures, and precipitation strengthening becomes essential.

The International Annealed Copper Standard (IACS; a high purity copper with a resistivity of 0.0000017 Ω cm) is sometimes used as an electrical conductivity standard for metals, and the effect of alloying on electrical conductivity is often expressed by the resultant electrical conductivity value of the alloy as a percentage of IACS. For instance, it was found that in Cu–0.4%Cr–0.08%Zr, the maximum of electrical conductivity, which is between 89% and 92% IACS, appears at 480°C.[34]

Sticking of the electrodes to the workpiece is a major problem when welding galvanized steels. The reaction of the galvanized Zn and Cu can produce a bond between the electrode and the steel sheet and cause the electrode to stick to the sheet. This may result in the alloyed layer of brass on the electrode to be peeled from the electrode, or even the electrode pulled from its holder.[37] Using Cu–Zr electrodes can dramatically reduce sticking, and another type of material, DSC, has better sticking resistance.[33] Both Cu–Zr alloys and DSC have excellent high-temperature stability and, therefore, prolonged electrode life. Because dispersed oxides such as alumina are often used in making DSC, they are often referred to as oxide dispersion-strengthened copper (ODSC or ODS copper). The high thermal stability of ODSC comes from the fact that the aluminum oxide particles can retain their original size and spacing, and retard the copper matrix from recrystallization even after prolonged heating.[38]

There are several means of preparing ODS coppers. One is powder metallurgy, in which a mixture of very fine powdered copper and oxides are compacted and sintered to form a solid metal. A more commonly used method nowadays is internal oxidation, which forms oxides of a reactive alloy constituent *in situ*. ODS coppers are commercially available in three grades: C15715, C15725, and C15760, with 0.3, 0.5, and 1.1 wt.% Al_2O_3, respectively. For instance, Glidcop® AL-15, a C15715 material, is a low-alumina content grade of DSC with 0.15 wt.% aluminum as Al_2O_3.[39] It is strengthened by an ultrafine dispersion of Al_2O_3 particles through *in situ* internal oxidation of the aluminum in a dilute solid solution copper–aluminum alloy powder. Along with superior strength retention, an ODS copper's thermal and electrical conductivities are higher than conventional copper alloys. Its electrical conductivity is rated at 92% IACS at 20°C.

1.2.4.2 Classifications of Electrodes

Electrode tips for resistance welding are made of copper alloys and other materials. The Resistance Welder Manufacturers' Association has classified electrode tips into two groups according to the chemical compositions of the materials[40]—Group A: copper-base alloys, and Group B: refractory metals. These groups are further classified according to the chemical compositions and performance characteristics of the materials.

Group A, made of copper alloys, is further divided into five classes (I, II, III, IV, and V) with Class I electrodes the closest in composition to pure copper. As the class number goes up, the hardness and annealing temperature increase, whereas the thermal and electrical conductivities decrease. In Group B, Classes 10, 11, 12, 13, and 14 are the refractory alloys, made of sintered mixtures of copper and tungsten, etc., designed for wear resistance and compressive strength at high temperatures. Refractory metals, including the tungsten–copper composites (Classes 10–12), are used in specialty applications in which the high heat, long weld time, inadequate cooling, and high pressure involved may cause rapid deterioration of DSC-base alloys (Group A).[38] The main metallurgical aspects of these classes of electrodes are presented in the following.

GROUP A: Copper-Base Alloys

Class 1. Cadmium–copper is suitable for welding aluminum and magnesium alloys, coated materials, and brass and bronze. It is not heat treatable. This alloy is superior to pure copper as an electrode material because of its high electrical conductivity and reasonable strength at elevated temperatures.

Class 2. Chromium–copper is suitable for welding cold- and hot-rolled steels, stainless steel, and low-conductive brasses and bronzes. It is heat treatable. It has good strength, and when hardened, has a conductivity of 80% that of pure copper. It is recommended for high-production operations. A special heat-treated alloy that meets the minimum electrical conductivity and hardness specifications of Class 2 alloy is Zr–Cr–Cu. It is suited to welding galvanized steel and other metallic-coated steel.

Class 3. Nickel–copper and beryllium–nickel–Copper are suitable for welding steels having high electrical resistance, such as stainless steels. They are heat treatable. These alloys have higher strength than the previous classes and, therefore, they are often used as electrode shanks and electrode holders.

Class 4. Beryllium–copper has lower conductivity than Class 3 alloys but has exceptional strength and hardness, in some cases approaching the levels attained in heat-treated steels. It is available in the annealed condition that is more readily machined and then heat treated. It is often used in the form of inserts, die facings, and seam welder bushings.

GROUP B: Refractory Metals

Class 10. Tungsten55%–copper45%, is recommended where (relatively) high electrical conductivity and some degree of malleability are desirable. It is suitable for facings and inserts for projection welding electrodes and flash and butt welding dies.

Class 11. Tungsten75%–copper25%, is harder than Class 10 alloys, and suited to similar applications as Class 10 for facing on electrode forming dies, and for projection welding electrodes.

Class 12. Tungsten80%–copper20%, is suitable for electro-forming and electro-forging die facings, and for electrode facings used as upset studs and rivets.

Class 13 (tungsten) and **Class 14** (molybdenum). These two classes of materials are used primarily for welding or electro-brazing nonferrous metals having relatively high electrical conductivities. They are suitable for cross-wire welding of copper and brass, and for welding copper wire braid to brass or bronze terminals. Special setups and procedures are required.

1.2.4.3 Copper Electrode and Coating/Sheet Interaction

The interaction between Cu electrodes and coating/sheets is a complicated process consisting of mechanical, electrical, and thermal, in addition to metallurgical factors. When Cu-base alloy electrodes are used for welding coated metals, certain metallurgical reactions may happen between Cu and the coating, and such interaction may significantly affect the welding process and electrode life. For instance, Cu may form a brittle low-melting intermetallic with Zn. The alloyed electrode surface has a lower electrical conductivity, and during welding, the temperature at the electrode–workpiece interface increases as a result. This may promote sticking of electrodes to the coated workpieces when welding galvanized steels. Such alloying may happen between Cu electrodes and a number of coating and substrate materials such as Ni, Sn, Al, and Mg. The alloying of electrode material with the coating/substrate is the primary reason for electrode deterioration. Examples illustrating the interaction between Cu electrodes and Zn-coated steels, and that between Cu and Al sheets are shown in the following.

GALVANIZED STEEL WELDING

In a study on the electrode wear mechanisms, Gugel et al.[41] systematically investigated the evolution of electrode face in terms of surface chemistry through secondary electron imaging and EDX analysis. The chemical change of the Cu–Cr electrode face clearly shows the severe interaction between the electrode and the Zn coating, as seen in Figure 1.24. The first weld already picked up substantial amount of zinc, and by 10 welds, zinc overtook Cu on the electrode surface. The concentration of zinc steadily increases to nearly 80 wt.% by 1000 welds, and the concentration of iron remains around 10%. Since the Cu–Zn alloy has higher electrical resistivity than Cu–Cr, a large amount of heat was generated at the electrode–sheet interface. This was evidenced by the substantial sticking. Similar trends were observed when welding using Cu–Zr electrodes (Figure 1.25), and a Glidcop AL60 grade DSC electrode (Figure 1.26). Although there are similarities among these three types of electrodes in reacting with the Zn coating, the DSC electrodes had shorter electrode life than the other two, possibly because the higher relative hardness of the DSC electrodes may hinder the plastic deformation of the Cu, and are unable to heal small surface imperfections.[42] It was also observed that oxides existed in the depressions on the electrode faces; the effect of which on electrode deterioration is not clear.

The interaction between Cu electrodes and Zn coating of the steel sheets is also affected by the Al content in the coating. Matsuda et al.[43] studied the effect of Al in the coating on electrode life by intentionally varying the Al content in the range from 0.22 to 0.87 wt.% in hot-dip galvanized steel sheets, and from 0.19 to 0.78 wt.% in the galvannealed steel sheets. They found that when the aluminum content in the coating is sufficiently high (more than 0.4 wt.%), a thin layer of intermetallic $Fe_2Al_{5-x}Zn_x$ is present at the interface between the coating and substrate in hot-dip galvanized steel sheets. This layer inhibits Fe diffusion into the coating, and a low Fe content in the coating makes the coating low in melting temperature with high Zn concentration, promotes the Cu–Zn alloying, and accelerates electrode wear. On the other hand, there is no such intermetallic layer between the coating and substrate in galvannealed steel sheets, possibly resulting from the post-heating process of galvannealing. The aluminum content in the coating, therefore, has no effect on electrode

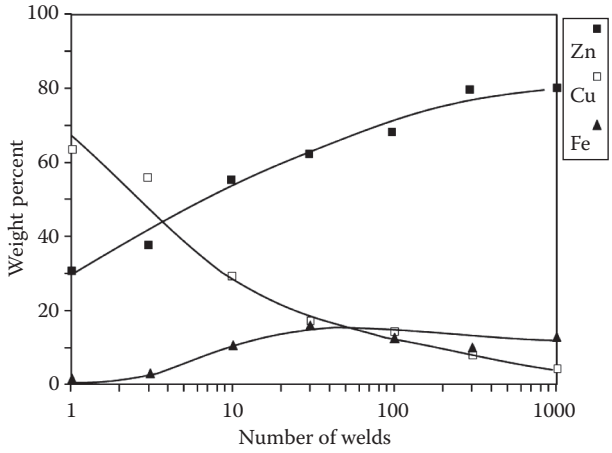

FIGURE 1.24
Evolution of element concentrations on Cu–Cr electrode face. (From Gugel, M.D. et al., Progression of electrode wear during RSW of EG steel, SMWC V, Paper A4, 1992. With permission.)

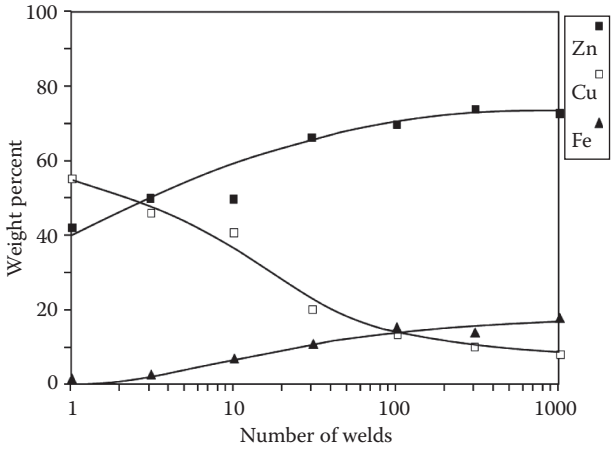

FIGURE 1.25
Evolution of element concentrations on Cu–Zr electrode face. (From Gugel, M.D. et al., Progression of electrode wear during RSW of EG steel, SMWC V, Paper A4, 1992. With permission.)

life in this welding material. The coating of galvannealed steel has a high concentration of the Fe–Zn intermetallic compounds formed during galvannealing, which have higher melting temperatures and hardness than mostly free Zn in the hot-dip galvanized steel coating. Therefore, in general, the electrode life is significantly longer when welding galvannealed steels than welding galvanized steels.

As revealed by Matsuda et al.,[43] the amount of free Zn in the coating directly affects the reaction between the electrode and the coating. Figure 1.27 shows the differences in geometry and composition of the depressions on the electrode faces. In the two types of galvannealed steels with different Al contents in the coating, there is a significant amount of Fe in the material picked up by the electrodes from the coatings, which largely consist of Fe–Zn

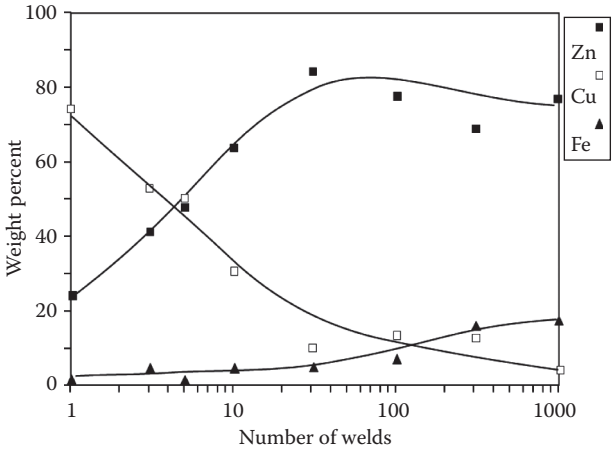

FIGURE 1.26
Evolution of element concentrations on DSC electrode face. (From Gugel, M.D. et al., Progression of electrode wear during RSW of EG steel, SMWC V, Paper A4, 1992. With permission.)

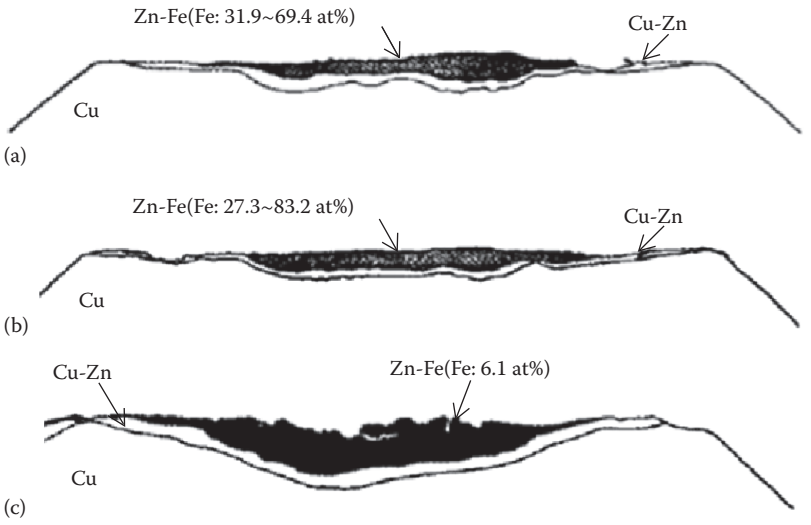

FIGURE 1.27
Cross-sectional structures of electrode tip faces after 1500 welds on galvannealed (GA) and hot-dip galvanized (HDG) steels.[43] (a) GA-2 (Al: 0.78 mass%); (b) GA-6 (Al: 0.23 mass%); (c) HDG-6 (Al: 0.22 mass%).

intermetallic compounds. Al content has no impact on the depression on the electrodes. The electrode used for welding hot-dip galvanized steel, however, has a much deeper depression on the surface, filled with metals picked from the coating of mostly free zinc.

The low-melting intermetallic formed between Cu and Zn on the surface of a galvanized steel may attack the grain boundaries and create cracks. This effect is called liquid metal embrittlement (LME) cracking, and it has significant impact on the integrity of certain Zn-coated steels. More detail can be found in Section 1.4. When the alloying process completely covers the contacting electrode tip surface, weld quality degradation slows down considerably but still continues because mechanical wear creates newly exposed copper surfaces. Thus, pre-seasoning (conditioning) the electrodes is necessary not for prolonged electrode life, but for stabilization of the welding process.[44]

AL WELDING

A study on the effects of sheet surface conditions on electrode life revealed that electrode wear is the result of localized heating at the interface, which creates the condition for metallurgical reaction between the elements in the electrode and sheet/surface.[45] 5A02 aluminum sheets (2 mm in thickness), and a number of surface condition and welding schedule combinations were used in the study.

The effects of electrode force and welding time on electrode alloying are clearly seen in Figure 1.28. The line scanning of the chemical composition along the center of an electrode shows the percentage of Cu, Al, and Mg at each location on a line through the electrode center. When the electrode force is small (4.5 kN), long welding time (180 ms) generates more heat at the electrode–sheet interface and, therefore, a larger amount of alloying with Al and Mg (Figure 1.28b) than shorter welding time (Figure 1.28a). The effect of welding time is similar when electrode force is higher (9.0 kN, as in Figure 1.28c and d), but the severity of alloying is significantly lessened with high electrode force, as can be seen by comparing Figure 1.28a with 1.28c and Figure 1.28b with 1.28d. This is because a large

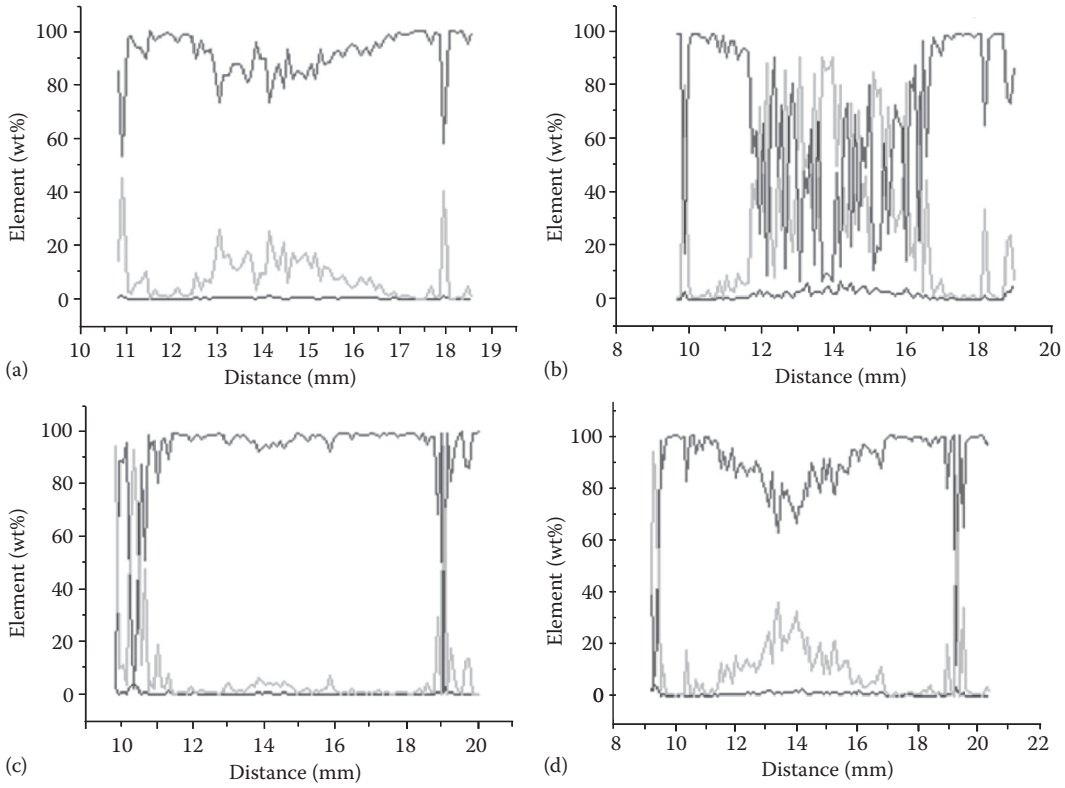

FIGURE 1.28
(See color insert.) Composition profiles of electrode surfaces after 60 welds using schedules of (a) $F = 4.5$ kN, $\tau = 60$ ms; (b) $F = 4.5$ kN, $\tau = 180$ ms; (c) $F = 9.0$ kN, $\tau = 60$ ms; and (d) $F = 9.0$ kN, $\tau = 180$ ms. Red line is for Cu, green is for Al, and blue is for Mg.

electrode force results in a low contact resistance and, therefore, less heat generation and alloying at the electrode–sheet interface.

1.3 Embrittlement of Weldment

Embrittlement of metals refers to the loss of ductility resulting from metallurgical reactions or other processes. In general, its occurrence in certain material systems requires specific conditions. There are several types of embrittlement in metals and the most common ones are described below:

1. Liquid metal embrittlement. It is also known as liquid metal-assisted cracking, or liquid metal-induced cracking. Deep liquid grooves may form at the grain boundaries when a specific liquid metal is in contact with a polycrystalline solid in certain material systems. The most common LME-causing material is mercury (melting point –38.8°C), which is liquid at room temperature. It presents a significant danger for airplanes as the aircraft material Al–Zn–Mg–Cu alloy DTD 5050B

is especially susceptible to LME by Hg.[46] Another commonly cited example is the Al–Ga system in which liquid Ga quickly penetrates into grain boundaries in Al, leading to intergranular fracture even under very small stresses. As elevated temperature is needed in order for most metals to melt, LME generally occurs only above a certain temperature. A tensile stress is usually needed for LME to occur, which is readily available in most metals, and only modest levels of stresses are needed to break a polycrystalline structure in which the grains are only "glued" by the liquid metal. Such stresses may come from externally applied loading, or from residual stresses created during fabrication of the material such as cold working. Although this phenomenon is relatively common, the mechanisms of LME are not well understood.

2. Hydrogen embrittlement (HE). The presence of atomic hydrogen within the crystal lattice structure of a metal may significantly impair its mechanical strength, and may result in failure under a tensile loading. Hydrogen can be introduced into a metal at various stages such as in service or during material processing. Common causes of HE are pickling, electroplating, and welding. However, HE is not limited to these processes. High-strength steels, such as quenched and tempered steels or precipitation-hardened steels, are particularly susceptible to HE. The susceptibility to HE of steels is directly related to their strength. Steels with a tensile strength in the order of 1000 MPa or higher are generally subject to HE, whereas it is usually not a concern for steels of lower strength. Currently, the majority of hot-dip galvanized steels are generally in the range of 200–450 MPa and they are generally not so susceptible to HE. It can be avoided if necessary precautions are taken, for instance, using mechanical cleaning instead of acid pickling for preparing the surfaces before hot-dip galvanization of high-strength steels.
3. Strain age embrittlement. Strain aging is associated with the strains resulting from plastic deformation, usually generated from cold working. The residual stresses that resulted from plastic deformation are the driving force for the changes in structures and properties of metals. In steels, carbon atoms in the iron crystals tend to move to dislocations under the residual stress field produced by plastic deformation. The resultant high concentration of carbon atoms at dislocations impedes their mobility and, therefore, a reduction in ductility results in the steel. Because it depends on diffusion of carbon atoms, strain aging is a strong function of temperature, in addition to stress level.
4. Intermetallic-compound embrittlement. Formation of brittle intermetallic compounds, usually at the grain boundaries of a crystalline solid, may lower the strength and ductility of the material. Such intermetallic compounds may form during fabrication or during service, either due to segregation of alloying elements to grain boundaries, or diffusion of the elements from coating or environment. For instance, an improperly controlled casting process may create a brittle grain boundary network resulting from segregation of alloying elements. A long exposure of galvanized steel to temperature slightly below the melting point of zinc (420°C) causes zinc diffusion into the steel, resulting in the formation of a brittle iron–zinc intermetallic compound in the grain boundaries. For the same reason, it is difficult to weld Al directly to steels.

All of these four types of embrittlement may occur during resistance welding. For instance, if the surface of a steel sheet is not properly cleaned, hydrogen from decomposition of grease or surface treatment agents at the faying interface may be trapped in the molten

nugget and cause HE. A large sheet distortion/separation is an indication of large residual stresses, which may embrittle the weldment through strain aging. Certain confinement of sheets during welding, such as applying additional constraints to prevent cracking as discussed in Chapter 3, can effectively reduce the distortion and, therefore, the risk of strain age embrittlement. In general, these two types of embrittlement can be avoided if proper precaution is taken. On the other hand, it could be difficult to avoid LME and intermetallic-compound embrittlement in certain material systems as they are more material related than process related. Many structural alloys can be embrittled by low-melting-point metals. For instance, aluminum is embrittled by mercury, indium, tin, and zinc; steel by tin, cadmium, zinc, lead, copper, and lithium; stainless steels by cadmium, aluminum, lead, and copper; titanium by cadmium and mercury; and nickel by zinc, cadmium, and mercury.[47] Significant efforts have been made in understanding the mechanisms of LME. Brittle intermetallic compounds may form during welding, especially in the HAZ where stress concentration often occurs and fracture initiates. HE can be avoided if proper precaution is taken, and it is not common in resistance spot welds except under certain special conditions, such as when the welded structure is subject to corrosive environment with hydrogen charging. As the strain age embrittlement involves complex interaction between the deformation process and material structure and composition, it is case dependent and difficult to be singled out. The other three types of embrittlement are discussed in more detail in this section.

1.3.1 Liquid Metal Embrittlement

LME is basically a metallurgical process. The tendency and severity of LME strongly depend on the material systems. LME is significantly affected by alloying of the solid metals: some alloying elements may increase the severity, whereas others prevent LME. The alloying elements affect segregation to grain boundaries of the metal and, therefore, alter the grain boundary properties. Maximum LME is observed in cases where alloying elements have saturated the grain boundaries of the solid metal.[48] It is a strong function of the mutual solubility of a solid–liquid metal combination.[49] Excessive solubility makes sharp crack propagation difficult, yet zero solubility prevents wetting of the solid surfaces by the liquid metal and, therefore, prevents LME. Presence of an oxide layer on the solid metal surface also prevents good contact between the two metals and deters LME. Figure 1.29 shows the effects of solute elements on mechanical strength of a polycrystalline Al. Addition of third elements to the liquid metal may increase or decrease the embrittlement and also alters the temperature region over which embrittlement occurs. Metal combinations that form intermetallic compounds do not cause LME. The susceptibility to LME of a solid metal is also affected by its hardness and grain size. Harder metals are more severely embrittled, and solids with larger grains are more susceptible. The microstructure of LME cracks is shown in Figure 1.30.[50] The grains are separated along grain boundaries, that is, it is an intergranular fracture.

A complete review of LME mechanisms can be found from a huge amount of literature in the public domain on this subject, such as the work by Joseph[48] and Glickman,[51] and some of the theories are listed here[46]:

1. The dissolution–diffusion model[52,53]: Adsorption of the liquid metal on the solid metal induces dissolution and inward diffusion, leading to crack nucleation and propagation.
2. The brittle fracture theory[54,55]: Adsorption of the liquid metal atoms at the crack tip weakens inter-atomic bonds and promotes cracking.

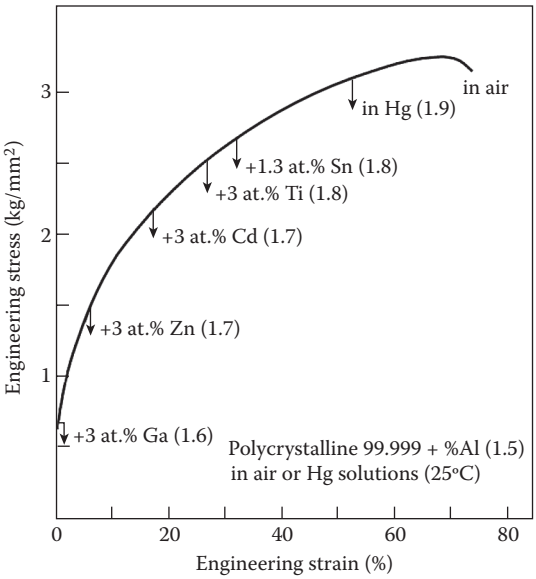

FIGURE 1.29
Polycrystalline pure Al embrittled by various Hg solutions. Electronegativities of solute elements are listed in parentheses. (From Westwood, A.R.C. et al., in Liebowitz, H. (ed.) *Fracture: An Advanced Treatise*, Academic Press, New York, 589–644, 1971. With permission.)

3. The diffusion–penetration model[56]: Crack nucleation and propagation are promoted through a diffusion–penetration process of liquid metal atoms into the grain boundaries.
4. The ductile failure model[57]: Nucleation and migration of dislocations under stress are promoted by adsorption of the liquid metal that weakens the atomic bonds. The dislocations pile up and work-harden the solid. In addition, such dissolution may also help the nucleation of voids that grow under stress and cause ductile failure.

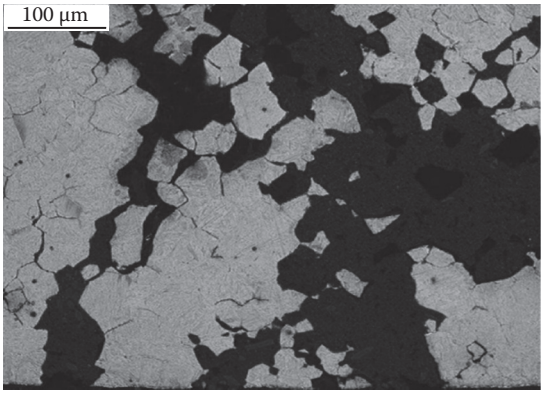

FIGURE 1.30
Microstructure of an LME fracture. (From AET_Service_Capability.pdf. Available online at http://www.aet-int.com/capability/AET_Service_Capability.pdf. Accessed in Nov. 2010. With permission.)

All of these theories are based on the fundamental assumption that the adsorption of liquid metal lowers the surface energy of the solid metal, which leads to LME. This mechanism of LEM can be easily understood through fracture mechanics consideration. The strength of a material to resist cracking is associated with the energy needed to create new surfaces, or the surface energy density, γ_s. Or, if such strength is expressed in terms of fracture stress, σ_f[58]

$$\sigma_f = \sqrt{\frac{2Ew_f}{\pi a}} \tag{1.9}$$

where E is Young's modulus and a represents the crack length. w_f is a unified fracture energy that could include elastic, plastic, viscoelastic, and other effects. During an LME, the adsorption of liquid at the crack tip (usually along a grain boundary) reduces w_f and, therefore, σ_f. Efforts have been spent on characterizing the dependence of w_f on alloying elements of a solid, solution composition, temperature stress, etc. Because of the large number of factors involved and the difficulties in measuring w_f, limited qualitative, and not quantitative, data have been obtained on certain material systems.

LME could occur in two separate but related processes that may have impact on the quality of a resistance spot weld. One is associated with hot-dip galvanizing, which is one of the most efficient ways of providing durable corrosion protection for steel components. When hot-dip galvanizing steel, the molten zinc interacts with the steel, and a layered coating is formed consisting of zinc–iron intermetallics as reaction products, covered by a layer of solid zinc, as shown in Figure 1.31. The coating thickness is normally in the order of 100 μm. During a galvanizing process, the free zinc (often with other additives) in its liquid state may attack the grain boundaries of the sheets, resulting in cracking and rendering the sheets unusable. In general, cracking in galvanized steel structures may occur at various stages of fabrication. For certain steels, especially some stainless steels or heavily cold-worked products such as rolled sheets, the condition for LME may exist when they are galvanized, that is, when they are in contact with molten zinc. For instance, a steel structure used in a sign bridge that spans the freeway and carries informational sign boards consisted of a triangulated space frame fabricated from four long parallel

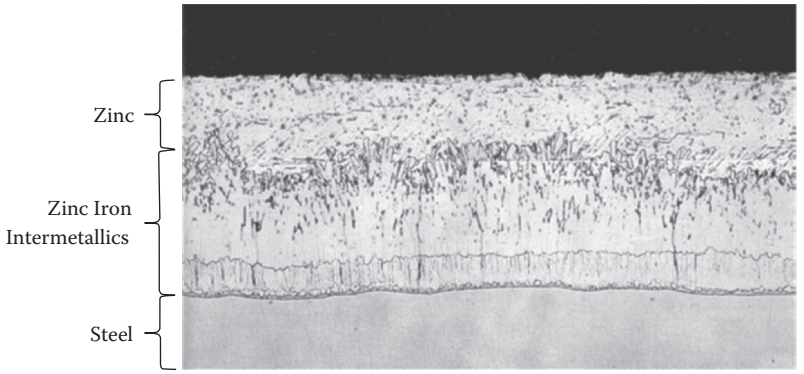

FIGURE 1.31
Microstructure of a galvanizing layer. (From Kinstler, T.J., Current knowledge of the cracking of steels during galvanizing—A synthesis of the available technical literature and collective experience for the American Institute of Steel Construction, GalvaScience LLC. Available online at http://www.aisc.org/uploadedFiles/Research/Files/Final5906.pdf. Accessed in Nov. 2010. With permission.)

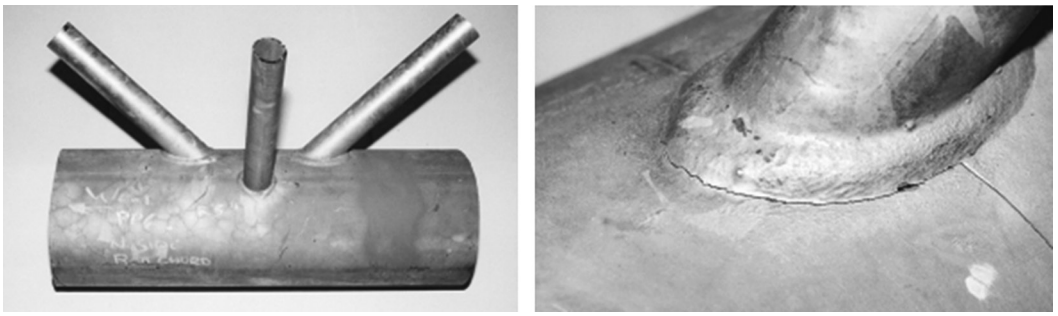

FIGURE 1.32
Cut-out section of cracked area on a sign bridge (left), and cracks at weld joining a diagonal tube to the chord (right). Note crack growth into chord at right. (From Website of Metallurgical Associates, Inc., http://www.metassoc.com/pdf/MAI_Minutes-6_04.pdf. Accessed in Nov. 2010. With permission.)

large diameter tubes, called chords, cross braced by smaller diameter perpendicular and diagonal tubes. After welding, the structure was hot-dip galvanized by submerging it in a bath of molten zinc to provide corrosion protection. While the welding was appropriately performed, cracking appeared after the structure was galvanized, as seen in Figure 1.32.[59] Metallurgical examination revealed that there was no sign of hot cracking, a defect associated with improper welding process, and all the cracks, near the weld or away from it, were filled with zinc. When galvanized steels are used in fabrication involving elevated temperature operation, LME may occur as well. Figure 1.33 shows a crack in a welded structure using galvanized steels, which initiates at the termination of the weld (in the HAZ) and propagates into the base metal.[60]

LME may happen during RSW. As shown in Figure 1.34, LME cracking is apparent near the surface of an HSLA steel weld that is in contact with the Cu electrode during welding.[50] The electron dispersive spectroscopy maps of elements clearly show that the cracks are filled with Cu and Zn (Figure 1.34b and c), which means that Zn in the coating and Cu

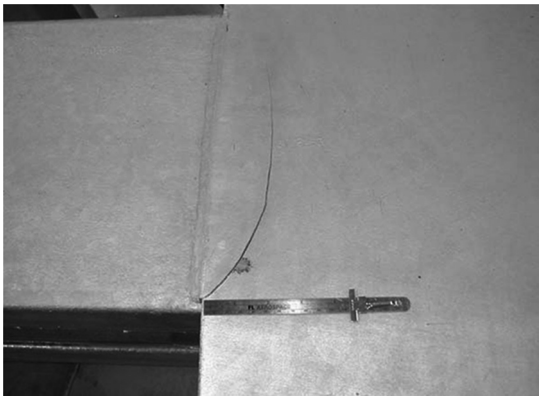

FIGURE 1.33
Crack at weld termination. (From Kinstler, T.J., Current knowledge of the cracking of steels during galvanizing—A synthesis of the available technical literature and collective experience for the American Institute of Steel Construction, GalvaScience LLC. Available online at http://www.aisc.org/uploadedFiles/Research/Files/Final5906.pdf. Accessed in Nov. 2010. With permission.)

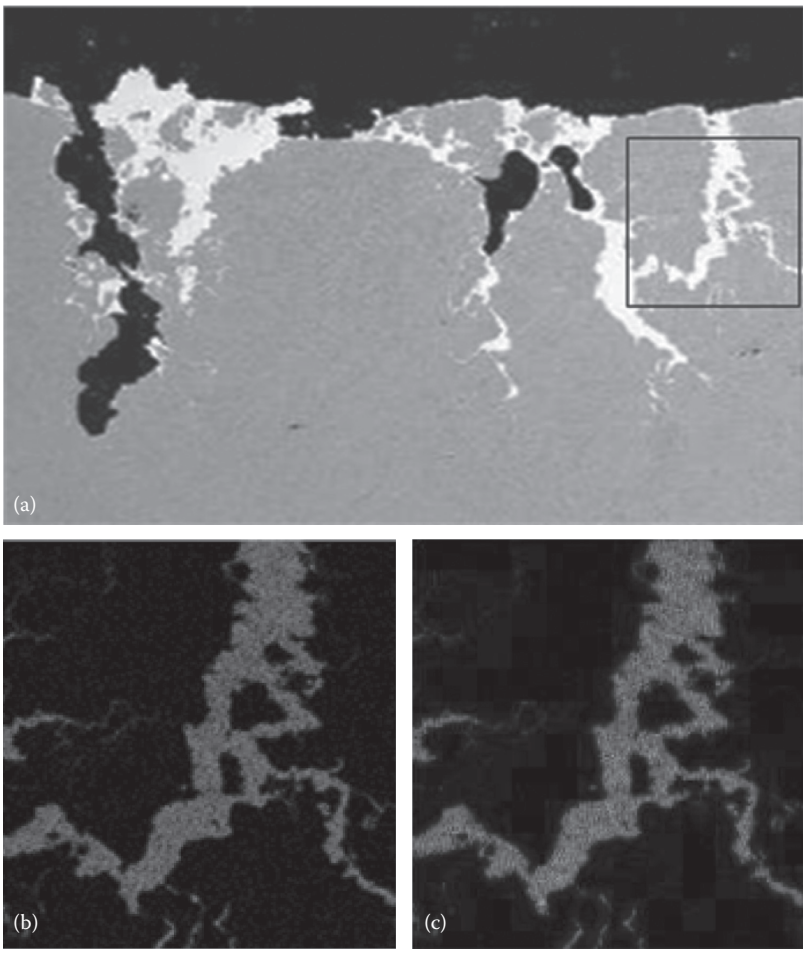

FIGURE 1.34
(See color insert.) Liquid metal embrittlement cracking in a Zn-coated HSLA steel spot weldment (a), and x-ray maps of Cu (b) and Zn (c) of area outlined in (a). (From AET_Service_Capability.pdf. Available online at http://www.aet-int.com/capability/AET_Service_Capability.pdf. Accessed in Nov. 2010. With permission.)

in the electrode were in liquid state during welding, possibly due to an improper welding schedule. LME-related cracking in RSW is further discussed in Section 3.1.1 of Chapter 3.

1.3.2 Hydrogen Embrittlement

Atomic hydrogen has to be introduced to the steel structure for HE to occur. Because only some of the steels are susceptible to it in service under certain conditions, there is very little research on HE in the context of RSW. Interstitial-free (IF) steels have been used in a number of studies on HE in RSW, because the high diffusivity and permeability of hydrogen in their ferritic microstructures make IF steels susceptible to HE. IF steels are commonly used in automobile body-in-white construction because of their good formability. In the work of Mukhopadhyay et al.,[62] the effect of HE was investigated on an IF steel of a tensile strength of 295 MPa, and interesting results were obtained. In their study, the RSW joints were submerged in an aqueous solution of 3.5% sodium chloride and

loaded quasistatically under *in situ* cathodic hydrogen charging in the solution. The effect of hydrogen charging on mechanical strength was measured.

There is a complex interaction between process variables in affecting the behavior of a spot weldment charged with hydrogen. The susceptibility of an IF steel to hydrogen is shown in Figure 1.35. The effect of HE is measured by the failure load, or load bearing capacity (LBC), and by the maximum displacement, or extension up to maximum loading (EML) of a weldment when tensile tested. The variables are hydrogen charging and pre-straining, and LBC and EML are used as responses. The specimens were either as-received or pre-strained in a certain range, and they were tested either with (submerged in a solution) or without (in air) hydrogen charging.

The hydrogen charging has a negligible effect on the spot weldments made on as-received sheets on the failure load, and it slightly increases the ductility, which is possibly statistically insignificant. Therefore, it can be concluded that HE has no effect on the performance of welds made on unstretched IF steel sheets. When the sheets are pre-strained, however, hydrogen charging clearly weakens the welds made on such sheets, and the weakening severs with the amount of pre-strain. In general, the trend in both peak (failure) load and ductility (or EML) is consistent with what has been observed in metallic materials, that is, cold work strengthens a metal but makes it less ductile. However, the level of influence of pre-straining is clearly different with and without HE. The increase of failure load with pre-straining level is clear in specimens tested in air, and at a very moderate level with hydrogen charging. The loss of ductility is more significant in hydrogen-charged specimens than in those tested in air. This is consistent with the findings of other researchers.[63] The effect of HE requires a critical level of hydrogen in the lattice. It is believed that cold work or plastic deformation helps hydrogen entrapment in the steel by generating dislocations and vacancies in the lattice that serve as the sites for trapping hydrogen atoms.

The pre-straining was found to affect the properties of the base metal, not the weld including the HAZ. The melting and solidification in a weld nugget, and recrystallization in the HAZ essentially erase the work hardening induced by cold work. As a result, the hardness of the HAZ was found by the researchers[62] to be unaltered by pre-straining. The hardness decreases from the base metal toward the HAZ in a pre-strained specimen, and the damage caused by hydrogen charging is limited in the base metal, up to its border

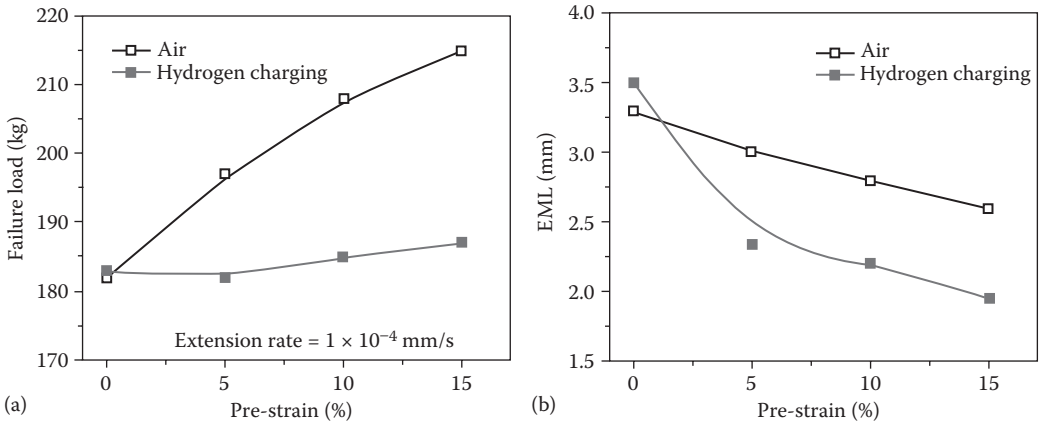

FIGURE 1.35
Peak load (a) and ductility (b) as a function of pre-strain level tested on spot welds with and without hydrogen charging. (From Mukhopadhyay, G. et al., *Mater. Corros.*, 61(5), 398–406, 2010. With permission.)

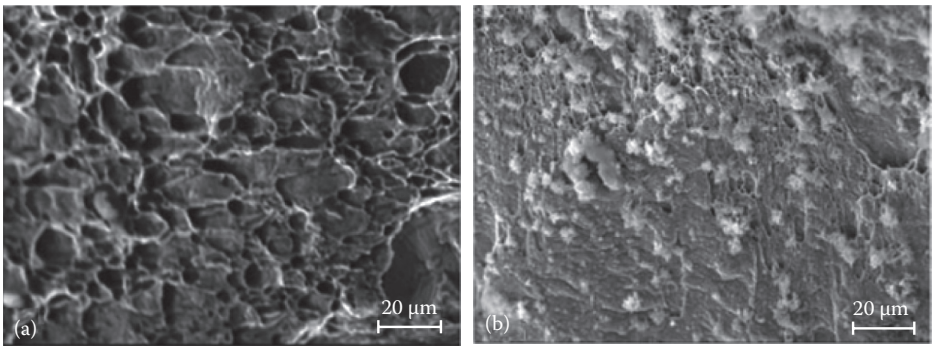

FIGURE 1.36
Fracture surfaces of specimens tested without (a) and with (b) hydrogen charging. (From Mukhopadhyay, G. et al., *Mater. Corros.*, 61(5), 398–406, 2010. With permission.)

with the HAZ. It is common to observe that fracture of a weldment starts from its HAZ, due to the stress concentration associated with its geometric location in the weld and the change of material properties in the region. The fluctuation in material properties was found to increase with the level of pre-straining and, therefore, large pre-straining generates a sharp change in mechanical strength. The fracture of the weld specimens was found to initiate in the region of the HAZ–base metal junctures, and the fracture surfaces clearly illustrate the effect of HE as shown in Figure 1.36. The specimen without hydrogen charging in Figure 1.36a has dimples on the fracture surface, whereas the one tested after immersion is fairly smooth, with small voids and certain corrosion products (Figure 1.36b).

1.3.3 Intermetallic-Compound Embrittlement

Most of the intermetallic compounds formed in structural materials are hard and brittle compared with their constituent metals, with the exception of several rare earth intermetallic compounds that are ductile at room temperature, discovered by researchers at the U.S. Department of Energy's Ames Laboratory at Iowa State University.[64] In controlled material fabrication processes, hard and brittle compounds may be used to strengthen the material, such as in dispersion–strengthening processes. In a study, particles of intermetallic-compounds Al_3Ni, Al_3Ti, Al_3Zr, Al_7Cr, and $Al_{12}Mo$ were produced by reactions when these metal powders were added to molten aluminum, and reinforced aluminum matrix composites were created as a result.[65]

Intermetallic compounds often deteriorate materials in unintended ways. In a study on casting AA6082 aluminum alloy, it was found that cracks initiate at the interface between the intermetallic β-Al_5FeSi or α-Al(FeMn)Si particles and the matrix through nucleation of voids.[66] Although such particles are generated during fabrication and mostly intended to strengthen the material, large hard and brittle intermetallic particles may break under loading, as shown in Figure 1.37, and they reduce the overall ductility of the alloy. Materials containing intermetallic compounds, intentionally and unintentionally created, may be affected in the following ways:

1. Brittle fracture of the compounds
2. Debonding at the interface
3. Loss of strength with low melting compounds

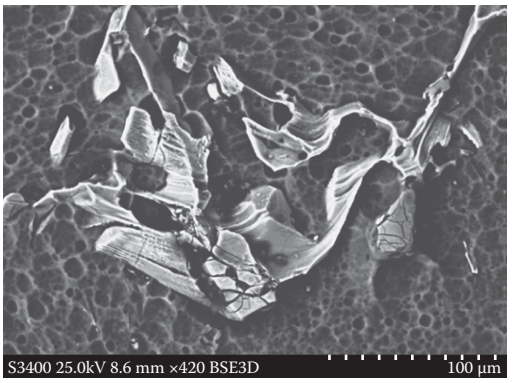

FIGURE 1.37
Broken particles at fracture surface in AA6082 alloy. (From Mrówka-Nowotnik, G., *J. Achievements Mater. Manuf. Eng.*, 30(1), 35–42, September 2008. With permission.)

In many cases, intermetallic compounds are unintentionally created and their shape, size, and distribution are not controlled. In Figure 1.38, the $Al_{12}Mg_{17}$ precipitates at the grain boundaries of a magnesium alloy AZ80 serving as the sites of stress concentration when the material is loaded. In addition, the coarse intermetallic compound particles embrittle the metal by fracture in the compounds, and debonding the interface between the compound particles and the matrix. As a result, the toughness of the material is adversely affected. There are numerous examples of such embrittlement in the literature. In Al–Cu joints for electric connection, intermetallic compounds Al_x–Cu_y can form after a certain period of service because of electric resistance heating, as shown in Figure 1.39.[67] A similar phenomenon may be observed in welding aluminum alloys using Cu electrodes. These intermetallics raise the electrical contact resistance between the electrode and sheet and promote localized heating at the interface. They tend to break off from the electrode and affect the integrity of the electrode face, and result in rapid electrode deterioration. On the other hand, such hard and brittle intermetallic compounds can be utilized to slow down the electrode deterioration process in the case of welding Zn-coated steel sheets, in which a layer of Cu–Zn intermetallic is formed after a number of welds (usually between

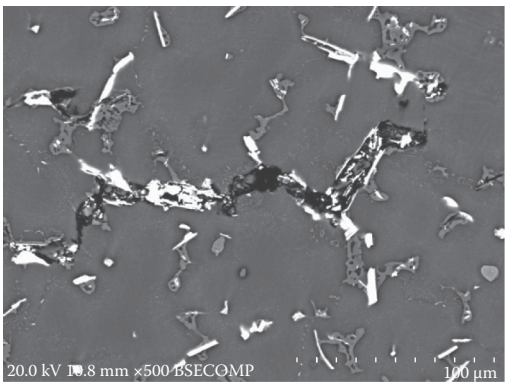

FIGURE 1.38
Precipitation of $Al_{12}Mg_{17}$ at grain boundaries of an AZ80 alloy. (Courtesy of B. Wang and J. Wang.)

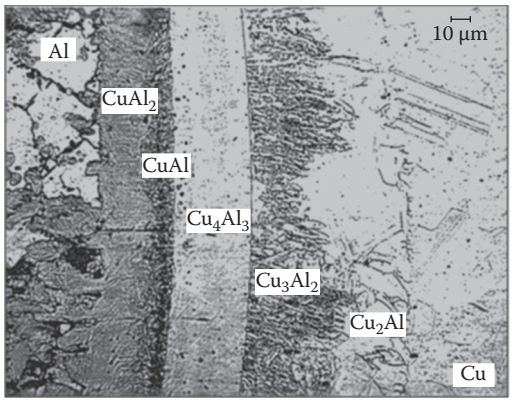

FIGURE 1.39
Various intermetallic compounds formed at an Al–Cu joint. (From Slade, P.G. (ed.), *Electrical Contacts: Principles and Applications*, Marcel Dekker, Inc., New York, 1999. With permission.)

20 and 50) are made using new electrodes. This is called pre-seasoning, or conditioning of electrodes. Welding schedules for production should be selected based on pre-seasoned/conditioned, not new electrodes.

Many of the intermetallic compounds have low melting temperature, and they may melt before the rest of the structure. This may have a serious implication in welding, especially when the volume of the compounds is large and their particles are interconnected in a structure. During RSW, the HAZ is usually heated to a temperature, although not high enough to melt the material, sufficient to melt certain low-melting intermetallic compounds such as eutectics in it. When the HAZ is stretched during welding, the liquid phase effectively provides no resistance to fracture. Even discretely distributed low-melting particles may weaken the structure as the molten volume of a precipitate may act as a crack or pore under loading. Fracture associated with the low-melting phases during welding, or liquation cracking, is presented in Section 1.4. In addition to the embrittlement such intermetallic compounds bring to the weldment during heating/cooling, a connected

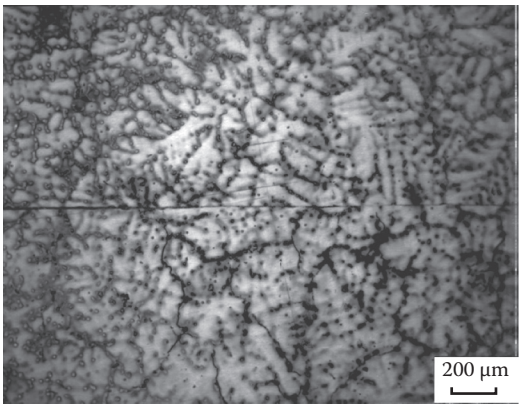

FIGURE 1.40
Microstructure of partial melting zone of AZ91D weld. (From Munitz, A. et al., Resistance spot welding of Mg–AM50 and Mg–AZ91D alloys. Magnesium Technology, TMS [The Minerals, Metals & Materials Society], 2002. With permission.)

liquid network in the HAZ also provides a pathway for the molten metal in the nugget to eject from the nugget to the faying interface. Such an expulsion phenomenon has been observed in Al and Mg welding and is discussed in Chapter 7.

In a study by Munitz et al.,[30] it was observed that in AZ91D sheets, a large amount of intermetallic β phase ($Al_{12}Mg_{17}$) exists in the form of a network at grain boundaries, in the partial melting zone of a spot weldment (Figure 1.40). In three-dimensions, the β phase forms a continuous "foam" made of grain boundaries. A portion of this network adjacent to a weld nugget during RSW may stay as liquid for a significant proportion of the welding time, which embrittles the material, as the melting temperature of the eutectic is only 437°C, far below that of Mg matrix (650°C for pure Mg).

1.4 Cracking

Cracking in RSW occurs in a similar manner as in other fusion welding processes. A weldment expands under Joule heating, and at the same time, it is distorted due to electrode squeezing and confinement from the surrounding metals. Such a distortion is irreversible and the weldment undergoes a restrained contraction during cooling. It induces tensile stresses in the joint that are directly responsible for cracking. Cracking may occur at all locations of a weldment: the nugget, HAZ, and parent metal. If it occurs during solidification of the liquid nugget, it is called *solidification cracking* or *hot cracking*. The tensile stresses may also induce cracking in the solid phases, that is, the HAZ or even the parent metal. Fracturing the low-melting components in the HAZ due to liquation is called *liquation cracking*, and cracking the weld or HAZ in high-carbon steels at low temperatures (below solidus temperatures) or even after welding is called *cold cracking*. In general, cracking requires two concurrent conditions: a weakened structure, such as one embrittled due to melting of low-melting eutectics or corrosion, and a tensile stress field. This section discusses the metallurgical aspect of cracking. Examples of cracking and its suppression can be found in Chapter 3.

1.4.1 Solidification Cracking

The stress level on the just solidified nugget, together with the mechanical strength of the material at elevated temperatures, determines the occurrence of solidification cracking. The stresses induced by the restrained contraction are proportional to the cooling, and they are released if the material is plastically deformed under such stresses. Cracking occurs when the material is relatively weak, yet the stresses reach a certain level, usually in the *brittle temperature range*. It is between the temperature at which ductility sharply drops and the liquidus temperature.

Figure 1.41 shows that the ductility of AA5754 increases rapidly right after the solidus temperature is reached during cooling, whereas the ultimate strength grows at a slower pace. In the figure, the solidus temperatures for two AA5754 alloys with 2.6 and 3.6 wt.% Mg, respectively, are also plotted. The brittle temperature range can be in this case approximated by the difference between solidus and liquidus temperatures. By comparing the liquidus and solidus in Figure 1.14, it can be seen that the brittle temperature range for the alloy with 3.6 wt.% Mg is larger than that for the alloy with 2.6 wt.% Mg. Therefore, a high concentration of Mg in AA5754 makes it more prone to cracking. Therefore, solidification

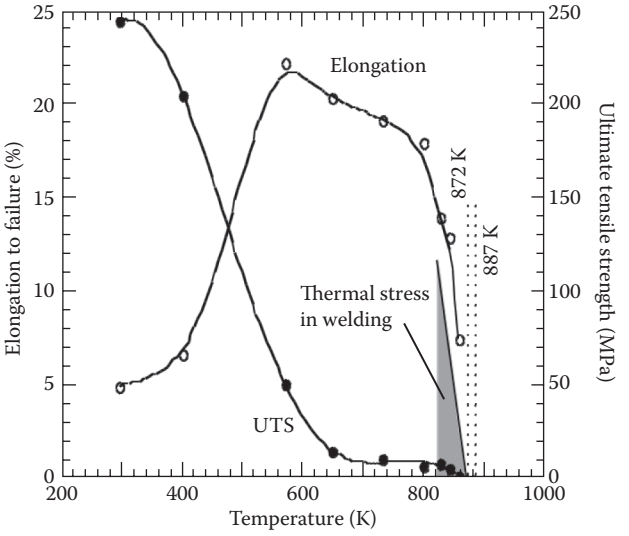

FIGURE 1.41
Dependence of ductility (elongation) and UTS on temperature. Dashed lines mark the solidus temperatures (887 and 872 K) for AA5754, with Mg content ranging from 2.6 to 3.6 wt.%. (From Zhang, H. et al., *Trans. ASME—J. Manuf. Sci. Eng.*, 124, 79, 2002. With permission.)

cracking of aluminum alloys is associated with the intentionally added alloying elements, and the presence of low-melting impurities.

Another type of cracking in the nuggets that is closely related to solidification is associated with the shrinkage of a nugget. The volume deficit created in a nugget by large expansion and deformation during heating under the electrode force, and by restrained contraction, may not be made up during cooling. Therefore, the last part of the nugget to solidify has an insufficient amount of liquid to form a coherence. Free solidification occurs as a result. A crack formed by this mechanism has a clear trace of free solidification on the crack surfaces, in the form of visible columnar or equiaxed grains. Higher strength heat-treatable aluminum alloys are prone to solidification cracking. Examples of solidification cracking in a weld are shown in Figures 1.2 and 1.3. Solidification cracking was also observed by Ma et al.[9] during welding of a DP600 steel, as seen in Figure 1.42. In addition to cracking, voids are also visible in the nugget, possibly formed because of expulsion as seen from the metal remnants on both sides of the weld at the interfaces.

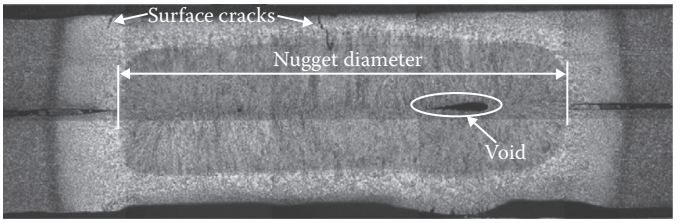

FIGURE 1.42
Microstructure of a DP600 steel weld. (From Ma, C. et al., *Mater. Sci. Eng. A*, 485, 334–346, 2008. With permission.)

1.4.2 Liquation Cracking

At certain moments during welding, the temperature at certain locations in a weldment may be lower than the solidus of the alloy, but higher than the melting temperatures of some low-melting components, such as eutectics or impurities. This may happen both at the HAZ near the nugget and in the solidified part of a nugget after it has cooled from the peak temperature. As such, components are usually solvent rich; they tend to have a higher concentration at grain boundaries than in the grains due to segregation. Therefore, continuous intergranular liquid films may present at elevated temperatures, and they have no strength to resist thermal stresses. As a result, cracking may occur. Cracks formed due to liquation have a clear intergranular characteristic. The amount of low-melting eutectics, such as sulfur and phosphorus eutectics in steel and Al–Mg eutectics in aluminum and magnesium alloys, depends on the solubility of the element at the eutectic's melting point. Only the excess of these elements over their solubility limits forms the respective eutectics and contributes to liquation cracking. Therefore, it is important to know the type, amount, and solubility of elements, as well as the melting temperatures of their eutectics, in order to determine the possibility of liquation cracking.

Cracking during welding and solidification cracking during casting have similar characteristics, and the knowledge of cracking in casting is helpful for understanding the cracking formation in welding. According to the classical works by Pellini and Flemings, hot tearing in casting alloys occurs at the last stage of crystallization, during which solid grains are surrounded by the liquid; such a structure has very low strength. Tensile stresses and strains, resulting from nonuniform temperature distribution and cooling, may cause material failure. Hot cracking tendency in casting increases with grain size, solidus–liquidus gap, and solidification shrinkage, which is especially high for Al as well as Mg alloys. The presence of impurities and grain boundary segregation also promotes cracking. The mechanism of hot cracking in welding, similar to that in casting, can be understood from the theory developed by Borland and Prokhorov. The occurrence of cracking in the coherence temperature range (Borland's definition) depends on both critical strain and critical strain rate. Comparisons of various Al alloys in casting and arc welding revealed that the Al–Mg system is second to the Al–Cu system in crack susceptibility among aluminum alloys, in spite of only a small amount of eutectics formed during solidification.

1.4.3 Corrosion Cracking

The spot-welded structures are usually protected against corrosion before they are put into service. Therefore, the corrosion resistance of spot welds is usually not an issue, and corrosion cracking of spot welds is rarely investigated. However, improper manufacturing and usage may expose resistance welds to corrosive environment. For instance, welding of zinc-coated steel sheets destroys the protective coating and exposes the indented weld area. Residual stresses along the periphery of the indentation marks may promote cracking if the weld surface is not properly protected. A study by Mukhopadhyay et al.[62] has found that the strength and ductility of an IF steel weld are reduced if the weldments are hydrogen charged and pre-strained, as discussed in Section 1.3.2, through a mechanism called hydrogen embrittlement. In the experiment, the welded specimens were cathodically charged with hydrogen for certain days in a 3.5% sodium chloride solution. The specimens were then tensile–shear tested with *in situ* hydrogen charging. Figure 1.43 shows the comparison between hydrogen-charged and original welded specimens. After 40 days of immersion in the sodium chloride solution, the weldment lost 11% of its thickness as

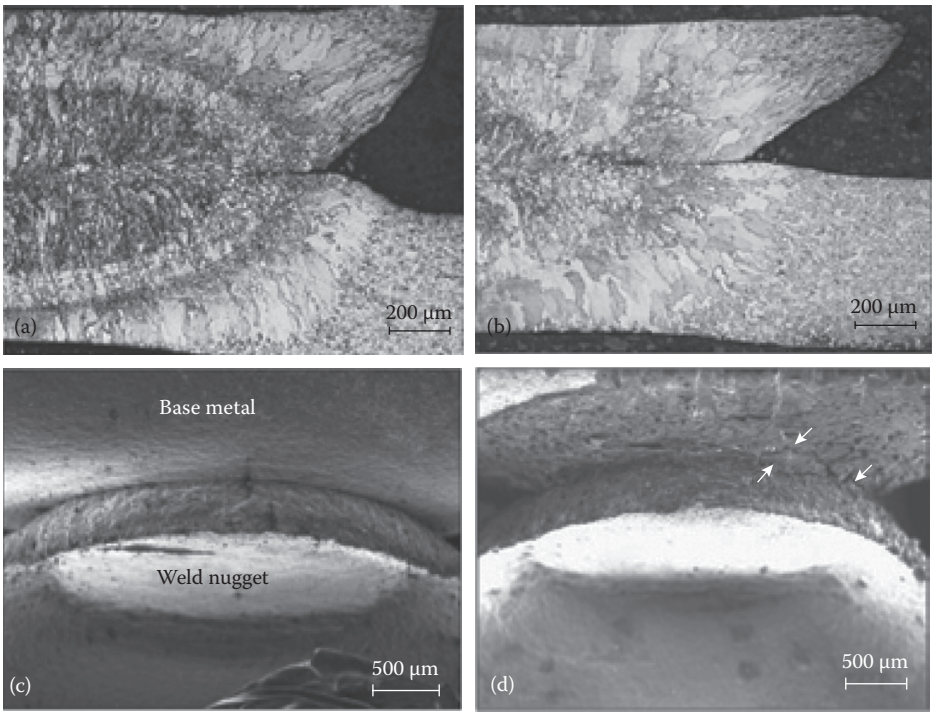

FIGURE 1.43
Effect of corrosion on welds and cracking.[62] Cross-sections of torn spot-welds without (a) and with (b) immersion, and pulled weld buttons without (c) and with (d) immersion in a corrosive environment. Arrows indicate secondary cracks near the fracture surface.

shown in Figure 1.43b, compared with the original one (Figure 1.43a). In addition, a large number of secondary cracks, indicated by the arrows in Figure 1.43d, are observed in the tested specimen, in the periphery of a hydrogen-charged weld nugget. The one without immersion in the solution, shown in Figure 1.43c, does not have any secondary cracks. Clearly, the corrosive solution weakens the weldment by corroding the faying interface, and creating cracks at or near the HAZ. In general, the HAZ of a weld is particularly vulnerable to corrosion cracking because of the residual stresses resulting from welding, and a modified microstructure in the region that often loses certain corrosion resistance intentionally created in fabricating the base metal.

References

1. Easterling, K. E., *Introduction to the Physical Metallurgy of Welding*, 2nd edition, Butterworth-Heinemann, Cambridge, UK, 1992.
2. Granjon, H., *Fundamentals of Welding Metallurgy*, Woodhead Publishing, Abington, UK, 1991.
3. Kou, S., *Welding Metallurgy*, 2nd edition, J. Wiley & Sons, Inc., Hoboken, NJ, 2003.
4. Lancaster, J. F., *Metallurgy of Welding*, 6th edition, Abington Publishing, Abington, UK, 1999.

5. Linnert, G. E., *Welding Metallurgy: Carbon and Alloy Steels, Volume 2: Technology*, 3rd edition, American Welding Society, New York, 1967.
6. Linnert, G. E., *Welding Metallurgy: Carbon and Alloy Steels, Volume 1: Fundamentals*, 4th edition, American Welding Society, Miami, FL, 1994.
7. Lippold, J. C. and Kotecki, D. J., *Welding Metallurgy and Weldability of Stainless Steels*, John Wiley & Sons, Inc., New York, 2005.
8. Tumuluru, M. D., Effect of post-weld baking on the behavior of resistance spot welds in a 780-MPa TRIP Steel, SMWC XI, Paper 6-2, 2004.
9. Ma, C., Chen, D. L., Bhole, S. D., Boudreau, G., Lee, A., and Biro, E., Microstructure and fracture characteristics of spot-welded DP600 steel, *Materials Science and Engineering A*, 485, 334–346, 2008.
10. Luo, H., New joining techniques for magnesium alloy sheets, MS thesis, Institute of Metal Research, Chinese Academy of Sciences, May 2008.
11. Callister, W. D., Jr., *Materials Science and Engineering: An Introduction*, 6th edition, John Wiley & Sons, Inc., New York, 2003.
12. Hu, S. J., Senkara, J., and Zhang, H., Quality definition of resistance spot welds: A structural point of view, in *Proceedings of International Body Engineering Conference IBEC'96*, Body and Engineering Section, Detroit, MI, 1996, 91.
13. Krauss, G., Martensitic transformation, structure and properties in hardenable steels, *Hardenability Concepts with Applications to Steel*, edited by D. V. Doane and J. S. Kirkaldy, AIME, Warrendale, PA, 1978, 229–248.
14. http://www.leonghuat.com/articles/articles1.htm. Accessed Nov. 2010.
15. Dearden, J. and O'Neill, H., A guide to the selection and welding of low alloy structural steels, *Institute of Welding Transactions*, 3, 203–214, 1940.
16. Ito, Y. and Bessho, K., *Journal of Japan Welding Society*, 37 (9), 983, 1968.
17. Yurioka, N. et al., *Welding Journal*, 62 (6), 147s, 1983.
18. American Welding Society, *Structural Welding Code*, AWS D1.1, 2004.
19. Ginzburg, V. B. and Ballas, R., *Flat Rolling Fundamentals*, Marcel Dekker, New York, 2000.
20. Marya, M. and Gayden, X. Q., Development of requirements for resistance spot welding dual-phase (DP600) steels. Part 1—the causes of interfacial fracture, *Welding Journal*, 84 (11), 172s–182s, 2005.
21. Kuntz, M. L. and Bohr, J. C., Modeling projection welding of fasteners to AHSS sheet using finite-element method, Sheet Metal Welding Conference XII, Paper 8-6, 2006.
22. Khan, M. S., Bhole, S. D., Chen, D. L., Biro, E., Boudreau, G., and Deventer, J. V., Welding behaviour, microstructure and mechanical properties of dissimilar resistance spot welds between galvannealed HSLA350 and DP600 steels, *Science and Technology of Welding and Joining*, 14 (7), 616–625, 2009.
23. Hansen, M. and Anderko, K., *Constitution of Binary Alloys*, McGraw-Hill, New York, 106, 1958.
24. *Magnesium Vision 2020*, A North American Automotive Strategic Vision for Magnesium, USAMP, United States Automotive Materials Partnership, 2006.
25. Straumal, B., Lopez, G. A., Mittemeijer, E. J., Gust, W., and Zhiyaev, A. P., Grain boundary phase transitions in the Al–Mg system and their influence on high-strain rate superplasticity, *Defect and Diffusion Forum*, 216–217, 307–321, 2003.
26. Munitz, A., Cotler, C., Shaham, H., and Kohn, G., Electron beam welding of magnesium AZ91D plates, *Welding Journal*, 79, 202s–208s, 2000.
27. Munitz, A., Cotler, C., Stern, A., and Kohn, G., Mechanical properties and microstructure of gas tungsten arc welded magnesium AZ91D plates, *Materials Science and Engineering A* 302, 68–73, 2001.
28. Wang, Y., Feng, J., and Zhang, Z., Influence of surface condition on expulsion in spot welding AZ31B magnesium alloy, *Journal of Materials Science and Technology*, 21 (5), 749–752, 2005.
29. Wang, Y., Zhang, Z., and Feng, J., Effect of welding current on strength and microstructure in resistance spot welding of AZ31 Mg alloy, *Chinese Welding Journal*, 16 (4), 37–41, 2007.
30. Munitz, A., Kohn, G., and Cotler, C., Resistance spot welding of Mg–AM50 and Mg–AZ91D alloys. Magnesium Technology, TMS (The Minerals, Metals & Materials Society), 2002.

31. Luo, H., Hao, C., Zhang, J., Gan, Z., Chen, H., and Zhang, H., Characteristics of resistance welding magnesium alloys AZ31 and AZ91, *Welding Journal*, in print, July 2011.
32. Sun, D. Q., Lang, B., Sun, D. X., and Li, J. B., Microstructure and mechanical properties of resistance spot welded magnesium alloy joints, *Materials Science and Engineering A*, 460, 461, 494–498, 2007.
33. Nippert, R. A., Composite resistance welding electrode, AWS Sheet Metal Welding Conference IX, Paper 3-4, 2000.
34. Jovanovic, M. T. and Rajkovic, V., High electrical conductivity Cu-based alloys, Association of Metallurgical Engineers of Serbia, *Metalurgija, Journal of Metallurgy*, 15 (2), 125–133, 2009.
35. Li, H., Xie, S., Wu, P., and Mi, X., Study on improvement of conductivity of Cu–Cr–Zr alloys, *Rare Metals*, 26 (2), 124–130, 2004.
36. Holzwarth, U. and Stamm, H., *Journal of Nuclear Materials*, 279, 31, 2000.
37. Kimchi, M., Gould, J. E., Helenius, A., Keippi, K., and Nippert, R. A., The evaluation of various electrode materials for resistance spot welding galvanized steel, SMWC IV, Paper 7, 1990.
38. ASM Specialty Handbook, *Copper and Copper Alloys*, edited by J. R. Davis, ASM International, 2001.
39. http://www.spotweldingconsultants.com/GlidCop_AL_15.pdf. Accessed in Nov. 2010.
40. Resistance Welder Manufacturers' Association Bulletins #16—Resistance Welding Equipment Standards, 1996.
41. Gugel, M. D., White, C. L., and Wist, J. A., Progression of electrode wear during RSW of EG steel, SMWC V, Paper A4, 1992.
42. Wist, J. A. and White, C. L., Metallurgical aspects of electrode wear during resistance spot welding of zinc-coated steels, SMWC IV, Paper 7, 1990.
43. Matsuda, H., Matsuda, Y., Nagae, M., and Kabasawa, M., Effect of aluminum on spot weldability of hot-dipped galvanized and galvannealed steel sheets, SMWC VIII, Paper 1-5, 1998.
44. Steinmeier, D., Resistance welding—Electrode seasoning-1, microJoining Solutions—microTips, Available online at http://www.microjoining.com/microTip_Library/microTip_Resistance_Electrode_Seasoning-1.pdf. Accessed in Nov. 2010.
45. Li, Z., Hao, C., Zhang, J., and Zhang, H., Effects of sheet surface conditions on electrode life in aluminum welding, *Welding Journal*, 86 (4), 34s–39s, 2007.
46. http://en.wikipedia.org/wiki/Liquid_metal_embrittlement. Accessed in Nov. 2010.
47. Lai, G. Y., *High Temperature Corrosion and Materials Applications*, ASM International, Materials Park, OH 44073, 2007.
48. Joseph, B., Picat, M., and Barbier, F., Liquid metal embrittlement: A state-of-the-art appraisal, *European Physical Journal Applied Physics*, 5, 19–31, 1999.
49. Liquid metal assisted cracking of galvanized steel work, Topic Paper, SC/T/04/02, Standing Committee on Structural Safety, London, U.K., June 2004. Available online at www.scoss.org.uk. Accessed in Nov. 2010.
50. AET_Service_Capability.pdf. Available online at http://www.aet-int.com/capability/AET_Service_Capability.pdf. Accessed in Nov. 2010.
51. Glickman, E. E., Mechanism of liquid metal embrittlement by simple experiments: From atomics to life-time, *Multiscale Phenomena in Plasticity*, Kluwer Academic Publisher, Ouranopolis, Greece, 2000.
52. Robertson, W. M., Propagation of a crack filled with liquid metal, *Transactions of the Metallurgical Society of AIME*, 236, 1478–1482, 1966.
53. Glickman, E. E. et al., Round table discussion: II. Grain boundary wetting and liquid grooving, *Defect and Diffusion Forum*, 156, 265–272, 1998.
54. Stoloff, N. S. and Johnston, T. L., Crack propagation in a liquid metal environment, *Acta Materialia*, 11 (4), 251–256, 1963.
55. Westwood, A. R. and Kamdar, M. H., Concerning liquid metal embrittlement, particularly of zinc monocrystals by mercury, *Philosophical Magazine*, 8 (89), 787–804, 1963.
56. Gordon, P., Metal-induced-embrittlement of metals—An evaluation of embrittler transport mechanisms, *Metallurgical Transactions A*, 9A, 267–273, 1978.

57. Lynch, S. P., Environmentally assisted cracking: Overview of evidence for an adsorption-induced localised-slip process, *Acta Metallurgica*, 36 (10), 2639–2661, 1988.
58. Anderson, T. L., *Fracture Mechanics: Fundamentals and Applications*, 2nd edition, CRC Press, Boca Raton, FL, 1995.
59. Website of Metallurgical Associates, Inc., http://www.metassoc.com/pdf/MAI_Minutes-6_04.pdf. Accessed in Nov. 2010.
60. Kinstler, T. J., Current knowledge of the cracking of steels during galvanizing—A synthesis of the available technical literature and collective experience for the American Institute of Steel Construction, GalvaScience LLC. Available online at http://www.aisc.org/uploadedFiles/Research/Files/Final5906.pdf. Accessed in Nov. 2010.
61. Westwood, A. R. C., Preece, C. M., and Kamdar, M. H., Adsorption-induced brittle fracture in liquid–metal environments, *Fracture: An Advanced Treatise*, edited by H. Liebowitz, Academic Press, New York, 1971, 589–644.
62. Mukhopadhyay, G., Bhattacharya, S., and Ray, K. K., Strength of spot-welded steel sheets in corrosive environment, *Materials and Corrosion*, 61 (5), 398–406, 2010.
63. Liu, P. W. and Wu, J. K., *Materials Letters*, 57, 1224, 2003.
64. Ductile intermetallic compounds discovered, Public release date: 15-Sep-2003, DOE/Ames Laboratory. Available online at http://www.eurekalert.org/pub_releases/2003-09/dl-dic091503.php.
65. Mitsumaki, M. and Tadashi, K., In-situ fabrication of intermetallic compound-dispersed Al matrix composites by addition of metal powders, *Osaka Furitsu Sangyo Gijutsu Sogo Kenkyujo Hokoku*, 20, 63–67, 2006 (in Japanese).
66. Mrówka-Nowotnik, G., The effect of intermetallics on the fracture mechanism in AlSi1MgMn alloy, *Journal of Achievements in Materials and Manufacturing Engineering*, 30 (1), 35–42, September 2008.
67. Slade, P. G. (ed.) *Electrical Contacts: Principles and Applications*, Dekker, Inc., New York, 1999.
68. Zhang, H., Senkara, J., and Wu, X., Suppressing cracking in RSW AA5754 aluminum alloy by mechanical means, *Transactions of the ASME—Journal of Manufacturing Science and Engineering*, 124, 79, 2002.

References

1 Chapter 1 - Welding Metallurgy

1. Easterling, K. E., Introduction to the Physical Metallurgy of Welding, 2nd edition, ButterworthHeinemann, Cambridge, UK, 1992.

2. Granjon, H., Fundamentals of Welding Metallurgy, Woodhead Publishing, Abington, UK, 1991.

3. Kou, S., Welding Metallurgy, 2nd edition, J. Wiley & Sons, Inc., Hoboken, NJ, 2003.

4. Lancaster, J. F., Metallurgy of Welding, 6th edition, Abington Publishing, Abington, UK, 1999. (a) 200 µm (b) 200 µm (c) (d) 500 µm 500 µm Weld nugget Base metal

FIGURE 1.43

Effect of corrosion on welds and cracking. 62
Cross-sections of torn spot-welds without (a) and with (b) immer

sion, and pulled weld buttons without (c) and with (d) immersion in a corrosive environment. Arrows indicate

secondary cracks near the fracture surface.

5. Linnert, G. E., Welding Metallurgy: Carbon and Alloy Steels, Volume 2: Technology, 3rd edition, American Welding Society, New York, 1967.

6. Linnert, G. E., Welding Metallurgy: Carbon and Alloy Steels, Volume 1: Fundamentals, 4th edition, American Welding Society, Miami, FL, 1994.

7. Lippold, J. C. and Kotecki, D. J., Welding Metallurgy and Weldability of Stainless Steels, John Wiley & Sons, Inc., New York, 2005.

8. Tumuluru, M. D., Effect of post-weld baking on the behavior of resistance spot welds in a 780MPa TRIP Steel, SMWC XI, Paper 6-2, 2004.

9. Ma, C., Chen, D. L., Bhole, S. D., Boudreau, G., Lee, A., and Biro, E., Microstructure and fracture characteristics of spot-welded DP600 steel, Materials Science and Engineering A, 485, 334–346, 2008.

10. Luo, H., New joining techniques for magnesium alloy sheets, MS thesis, Institute of Metal Research, Chinese Academy of Sciences, May 2008.

11. Callister, W. D., Jr., Materials Science and Engineering: An Introduction, 6th edition, John Wiley & Sons, Inc., New York, 2003.

12. Hu, S. J., Senkara, J., and Zhang, H., Quality de

nition of resistance spot welds: A structural point of view, in Proceedings of International Body Engineering Conference IBEC'96, Body and Engineering Section, Detroit, MI, 1996, 91.

13. Krauss, G., Martensitic transformation, structure and properties in hardenable steels, Hardenability Concepts with Applications to Steel, edited by D. V. Doane and J. S. Kirkaldy, AIME, Warrendale, PA, 1978, 229–248.

14. http://www.leonghuat.com/articles/articles1.htm. Accessed Nov. 2010.

15. Dearden, J. and O'Neill, H., A guide to the selection and welding of low alloy structural steels, Institute of Welding Transactions, 3, 203–214, 1940.

16. Ito, Y. and Bessho, K., Journal of Japan Welding Society, 37 (9), 983, 1968.

17. Yurioka, N. et al., Welding Journal, 62 (6), 147s, 1983.

18. American Welding Society, Structural Welding Code, AWS D1.1, 2004.

19. Ginzburg, V. B. and Ballas, R., Flat Rolling Fundamentals, Marcel Dekker, New York, 2000.

20. Marya, M. and Gayden, X. Q., Development of requirements for resistance spot welding dual-phase (DP600) steels. Part 1—the causes of interfacial fracture, Welding Journal, 84 (11), 172s–182s, 2005.

21. Kuntz, M. L. and Bohr, J. C., Modeling projection welding of fasteners to AHSS sheet using

nite-element method, Sheet Metal Welding Conference XII, Paper 8-6, 2006.

22. Khan, M. S., Bhole, S. D., Chen, D. L., Biro, E.,

Boudreau, G., and Deventer, J. V., Welding behaviour, microstructure and mechanical properties of dissimilar resistance spot welds between galvannealed HSLA350 and DP600 steels, Science and Technology of Welding and Joining, 14 (7), 616–625, 2009.

23. Hansen, M. and Anderko, K., Constitution of Binary Alloys, McGraw-Hill, New York, 106, 1958.

24. Magnesium Vision 2020, A North American Automotive Strategic Vision for Magnesium, USAMP, United States Automotive Materials Partnership, 2006.

25. Straumal, B., Lopez, G. A., Mittemeijer, E. J., Gust, W., and Zhiyaev, A. P., Grain boundary phase transitions in the Al–Mg system and their in□uence on high-strain rate superplasticity, Defect and Diffusion Forum, 216–217, 307–321, 2003.

26. Munitz, A., Cotler, C., Shaham, H., and Kohn, G., Electron beam welding of magnesium AZ91D plates, Welding Journal, 79, 202s–208s, 2000.

27. Munitz, A., Cotler, C., Stern, A., and Kohn, G., Mechanical properties and microstructure of gas tungsten arc welded magnesium AZ91D plates, Materials Science and Engineering A 302, 68–73, 2001.

28. Wang, Y., Feng, J., and Zhang, Z., In□uence of surface condition on expulsion in spot welding AZ31B magnesium alloy, Journal of Materials Science and Technology, 21 (5), 749–752, 2005.

29. Wang, Y., Zhang, Z., and Feng, J., Effect of welding current on strength and microstructure in resistance spot welding of AZ31 Mg alloy, Chinese Welding Journal, 16 (4), 37–41, 2007.

30. Munitz, A., Kohn, G., and Cotler, C., Resistance spot welding of Mg–AM50 and Mg–AZ91D alloys. Magnesium Technology, TMS (The Minerals, Metals & Materials Society), 2002.

31. Luo, H., Hao, C., Zhang, J., Gan, Z., Chen, H., and Zhang, H., Characteristics of resistance welding magnesium alloys AZ31 and AZ91, Welding Journal, in print, July 2011.

32. Sun, D. Q., Lang, B., Sun, D. X., and Li, J. B., Microstructure and mechanical properties of resistance spot welded magnesium alloy joints, Materials Science and

Engineering A, 460, 461, 494-498, 2007.

33. Nippert, R. A., Composite resistance welding electrode, AWS Sheet Metal Welding Conference IX, Paper 3-4, 2000.

34. Jovanovic, M. T. and Rajkovic, V., High electrical conductivity Cu-based alloys, Association of Metallurgical Engineers of Serbia, Metalurgija, Journal of Metallurgy, 15 (2), 125-133, 2009.

35. Li, H., Xie, S., Wu, P., and Mi, X., Study on improvement of conductivity of Cu-Cr-Zr alloys, Rare Metals, 26 (2), 124-130, 2004.

36. Holzwarth, U. and Stamm, H., Journal of Nuclear Materials, 279, 31, 2000.

37. Kimchi, M., Gould, J. E., Helenius, A., Keippi, K., and Nippert, R. A., The evaluation of various electrode materials for resistance spot welding galvanized steel, SMWC IV, Paper 7, 1990.

38. ASM Specialty Handbook, Copper and Copper Alloys, edited by J. R. Davis, ASM International, 2001.

39. http://www.spotweldingconsultants.com/GlidCop_AL_15.pdf. Accessed in Nov. 2010.

40. Resistance Welder Manufacturers' Association Bulletins #16—Resistance Welding Equipment Standards, 1996.

41. Gugel, M. D., White, C. L., and Wist, J. A., Progression of electrode wear during RSW of EG steel, SMWC V, Paper A4, 1992.

42. Wist, J. A. and White, C. L., Metallurgical aspects of electrode wear during resistance spot welding of zinc-coated steels, SMWC IV, Paper 7, 1990.

43. Matsuda, H., Matsuda, Y., Nagae, M., and Kabasawa, M., Effect of aluminum on spot weldability of hot-dipped galvanized and galvannealed steel sheets, SMWC VIII, Paper 1-5, 1998.

44. Steinmeier, D., Resistance welding—Electrode seasoning-1, microJoining Solutions—microTips, Available online at

45. Li, Z., Hao, C., Zhang, J., and Zhang, H., Effects of

sheet surface conditions on electrode life in aluminum welding, Welding Journal, 86 (4), 34s-39s, 2007.

46. http://en.wikipedia.org/wiki/Liquid_metal_embrittlement. Accessed in Nov. 2010.

47. Lai, G. Y., High Temperature Corrosion and Materials Applications, ASM International, Materials Park, OH 44073, 2007.

48. Joseph, B., Picat, M., and Barbier, F., Liquid metal embrittlement: A state-of-the-art appraisal, European Physical Journal Applied Physics, 5, 19-31, 1999.

49. Liquid metal assisted cracking of galvanized steel work, Topic Paper, SC/T/04/02, Standing Committee on Structural Safety, London, U.K., June 2004. Available online at www.scoss.org .uk. Accessed in Nov. 2010.

50. AET_Service_Capability.pdf. Available online at http://www.aet-int.com/capability/AET_Service_Capability.pdf. Accessed in Nov. 2010.

51. Glickman, E. E., Mechanism of liquid metal embrittlement by simple experiments: From atomics to life-time, Multiscale Phenomena in Plasticity, Kluwer Academic Publisher, Ouranopolis, Greece, 2000.

52. Robertson, W. M., Propagation of a crack

lled with liquid metal, Transactions of the Metallurgical Society of AIME, 236, 1478-1482, 1966.

53. Glickman, E. E. et al., Round table discussion: II. Grain boundary wetting and liquid grooving, Defect and Diffusion Forum, 156, 265-272, 1998.

54. Stoloff, N. S. and Johnston, T. L., Crack propagation in a liquid metal environment, Acta Materialia, 11 (4), 251-256, 1963.

55. Westwood, A. R. and Kamdar, M. H., Concerning liquid metal embrittlement, particularly of zinc monocrystals by mercury, Philosophical Magazine, 8 (89), 787-804, 1963.

56. Gordon, P., Metal-induced-embrittlement of metals—An evaluation of embrittler transport mechanisms, Metallurgical Transactions A, 9A, 267-273, 1978.

57. Lynch, S. P., Environmentally assisted cracking: Overview of evidence for an adsorptioninduced localised-slip process, Acta Metallurgica, 36 (10), 2639–2661, 1988.

58. Anderson, T. L., Fracture Mechanics: Fundamentals and Applications, 2nd edition, CRC Press, Boca Raton, FL, 1995.

59. Website of Metallurgical Associates, Inc., http://www.metassoc.com/pdf/MAI_Minutes-6_04 .pdf. Accessed in Nov. 2010.

60. Kinstler, T. J., Current knowledge of the cracking of steels during galvanizing—A synthesis of the available technical literature and collective experience for the American Institute of Steel Construction, GalvaScience LLC. Available online at http://www.aisc.org/uploadedFiles/Research/Files/Final5906.pdf. Accessed in Nov. 2010.

61. Westwood, A. R. C., Preece, C. M., and Kamdar, M. H., Adsorption-induced brittle fracture in liquid-metal environments, Fracture: An Advanced Treatise, edited by H. Liebowitz, Academic Press, New York, 1971, 589–644.

62. Mukhopadhyay, G., Bhattacharya, S., and Ray, K. K., Strength of spot-welded steel sheets in corrosive environment, Materials and Corrosion, 61 (5), 398–406, 2010.

63. Liu, P. W. and Wu, J. K., Materials Letters, 57, 1224, 2003.

64. Ductile intermetallic compounds discovered, Public release date: 15-Sep-2003, DOE/Ames Laboratory. Available online at http://www.eurekalert.org/pub_releases/2003-09/dl-dic 091503 .php.

65. Mitsumaki, M. and Tadashi, K., In-situ fabrication of intermetallic compound-dispersed Al matrix composites by addition of metal powders, Osaka Furitsu Sangyo Gijutsu Sogo Kenkyujo Hokoku, 20, 63–67, 2006 (in Japanese).

66. Mrówka-Nowotnik, G., The effect of intermetallics on the fracture mechanism in AlSi1MgMn alloy, Journal of Achievements in Materials and Manufacturing Engineering, 30 (1), 35–42, September 2008.

67. Slade, P. G. (ed.) Electrical Contacts: Principles and

Applications, Dekker, Inc., New York, 1999.

68. Zhang, H., Senkara, J., and Wu, X., Suppressing cracking in RSW AA5754 aluminum alloy by mechanical means, Transactions of the ASME—Journal of Manufacturing Science and Engineering, 124, 79, 2002.

2 Chapter 2 - Electrothermal Processes of Welding

1. Zinov'yev, V. E., Metals at High Temperatures: Standard Handbook of Properties, translated and edited by V. P. Itkin, Hemisphere Publishing Corp., New York, 1990.

2. Aluminum: Properties and Physical Metallurgy, edited by J. E. Hatch, American Society for Metals, Metals Park, OH, 1984.

3. Baker, H., Physical Properties of Magnesium and Magnesium Alloys, Dow Chemical Company, Midland, MI, 1967.

4. ASM Specialty Handbook, Magnesium and Magnesium Alloys, edited by M. M. Avedesian and H. Baker, ASM International, Materials Park, OH, 1999.

5. Handbook of Thermophysical Properties of Solid Materials, Vol. 2, Alloys, edited by A. Goldsmith, T. Waterman, and H. Hirschhorn, Macmillan, New York, 1961.

6. Tsai, L., Jammal, O. A., Papritan, J. C., and Dickinson, D. W., Modeling of resistance spot weld nugget growth, Welding Journal, 47s–54s, 1992.

7. Eager, T. E. and Kim, E., Controlling parameters of resistance spot welding, SMWC IV, Paper 17, 1990.

8. Dilthey, U. and Hicken, S., Metallographic investigations into wear processes on electrodes during the resistance spot welding of aluminum, Welding and Cutting, 50 (1), 34, 1998.

9. Resistance Welding: Measurement of the Transition Resistance in Aluminium Materials, DVS 2929, Deustscher Verband fur Schweisstechnik e.V, Dusseldorf, Germany, 1985 (in German).

10. Li, Z., Hao, C., Zhang, J., and Zhang, H., Effects of sheet surface conditions on electrode life in aluminum welding, Welding Journal, 86 (4), 34s–39s, 2007.

11. Newton, C. J., Browne, D. J., Thornton, M. C., Boomer, D. R., and Keay, B. F., The fundamentals of resistance spot welding aluminum, in Proceedings of AWS Sheet Metal Welding Conference VI, Detroit, MI, Paper No. E2, 1994.

12. International Institute of Welding, Procedure for spot welding of uncoated and coated low carbon and high

strength steels, draft, Document No. III-1005-93, Section 6.

13. Howe, P., Spot weld spacing effect on weld button size, SMWC VI, Paper C03, 1994.

14. ASM Handbook, Vols. 1 and 2, ASM International, Materials Park, OH, 1990.

15. Speci c Heat of Solids, edited by A. Cezairliyan and A. Anderson, Hemisphere Publ. Corp., New York, NY, 1988.

16. Kimchi, M., Gould, J. E., and Nippert, R. A., The evaluation of resistance spot welding electrode materials for welding galvanized steels, SMWC III, Paper C8, 1988.

17. Gugel, M. D., Wist, J. A., and White, C. L., Comparisons of electrode wear in DSC electrodes having different hardnesses, SMWC V, Paper A03, 1992.

18. Wist, J. A. and White, C.L., Metallurgical aspects of electrode wear during resistance spot welding of zinc-coated steels, SMWC IV, Paper B6, 1990.

19. Kimchi, M., Gugel, M. D., White, C. L., and Pickett, K., Weldability and electrode wear during the RSW of various HDG steels, SMWC VI, Paper D02, 1994.

20. Gugel, M. D., White, C. L., Kimchi, M., and Pickett, K., The effect of aluminum content in HDG coatings on the wear of RSW electrodes, SMWC VI, Paper D03, 1994.

21. Wist, J. A., Gugel, M. D., White, C. L., and Lu, F., Electrode-workpiece sticking on electrogalvanized steel, SMWC VII, Paper E2, 1996.

22. Kusano, H., The importance of electrode management in modern resistance welding, SMWC XIV, Paper 3-7, 2010.

23. Howe, P., Resistance spot weldability and electrode wear mechanisms of ZnNi-UC EG sheet steel, SMWC V, Paper A1, 1992.

24. Thornton, M. C., Newton, C. J., Keay, B. F. P., Sheasby, P. G., and Evans, J. T., Some surface factors that affect the spot welding of aluminium, Transactions of Institute of Metal Finishing, 75 (4), 165–170, 1997.

25. Ikeda, R., Yasuda, K., and Hashiguchi, K., Resistance spot weldability and electrode wear characteristics of

aluminium alloy sheets, Welding in the World, 41, 492, 1998.

26. Resistance Welding Manual, 4th edition, Resistance Welder Manufacturers' Association (RWMA), 1989.

27. Okuda, T., Spot welding of thick plates: Part 1. The law of thermal similarity, Welding Technique, Japan Welding Society, 21 (9), 1973.

28. Fong, M., Tsang, A., and Ananthanarayanan, A., Development of the law of thermal similarity (LOTS) for low indentation cosmetic resistance welds, in Proceedings of Sheet Metal Welding Conference IX, Sterling Heights, MI, Paper No 5-6, 2000.

29. Ando, K. and Nakamura, T., On the thermal time constant in resistance spot welding, Report 1, Japan Welding Society, 26, 1957.

30. Welding Handbook, 2nd edition, American Welding Society, New York, NY, 1942.

31. Agashe, S. and Zhang, H., Selection of schedules based on heat balance in resistance spot welding, Welding Journal, 82 (7), 179s–183s, 2003.

32. Welding Handbook, Vol. 1, Welding Science and Technology, 9th edition, American Welding Society, Miami, FL, 2001.

33. Welding Handbook, Vol. 2, Welding Processes, 9th edition, American Welding Society, Miami, FL, 2004.

34. Matsuyama, K. and Chun, J., A study of splashing mechanism in resistance spot welding, in Proceedings of Sheet Metal Welding Conference IX, Sterling Heights, MI, Paper No 5-4, 2000.

35. Spinella, D. J., Aluminum resistance spot welding: Capital and operating costs vs. performance, SMWC VII, Paper A05, 1996.

36. Dilay, W., Rogola, E. A., and Zulinski, E. J., Resistance welding aluminum for automotive production, SAE Technical Paper 770305, 1977.

37. Brown, B. M., A comparison of AC and DC resistance welding of automotive steels, Welding Journal, 66 (1), 18–23, 1987.

38. Roth, D., Power conversion for resistance welding machines, SMWC I, Paper 01, 1984.

39. Moss, L. E. and Bates, F. E., Three phase D.C. flash welding, SMWC I, Paper 05, 1984.

40. Roth, D. K. and Hofman, K. A., Alternating current versus direct current in resistance welding, SMWC IV, Paper D19, 1990.

41. Michaud, E. J. and Renaud, S. T., A comparison of AC and mid-frequency DC resistance spot weld quality, SMWC VII, Paper A1, 1996.

42. Dupuy, T. and Fardoux, D., Spot welding zinc-coated steels with medium-frequency direct current, SMWC IX, Paper 1-2, 2000.

43. http://en.wikipedia.org/wiki/Skin_effect. Accessed in Nov. 2010.

44. Military Handbook: Grounding, Bonding, and Shielding for Electronic Equipments and Facilities, MILHDBK-419A, Vol. 2, 1987.

45. Tawade, G., Bhole, S. D., Lee, A., and Boudreau, G. D., Robust schedules for spot welding zinccoated advanced high strength automotive steels, in Proceedings of AWS Sheet Metal Welding Conference XI, Sterling Heights, MI, Paper No. 6-3, 2004.

46. Hao, M., Osman, K. A., Boomer, D. R., and Newton, C. J., Developments in characterization of resistance spot welding of aluminum, Welding Journal, 75, 1s, 1996.

47. Karagoulis, M. J., Control of materials processing variables in production resistance spot welding, in Proceedings of AWS Sheet Metal Welding Conference V, Detroit, MI, Paper B5, 1992.

48. Kimchi, M. J., Spot weld properties when welding with expulsion—A comparative study, Welding Journal, 63, 58s, 1992.

49. Schumacher, B. W. and Soltis, M., Getting maximum information from welding lobe tests, in Proceedings of AWS Sheet Metal Welding Conference III, Detroit, MI, Paper No 16, 1988.

50. Yadav, K., Study of interactions between electrical, magnetic, and mechanical

elds in resistance spot welding, MS thesis, University of Toledo, 2005.

51. Spinella, D. J., Aluminum resistance spot welding: Capital and operating costs vs. performance, SMWC VII, Paper A05, 1996.

52. http://www.isomatic.co.uk/MFtransformers.htm. Accessed in Nov. 2010.

53. Osman, K. A., Hao, M., Newton, C. J., and Boomer, D. R., A comprehensive approach to the monitoring of aluminum spot welding, SMWC VII, Paper B2, 1996.

3 Chapter 3 - Weld Discontinuities

1. AWS D8.7: Recommended Practices for Automotive Weld Quality—Resistance Spot Welding, American Welding Society, Miami, FL, 2004.

2. AWS D8.9: Recommended Practices for Test Methods for Evaluating the Resistance Spot Welding Behavior of Automotive Sheet Steel Materials, American Welding Society, draft, 2005.

3. Jiang, C., Thompson, A. K., Shi, M. F., Agashe, S., Zhang, J., and Zhang, H., Liquid metal embrittlement in resistance spot welds of AHSS steels, American Welding Society Annual Convention 2003, Detroit, MI, Paper 9A, April 2003.

4. Automotive Sheet Speci□cation, Alcan Rolled Products Comp., Farmington Hills, MI, 1994.

5. Senkara, J., Zhang, H., and Hu, S.J., Expulsion prediction in resistance spot welding, Welding Journal, 83, 123-s, 2004.

6. Lide, D. R., Handbook of Chemistry and Physics, 74th edition, CRC Press, Boca Raton, FL, 1993-1994.

7. Ma, C., Chen, D. L., Bhole, S. D., Boudreau, G., Lee, A., and Biro, E., Microstructure and fracture characteristics of spot-welded DP600 steel, Materials Science and Engineering A, (485), 334-346, 2008.

8. Khan, M. S., Bhole, S. D., Chen, D. L., Biro, E., Boudreau, G., and van Deventer, J., Welding behaviour, microstructure and mechanical properties of dissimilar resistance spot welds between galvannealed HSLA350 and DP600 steels, Science and Technology of Welding and Joining, 14 (7), 616-625, 2009.

9. Anik, S. and Dorn, L., Metal physical processes during welding—Weldability of aluminum alloys, Welding Research Abroad, XXXVII, 41, 1991.

10. Lippold, J. C., Nippes, E. F., and Savage, W. F., An investigation of hot cracking in 5083-O aluminum alloy weldments, Welding Journal, 56, 171-s, 1977.

11. Jones, J. A., Yoon, J. W., Riches, S. T., and Wallach, E. R., Improved mechanical properties for laser welded automotive aluminum alloy sheets, in Proceedings of AWS

Sheet Metal Welding Conference, VI, Detroit, MI, Paper No. B2, 1994.

12. Pellini, W. S., Strain theory of hot tearing, The Foundry, 80, 125, 1952.

13. Borland, J. C., Suggested explanation of hot cracking in mild and low alloy steel welds, British Welding Journal, 8, 526, 1961. TABLE 3.4 Dependence of Cracking Tendency on Welding Conditions Variable In□uence on Cracking Electrode type Domed (+), □at (–) Increase in specimen width (–) Constraining by washer (–) Constraining by neighboring welds (–) Using insulator with washers (0) Note: (+) = increasing cracking tendency; (–) = decreasing cracking tendency; (0) = no clear in□uence on cracking.

14. Prokhorov, N. N., Theorie und Verfahren zum Bestimmen der technologischen Festigkeit von Metallen beim Schweißen, Schweißtechnik, 19, 8, 1968.

15. Watanabe, G. and Tachikawa, H., Behavior of cracking formed in aluminum alloy sheets on spot welding, presented at 48th Annual Assembly of IIW, Stockholm, IIW Doc. No. III-1041-95, 1995.

16. Michie, K. J. and Renaud, S. T., Aluminum resistance spot welding: How weld defects affect joint integrity, in Proceedings of AWS Sheet Metal Welding Conference VII, Detroit, MI, Paper No. B5, 1996.

17. Thornton, P. H., Krause, A. R., and Davies, R. G., The aluminum spot weld, Welding Journal, 75, 101-s, 1996.

18. Senkara, J. and Zhang, H., Cracking in multi-spot welding aluminum alloy AA5754, Welding Journal, 79, 194-s, 2000.

19. Zhang, H., Senkara, J., and Wu, X., Suppressing cracking in RSW AA5754 aluminum alloys by mechanical means, Transactions of ASME—Journal of Manufacturing Science and Technology, 124, 79, 2002.

20. Rosenberg, R. A., Flemings, M. C., and Taylor, H. F., Nonferrous binary alloys hot tearing, Transactions of American Foundrymen's Society, 68, 518, 1960.

21. Hemsworth, B., Boniszewski, T., and Eaton, N. F., Classi

cation and de

nition of high temperature welding cracks in alloys, Metallurgy, 5, 1969.

22. Randhakrishnan, B. and Thompson, R. G., A model for the formation and solidi

cation of grain boundary liquid in the heat-affected zone (HAZ) of welds, Metallurgical Transactions A, 23A, 1783, 1992.

23. Thompson, R. G., Inter-granular liquation effects on weldability, in Weldability of Materials, edited by R. A. Patterson and K. W. Mahin, ASM International, Metals Park, OH, 1990, 57.

24. Zhang, H., Huang, Y., and Hu, S. J., Nugget growth in spot welding of steel and aluminum, in Proceedings of AWS Sheet Metal Welding Conference VII, Detroit, MI, Paper No. B3, 1996.

25. Gupta, O. P. and De, A., An improved numerical modeling for resistance spot welding process and its experimental veri

cation, Transaction of ASME—Journal of Manufacturing Science and Engineering, 120, 246, 1998.

4 Chapter 4 - Mechanical Testing

1. Zhou, M., Hu, S. J., and Zhang, H., Critical specimen sizes for tensile-shear testing of steel sheets, Welding Journal, 78, 305-s, 1999.

2. Resistance Welding—Destructive Tests of Welds—Failure Types and Geometric Measurements for Resistance Spot, Seam and Projection Welds, International Standard, ISO 14329, 2003.

3. Wang, P. C., Chisholm, S. K., Banas, G., and Lawrence, F. V., The role of failure mode, resistance spot weld and adhesive on the fatigue behavior of weld-bonded aluminum, Welding Journal, 72, 41-s, 1995.

4. Resistance Spot Welding—Destructive Tests of Welds—Method for the Fatigue Testing of Spot Welded Joints, International Standard, ISO/FDIS 14324, Final draft, 2003.

5. Speci□cation for Resistance Welding of Coated and Uncoated Carbon and Low Alloy Steels, ANSI/ AWS C1.4.

6. Military Speci□cation—Welding, Resistance: Spot and Seam, MIL-W-6858D, U.S. Department of Defense, Washington, DC, 1992.

7. Specimen Dimensions and Procedure for Shear Testing Resistance Spot and Embossed Projection Welds, International Standard, ISO/DIS 14273, 1994.

8. AWS D8.7: Recommended Practices for Automotive Weld Quality—Resistance Spot Welding, American Welding Society, Miami, FL, 2003.

9. AWS C1.1: Recommended Practices for Resistance Welding, American Welding Society, Miami, FL, 1966.

10. Specimen Dimensions and Procedure for Cross Tension Testing Resistance Spot and Embossed Projection Welds, ISO 14272, 2000.

11. Mukhopadhyay, G., Bhattacharya, S., and Ray, K. K., Strength assessment of spot-welded sheets of interstitial free steels, Journal of Materials Processing Technology, 209 (4), 1995–2007, 2009.

12. Specimen Dimensions and Procedure for Shear Testing Resistance Spot, Seam and Embossed Projection Welds,

International Standard, ISO 14273, 1994.

13. Recommended Practices for Test Methods for Evaluating the Resistance Spot Welding Behavior or Automotive Sheet Steel Materials, AWS D8.9-97, SAE D8.9-97, ANSI D8.9-97, Miami, FL, 1997.

14. Zhou, M., Relationship between spot weld attributes and weld performance, PhD dissertation, University of Michigan, Ann Arbor, MI, 2000.

15. Rivett, R. M., Final contract report: Resistance spot welding of steel sheet (for the European Coal and Steel Community), The Welding Institute, Report 3570/7/81, March 1982.

16. Lee, Y., Wehner, T., Lu, M., Morrissett, T., Pakalnins, E., and Tsai, C., Test of resistance spot welds under combined tension and shear, SMWC VII, Paper C2, 1996.

17. Maddox, S. J., Fatigue Strength of Welded Structures, 2nd edition, Woodhead Publ. Ltd., Abington Hall, Abington, GB, 1998.

18. Wilson, R. B. and Fine, T. E., Fatigue behavior of spot welded high strength steel joints, Society of Automotive Engineers, SAE, Paper No. 810354, 1981.

19. McMahon, J. C., Smith, G. A., and Lawrence, F. V., Fatigue Crack Initiation and Growth in Tensile- Shear Spot Weldments, ASTM STP 1058, edited by H. I. McHenry and J. M. Potter, American Society for Testing and Materials, Philadelphia, PA, 47-77, 1990.

20. Rui, Y., Borsos, R. S., Gopalakrishnan, R., Agrawal, H. N., and Rivard, C., Fatigue life prediction method for multi-spot-welded structures, Society of Automotive Engineers, SAE, Paper No. 930571, 1981.

21. Ma, C., Chen, D. L., Bhole, S. D., Boudreau, G., Lee, A., Biro, E., Microstructure and fracture characteristics of spot-welded DP600 steel, Materials Science and Engineering A, 485, 334-346, 2008.

22. Khan, M. S., Bhole, S. D., Chen, D.L., Biro, E., Boudreau, G., and van Deventer, J., Welding behaviour, microstructure and mechanical properties of dissimilar resistance spot welds between galvannealed HSLA350 and DP600 steels, Science and Technology of Welding and Joining, 14 (7), 616-625, 2009.

23. Zhang, H., Zhou, M., and Hu, S. J., Impact strength measurement and a new impact tester, Journal of Mechanical Manufacture, 215B, 403, 2001.

5 Chapter 5 - Resistance Welding Process Monitoring and Control

1. Gedeon, S. A., Sorensen, C. D., Ulrich, K. T., and Eagar, T. W., Measurement of dynamic electrical and mechanical properties of resistance spot welds, Welding Journal, 66, 378-s, 1987.

2. Tsai, C. L., Dai, W. L., Dickinson, D. W., and Papritan, J. C., Analysis and development of a realtime control methodology in resistance spot welding, Welding Journal, 335-s, 1991.

3. Li, W., Monitoring and diagnosis of resistance spot welding process, PhD dissertation, University of Michigan, Ann Arbor, 1999.

4. Haefner, K., Carey, B., Bernstein, B., Overton, K., and D'Andrea, M., Real time adaptive spot welding control, Transactions of ASME—Journal of Dynamic Systems, Measurement, and Control, 113, 104, 1991.

5. Nakata, S., Aono, S., Suzuki, M., Kawaguchi, Y., and Inoue, M., Quality assurance characteristics in resistance spot welds by adaptive control system and its

eld applications, presented at Annual Assembly of IIW, Ljubljana, Yugoslavia, IIW Doc. No. III-720-82, 1982.

6. Ma, C., Bhole, S. D., Chen, D. L., Lee, A., Biro, E., and Boudreau, G., Expulsion monitoring in spot welded advanced high strength automotive steels, Science and Technology of Welding and Joining, 11 (4), 480–487, 2006.

7. Cleveland, D. and O'Brien, L. J., Acoustic emission spot welding monitor, Final Technical Report, NSF under Award, No. MEA 82-60345, 1983.

8. Stiebel, A., Apparatus and method for monitoring and controlling resistance welding, U.S. Patent No. 4419558, 1983.

9. Stiebel, A., Ulmer, C., Kodrack, D., and Holmes, B., Monitoring and control of spot weld operations, SAE Technical Paper, No. SAE 860579, 1986.

10. Dickinson, D. W., Franklin, J. E., and Stanya, A., Characterization of spot welding behavior by dynamic electrical parameter monitoring, Welding Journal, 59, 170s, 1980.

11. Li, W., Hu, S. J., and Zhang, H., Signal processing issues in resistance spot welding, Sheet Metal Welding Conference IX, Sterling Heights, MI., Paper 32, 2000.

12. NIST–ATP Intelligent Resistance Welding Quarterly Progress Report, No. 103, Ann Arbor, MI, 1996.

13. NIST–ATP Intelligent Resistance Welding Quarterly Progress Report, No. 203, Ann Arbor, MI, 1997.

14. NIST–ATP Intelligent Resistance Welding Quarterly Progress Report, No. 402, Ann Arbor, MI, 1999.

15. Haykin, S., Adaptive Filter Theory, 2nd edition, Prentice Hall Information and System Science Series, Prentice Hall, Englewood Cliffs, NJ, 1991.

16. NIST–ATP Intelligent Resistance Welding Quarterly Progress Report, No. 202, Ann Arbor, MI, 1997.

17. Boilard, R. and Farrow, J., Automatic current steppers for improved weld quality, SMWC IV, Paper 8, 1990.

18. AWS/SAE D8.9M, Recommended Practices for Test Methods for Evaluating the Resistance Spot Welding Behavior of Automotive Sheet Steel Materials, The American Welding Society, Miami, FL, 2002.

19. Gould, J. E., Kimchi, M., Leffel, C. A., and Dickinson, D. W., Resistance seam weldability of coated steels: Part I. Weldability envelopes, Edison Welding Institute Research Report, No. MR9112, 1991.

20. Kaiser, J. G., Dunn, G. J., and Eagar, T. W., The effect of electrical resistance on nugget formation during spot welding, Welding Journal, 61, 167-s, 1982.

21. Nagel, G. L. and Lee, A., A new approach to spot welding feedback control, SAE Technical Paper, No. SAE 880371, 1988.

22. Karagoulis, M. J., Process control in manufacturing: Control of materials processing variables in production resistance spot welding, in Proceedings of AWS Sheet Metal Welding Conference V, Detroit, MI, Paper No. B5, 1992.

23. Rivett, R. M. and Hurley, J. P., Weld bonding of zinc-coated sheet steels, SMWC IV, Paper 4, 1990.

24. Zhang, H., Hu, J. S., Senkara, J., and Cheng, S., Statistical analysis of expulsion limits in resistance spot welding, Transactions of ASME—Journal of Manufacturing Science and Engineering, 122, 501, 2000.

25. Ma, C., Chen, D. L., Bhole, S. D., Boudreau, G., Lee, A., and Biro, E., Microstructure and fracture characteristics of spot-welded DP600 steel, Materials Science and Engineering A, 485, 334-346, 2008.

26. Zhang, H., Expulsion and its in uence on weld quality, Welding Journal, 78, 373s, 1999.

27. NIST—ATP Intelligent Resistance Welding Quarterly Progress Report, No. 403, Ann Arbor, MI, 1999.

28. Tack, J., Pavement performance prediction using pattern recognition: Arti

cial neural networks and statistical analysis, PhD Thesis, The University of Toledo, Toledo, OH, 2002.

29. Ballard, D. H., An Introduction to Natural Computation, MIT Press, Cambridge, MA, 1997.

30. McCulloch, W. S. and Pitts, W. H., A logical calculus of the ideas imminent in nervous activity, Bulletin of Mathematical Biophysics, 115-133, 1943.

31. McClelland, J. L. and Rumelhart, D. E., Explorations in Parallel Distributed Processing, MIT Press, Cambridge, MA, 1988.

32. Zurada, J. M., Introduction to Arti cial Neural Systems, West Publishing Company, New York, 1992.

33. NIST—ATP Intelligent Resistance Welding Quarterly Progress Report, No. 204, Ann Arbor, MI, 1996.

34. NIST—ATP Intelligent Resistance Welding Quarterly Progress Report, No. 301, Ann Arbor, MI, 1997.

35. Androvich, D. A., New approaches in resistance welding controls, SMWC III, Paper 18, 1988.

36. Stiebel, A., Ulmer, C., Kodrack, D., and Holmes, B. B., Monitoring and control of spot weld operations, SMWC II, Paper 4, 1986.

37. Kuo, M., Kelly, D., Boguslawski, V., Liu, P. S., Lario,

T., Orsette, C., and Tann, L., Methodology development of tip dresser application in the production environment, SMWC IX, Paper 3-3, 2000.

38. Boilard, R. and Farrow, J., Automatic current steppers for improved weld quality, SMWC IV, Paper 8, 1990.

6 Chapter 6 - Weld Quality and Inspection

1. AWS A3.0:2001, Standard Welding Terms and De nitions; Includes Terms for Adhesive Bonding, Brazing, Soldering, Thermal Cutting, and Thermal Spraying, The American Welding Society (AWS) and the American National Standards Institute (ANSI), Miami, FL, 2001.

2. AWS D8.7: Recommended Practices for Automotive Weld Quality—Resistance Spot Welding, American Welding Society, Miami, FL, 2004.

3. Zuniga, S. M. and Sheppard, S. D., Determining the constitutive properties of the heat-affected zone in a resistance spot weld, Modeling & Simulation in Materials Science & Engineering, 3 (3), 391-416, 1995.

4. Gao, Z. and Zhang, K., Comparison of the fracture and fatigue properties of 16MnR steel weld metal, the HAZ and the base metal, Journal of Materials Processing Technology, 63 (1-3), 559-562, 1997.

5. Procedure for Spot Welding of Uncoated and Coated Low Carbon and High Strength Steels, Resistance and Related Welding Processes, International Institute of Welding, Doc III-1005-93, 1993.

6. Spinella, D. J., Using fuzzy logic to determine operating parameters for resistance spot welding of aluminum, Sheet Metal Welding Conference VI, Detroit, Michigan, 1994.

7. Newton, C. J., Browne, D. J., Thornton, M. C., Boomer, D. R., and Keay, B. F., The fundamentals of resistance spot welding aluminum, Sheet Metal Welding Conference VI, Detroit, MI, 1994.

8. Zhou, M., Hu, S. J., and Zhang, H., Critical specimen sizes for tensile-shear testing of steel sheets, Welding Journal, 78, 305-s, 1999. Interfacial fracture Button pull-out Complete button 0 10 20 30 40 50 60 70 0 0.2 0.4 0.6 0.8 1 Indentation depth (mm) P e a k l o a d (k N)

FIGURE 6.43

Relation between peak load and indentation depth.

9. Zhou, M., Relationship between spot weld attributes and weld performance, PhD Dissertation, University of

Michigan, Ann Arbor, MI, 2000.

10. Keller, F. and Smith, D. W., Correlation of the strength and structure of spot welds in aluminum alloys, Welding Journal, 23 (1), 23-s-26-s, 1944.

11. McMaster, R. C. and Lindrall, F. C., The Interpretation of radiographs of spot welds in alclad 24S-T and 75S-T aluminum alloys, Welding Journal, 25 (8), 707-s-723-s, 1946.

12. Heuschkel, J., The expression of spot-weld properties, Welding Journal, 31 (10), 931-s-943-s, 1952.

13. Sawhill, J. M. and Baker, J. C., Spot weldability of high-strength sheet steels, Welding Journal, 59 (1), 19-s-30-s, 1980.

14. Thornton, P. M., Krause, A. R., and Davies, R. G., The aluminum spot weld, Welding Journal, 75 (3), 101-s-108-s, 1996.

15. Ewing, K. W., Cheresh, M., Thompson, R., and Kukuchek, P., Static and impact strengths of spot-welded HSLA and low carbon steel joints, SAE Paper 820281, 1982.

16. Koehler, J. R. and Owen, A. B., Computer experiments in design and analysis of experiments, In: Ghosh, S., Rao, C.R. (Eds.), Handbook of Statistics, Elsevier, Amsterdam, 261-308, 1996.

17. Ye, K. Q., Orthogonal column Latin hypercubes and their application in computer experiments, Journal of the American Statistical Association, 93 (444), 1430-1439, 1998.

18. AWS D8.9: Recommended Practices for Test Methods for Evaluating the Resistance Spot Welding Behavior of Automotive Sheet Steel Materials, American Welding Society, Miami, FL, draft, 2005.

19. Krautkramer, J. and Krautkramer, H., Ultrasonic Testing of Materials, Springer-Verlag, New York, NY, 1983.

20. Mansour, T. M., Ultrasonic inspection of spot welds in thin-gage steel, Materials Evaluation, 46, 650-658, 1988.

21. Raj, B., Subramanian, C. V., and Jayakumar, T., Non-destructive Testing of Welds, Narosa Publishing House, New Delhi, India, 2000.

22. SWIS Operation Manual, Applied Metrics, Fremont, CA, 2003.

23. Zhang, J., Ultrasonic evaluation of resistance spot weld quality, M.Sc. thesis, University of Toledo, Toledo, OH, 2003.

24. Mucciardi, A. N. and Gose, E. E., A comparison of seven techniques for choosing subsets of pattern recognition properties, IEEE Transactions on Computers, C-20, 1023, 1971.

25. Murthy, S. K., Automatic Construction of Decision Trees from Data, Siemens Corporate Research, Princeton, NJ, 1997.

26. Roye, W., Ultrasonic Testing of Spot Welds in the Automotive Industry, Special Issue no. SD 298, Krautkrämer GmbH & Co., Huerth, Germany, 1999.

27. Chertov, A. M., Maev, R. Gr., and Severin, F. M., Acoustic microscopy of internal structure of resistance spot welds. Available online at http://www.andrey-chertov.com/SAM%20for%20 Industry%20Final%20Version%202006%2006.pdf. Accessed on Jan. 26, 2011.

28. Polrolniczak, H., Ultrasonic Testing as a Means for Quality Assurance in Resistance Spot Welding, A Special Issue no. SD 297, Krautkrämer, GmbH & Co., Huerth, Germany, 1999.

29. Shayan, A., Zhang, H., and Gan, Z., Quality test of AHSS steel spot welds using ultrasonic technique, SMWC XIV, Paper 3-2, 2010.

30. Saaty, T. L., Fundamentals of Decision Making and Priority Theory with the Analytic Hierarchy Process, RWS Publications, Pittsburgh, PA, 1994.

31. Saaty, T. L. and Vargas, L. G., Models, Methods, Concepts, & Applications of the Analytic Hierarchy Process, Kluwer Academic Publishers, Boston, 2001.

32. http://www.123ahp.com/OMetodi.aspx. Accessed on April 20, 2010.

33. Zhang, H., Jayatissa, A. H., and Gan, Z., Monitoring resistance spot welding using ultrasonic B-scan

techniques, EIT Conference, IEEE, Illinois, May 20-22, 2010.

34. Karve, G., An impact tester and impact strength measurement of advanced high strength steel welds, M.Sc. thesis, University of Toledo, Toledo, OH, 2004.

35. Karve, G. and Zhang. H., Impact strength measurement of advanced high strength steel welds, in Proceedings of Sheet Metal Welding Conference XI, Sterling Heights, MI, Paper 5-3, 2004.

7 Chapter 7 - Expulsion in Resistance Spot Welding

1. Kimchi, M., Spot weld properties when welding with expulsion—A comparative study, Welding Journal, 63, 58-s, 1984.

2. Karagoulis, M. J., Control of materials processing variables in production resistance spot welding, in Proceedings of AWS Sheet Metal Welding Conference V, Detroit, MI, Paper No. B5, 1992.

3. Newton, C. J., Browne, D. J., Thornton, M. C., Boomer, D. R., and Keay, B. F., The fundamentals of resistance spot welding aluminum, in Proceedings of AWS Sheet Metal Welding Conference VI, Detroit, MI, Paper No. E2, 1994.

4. Hao, M., Osman, K. A., Boomer, D. R., and Newton, C. J., Developments in characterization of resistance spot welding of aluminum, Welding Journal, 75, 1-s, 1996.

5. Zhang, H., Expulsion and its in uence on weld quality, Welding Journal, 78, 373-s, 1999.

6. Davies, A. C., The Science and Practice of Welding, Vol. 2, The Practice of Welding, 10th edition, Cambridge University Press, United Kingdom, 1993.

7. Dickinson, D. W., Franklin, J. E., and Stanya, A., Characterization of spot welding behavior by dynamic electrical parameter monitoring, Welding Journal, 59, 170-s, 1980.

8. Wu, K. C., The mechanism of expulsion in weldbonding of anodized aluminum, Welding Journal, 56, 238-s, 1977.

9. Senkara, J., Zhang, H., and Hu, S. J., Expulsion prediction in resistance spot welding, Welding Journal, 83, 123-s, 2004.

10. Gould, J. E., An examination of nugget development during spot welding using both experimental and analytical techniques, Welding Journal, 66, 1-s, 1987.

11. Vahaviolos, S. J., Carlos, M. F., and Slykhouse, S. J., Adaptive spot-weld feedback control loop via acoustic emission, Materials Evaluation, 39, 1057, 1981.

12. Kilian, M. and Hutchenrenther, A., Monitoring and control of electrode indentation, in Proceedings of AWS

Sheet Metal Welding Conference VI, Detroit, MI, Paper No. C4, 1994.

13. Hao, M., Osman, K. A., Boomer, D. R., Newton, C. J., and Sheasby, P. G., On-line nugget expulsion detection for aluminum spot welding and weld bonding, SAE Paper No. 960172, 1996.

14. Han, Z., Indacochea, J. E., Chen, C. H., and Bhat, S., Weld nugget development and integrity in resistance spot welding of high-strength cold-rolled sheet steels, Welding Journal, 72, 209-s, 1993.

15. Browne, D. J., Chandler, H. W., Evans, J. T., and Wen, J., Computer simulation of resistance spot welding in aluminum-part I, Welding Journal, 74, 339-s, 1995.

16. Browne, D. J., Chandler, H. W., Evans, J. T., James, P. S., Wen, J., and Newton, C. J., Computer simulation of resistance spot welding in aluminum—Part II, Welding Journal, 74, 417-s, 1995.

17. Lide, D. R., editor, Handbook of Chemistry and Physics, 74th edition, CRC Press, Boca Raton, FL, 1993–1994.

18. Metals Handbook, Vol. 1, 8th edition, ASM, Metals Park, OH, 1977.

19. ASM Metals Reference Book, 2nd edition, ASM, Metals Park, OH, 1984.

20. Hatch, J. E., Aluminum: Properties and Physical Metallurgy, ASM, Metals Park, OH, 1984.

21. Prigogine, I. and Defay, R., Chemical Thermodynamics, Longmans, London, 1967, 156.

22. Hultgren, R., Orr, R. L., Anderson, P. D., and Kelley, K. K., Selected Values of Thermodynamic Properties of Metals and Alloys, Wiley, London, 1974.

23. Krupkowski, A., Basic Problems in Theory of Metallurgical Processes, Polish Science Publications, Warsaw (in Polish), 1974.

24. Tsai, C. L., Jammal, O. A., Papritan, C., and Dickinson, D. W., Modeling of resistance spot welding nugget growth, Welding Journal, 71, 47-s, 1992.

25. Zhang, H., Huang, Y., and Hu, S. J., Nugget growth in

spot welding of steel and aluminum, in Proceedings of AWS Sheet Metal Welding Conference VII, Troy, MI, Paper No. B3, 1996.

26. Luo, H., Hao, C., Zhang, J., Gan, Z., Chen, H., and Zhang, H., Characteristics of resistance welding magnesium alloys AZ31 and AZ91, Welding Journal, in print, July 2011.

27. Salman, S. A., Ichino, R., and Okido, M., A comparative electrochemical study of AZ31 and AZ91 magnesium alloy, International Journal of Corrosion, 2010, Article ID 412129, 2010.

28. Luo, H., New joining techniques for magnesium alloy sheets, MS thesis, Institute of Metal Research, Chinese Academy of Sciences, June, 2008.

29. Munitz, A., Kohn, G., and Cotler, C., Resistance spot welding of Mg-AM50 and Mg-AZ91D alloys, Magnesium Technology, ed. Kaplan, H. I., TMS (The Minerals, Metals & Materials Society), Warrendale, PA, 2002.

30. Zhang, H., Hu, J. S., Senkara, J., and Cheng, S., Statistical analysis of expulsion limits in resistance spot welding, Transactions of ASME—Journal of Manufacturing Science and Engineering, 122, 501, 2000.

31. Browne, D. I., Newton, C. I., and Boomer, D. R., Optimization and validation of a model to predict the spot weldability parameter lobes for aluminum automotive body sheet, in Proceedings of International Body Engineering Conference IBEC'95, Advanced Technologies and Processes Section, Detroit, MI, 1995, 100.

32. Kaiser, J. G., Dunn, G. J., and Eagar, T. W., The effect of electrical resistance on nugget formation during spot welding, Welding Journal, 61, 167-s, 1982.

33. Gould, J. E., Kimchi, M., Leffel, C. A., and Dickinson, D. W., Resistance seam weldability of coated steels, Part I, Weldability envelopes, Edison Welding Institute Research Report, No. MR9112, Columbus, OH, 1991.

34. McCullagh, P. and Nelder, J. A., Generalized Linear Models, 2nd edition, Chapman & Hall, London, 1989, 21.

35. Automotive Sheet Specification, Alcan Rolled Products Comp., Farmington Hills, MI, 1994.

36. Alcini, W. V., Experimental measurement of liquid

nugget heat convection in spot welding, Welding Journal, 69, 177-s, 1990.

37. Auhl, J. R. and Patrick, E. P., A fresh look at resistance spot welding of aluminum automotive components, SAE Paper No. 940160, 1994.

38. Patrick, E. P. and Spinella, D. J., The effects of surface characteristics on the resistance spot weldability of aluminum sheet, in Proceedings of AWS Sheet Metal Welding Conference VII, Troy, MI, Paper No. B4, 1996.

8 Chapter 8 - Influence of Mechanical Characteristics of Welding Machines

1. Ganowski, F. J. and Williams, N. T., Advances in resistance spot and seam welding of zinc coated steel strip, Sheet Metal Industries, 49, 692, 1972.

2. Kolder, M. W., and Bosman, A. W. M., In□uence of the welding equipment on the weldability lobe of an HSLA-steel, IIW Doc. No. III-796-84, 1984.

3. Satoh, T., Katayama, J., and Okumura, S., Effects of mechanical properties of spot welding machine on electrode life on electrode life for mild steel, IIW Doc. No. III-912-88, 1988.

4. Satoh, T., Katayama, J., and Nakano, T., Effect of mechanical properties of spot welding machine on spot weld quality, IIW Doc. No. III-912-88, 1988.

5. Hahn, O, Budde, L., and Hanitzsch, D., Investigations on the in□uence of the mechanical properties of spot welding tongs on the welding process, Welding and Cutting, 42, 6, 1990.

6. Williams, N. T., Chilvers, K., and Wood, K., The relationship between machine dynamics of pedestal spot welding machines and electrode life, IIW Doc. No. III-994-92, 1992.

7. Howe, P., The effect of spot welding machine characteristics on electrode life behavior on two welders, in Proceedings of AWS Sheet Metal Welding Conference VII, Detroit, MI, Paper No. A3, 1996.

8. Dorn, L. and Xu, P., In□uence of the mechanical properties of resistance welding machines on the quality of spot welding, Welding and Cutting, 45, 12, 1993.

9. Dorn, L. and Xu, P., Relationship between static and dynamic machine properties in resistance spot welding, Welding and Cutting, 44, 19, 1992.

10. Tang, H., Hou, W., Hu, J. S., and Zhang, H., Force characteristics of resistance spot welding of steels, Welding Journal, 79, 175-s, 2000.

11. Tang, H., Hou, W., Hu, S. J., and Zhang, H. In□uence of machine mechanical characteristics on RSW process and weld quality, Welding Journal, 82 (5), 116-s–124-s, 2003.

12. Wang, Y., Mechanical characterization of resistance welding machines, MS Thesis, The University of Toledo, 2005.

13. Zhang, H., Expulsion and its in uence on weld quality, Welding Journal, 78, 373s, 1999.

14. Howe, P., The effect of spot welding machine characteristics on electrode life behavior, SMWC VII, Paper 3, 1996.

15. Gould, J. E. and Dale, W. N., Theoretical analysis of weld head motion, in Proceedings of AWS Sheet Metal Welding Conference VII, Detroit, MI, 1994.

16. Gould, J. E. Feng, Z., Chou, J., and Kimchi, M., Analytical models for the mechanical response of a resistance spot welding machine, CRP Report SR9902, Edison Welding Institute, Columbus, OH, 1999.

17. NIST–ATP Intelligent Resistance Welding Quarterly Progress Report, No. 304, Ann Arbor, MI, 1998.

18. Natale, T. V. and Pickett, K., The effect of workpiece

t-up and electrode composition on the resistance spot welding behavior of hot-dip galvanized sheet steel, SMWC IV, Paper 9, 1990.

9 Chapter 9 - Numerical Simulation in Resistance Spot Welding

1. ANSYS, Ansys Inc., Canonsburg, PA, 1999.

2. Nied, H. A., The

nite element modeling of the resistance welding process, Welding Journal, 70, 339-s, 1991.

3. Tsai, C. L., Jammal, O. A., Papritan, C., and Dickinson D. W., Modeling of resistance spot welding nugget growth, Welding Journal, 71, 47-s, 1992.

4. ABAQUS, Hibbitt, Karlsson & Sorensen Inc., Pawtucket, RI, 1988.

5. Bentley, K. P., Greenwood, J. A., Knowlson, P. M., and Backer, R. G., Temperature distribution in spot welds, British Welding Journal, 10, 613-619, 1963.

6. Rice, W. and Funk, E. S., An analytical investigation of temperature distributions during resistance welding, Welding Journal, 46, 175-s, 1967.

7. Gould, J. E., An examination of nugget development during spot welding, using both experimental and analytical techniques, Welding Journal, 66, 1-s, 1987.

8. Tsai, C. L., Jammal, O. A., Papritan, C., and Dickinson, D. W., Modeling of resistance spot welding nugget growth, Welding Journal, 71, 47-s, 1992.

9. Cho, H. S. and Cho, Y. J., A study of the thermal behavior in resistance spot welding, Welding Journal, 68, 236-s, 1989.

10. Huh, H. and Kang, W. J., Electrothermal analysis of electric resistance spot welding process by a 3-D

nite element method, Journal of Materials Processing Technology, 63, 672, 1997.

11. Wei, P. S. and Ho, C. Y., Axisymmetric nugget growth during resistance spot welding, Journal of Heat Transfer, 112, 309, 1990.

12. Wei, P. S. and Yeh, F. B., Factors affecting nugget growth with mushy-zone phase change during resistance spot welding, Journal of Heat Transfer, 113, 643, 1991.

13. Wei, P. S., Wang, S. C., and Lin, M. S., Transport phenomena during resistance spot welding, Journal of Heat Transfer, 118, 762, 1996.

14. Browne, D. I., Newton, C. I., and Boomer, D. R., Optimization and validation of a model to predict the spot weldability parameter lobes for aluminum automotive body sheet, in Proceedings of International Body Engineering Conference, IBEC'95, Advanced Technologies and Processes Section, Detroit, MI, 1995, 100.

15. Browne, D. J., Chandler, H. W., Evans, J. T., Wen, J., and Newton, C. J., Computer simulation of resistance spot welding in aluminum: Part I, Welding Journal, 74, 339-s, 1995.

16. Browne, D. J., Chandler, H. W., Evans, J. T., Wen, J., and Newton, C. J., Computer simulation of resistance spot welding in aluminum: Part II, Welding Journal, 74, 418-s, 1995.

17. Khan, J. A., Xu, L. J., and Chao, Y. J., Prediction of nugget development during resistance spot welding using a coupled thermal-electrical-mechanical model, Journal of Science and Technology of Welding and Joining, 4, 201, 1999.

18. Khan, J. A., Chao, Y. J., and Xu, L. J., Modeling and simulation of resistance spot welding process for Al-alloy, in Proceedings of AWS Sheet Metal Welding Conference IX, Sterling Heights, MI, Paper No. 5-1, 2000.

19. Khan, J. A., Xu, L. J., Chao, Y. J., and Broach, K., Numerical simulation of resistance spot welding process, Numerical Heat Transfer Part A—Applications, 37, 425-446, 2000.

20. Zhang, H., Huang, Y. J., and Hu, S. J., Nugget growth in resistance spot welding of aluminum alloys, in Proceedings of Sheet Metal Welding Conference VII, Detroit, MI, Paper No. B3, 1996.

21. Feng, Z., Babu, S. S., Santella, M. L., Riemer, B. W., and Gould, J. E., An incrementally coupled electrical-thermal-mechanical model for resistance spot welding, in Proceedings of the 5th International Conference on Trends in Welding Research, ASM International, Pine Mountain, GA, edited, 1998, 599.

22. Li, M. V., Dong, P., and Kimchi, M., Analysis of microstructure evolution and residual stress development in resistance spot welds of high strength steels, in Proceedings of Sheet Metal Welding Conference VII, Detroit, MI, Paper No. 5-6, 1998.

23. NIST—ATP Intelligent Resistance Welding Quarterly Progress Report, No. 202, Ann Arbor, MI, 1997.

24. NIST—ATP Intelligent Resistance Welding Quarterly Progress Report, No. 203, Ann Arbor, MI, 1997.

25. Babu, S., Web site: http://mjndeweb.ms.ornl.gov/Babu/default.html. Accessed in 2004.

26. Bay, N. and Wanheim, T., Real area of contact between a rough tool and a smooth workpiece at high normal pressures, Wear, 38, 225–234, 1976.

27. Vogler, M. and Sheppard, S., Electrical contact resistance under high loads and elevated temperatures, Welding Journal, 231-s–238-s, June, 1993.

28. Kohlrausch, F., An Introduction to Physical Measurements: With Appendices on Absolute Electrical Measurements (translated from the 2nd German edition by T. H. Waller and H. R. Proctor), D. Appleton and Company, New York, 1891.

29. Bowden, F. P. and Williamson, J. B. P., Electrical conduction in solids. I. In uence of the passage of current on the contact between solids, Proceedings of Royal Society of London, 1, 246, 1958.

30. Greenwood, J. A. and Williamson, J. B. P., Electrical conduction in solids: II. Theory of temperaturedependent conductors, Proceedings of Royal Society of London, 13, 246, 1958.

31. Ion, J. C., Easterling, K. E., and Ashby, M. F., A second report on diagrams of microstructure and hardness for heat-affected zones in welds, Acta Metallurgica, 32, 1949, 1984.

32. Watt, D. F., Coon, L., Bibby, M., Goldak, J., and Henwood, C., An algorithm for modelling microstructural development in weld heat affected zones (Part A). Reaction kinetics. Acta Metallurgica, 36, 3029, 1988.

33. Bhadeshia, H. and Svensson, L. E., Modelling the evolution of microstructure in steel weld metals, in Mathematical Modeling of Weld Phenomena, edited by H. Cerjak and K. E. Easterling, Institute of Materials, London, UK, 1993, 109.

34. Jones, S. J. and Bhadeshia, H., Kinetics of the simultaneous austenite into several transformation products, Acta Metallurgica, 45, 2911, 1997.

35. Kirkaldy, J. S. and Venugopolan, D., Phase Transformations in Ferrous Alloys, edited by A. R. Marder and J. I. Goldstein, AIME, Warrendale, PA, 1984, 125.

36. Brooks, J. A., Yang, N. C. Y., and Krafcik, J. S., On the origin of ferrite morphologies of primary ferrite solidi

ed austenitic stainless steel welds, Recent Trends in Welding Science and Technology, edited by S. A. David and J. M. Vitek, ASM International, Materials Park, OH, 1992, 73-80.

37. NIST-ATP Intelligent Resistance Welding Quarterly Progress Report, No. 201, Ann Arbor, MI, 1997.

10 Chapter 10 - Statistical Design, Analysis, and Inference in Resistance Welding Research

1. Montgomery, D. C., Design and Analysis of Experiments, 6th edition, John Wiley & Sons, New York, 2005.

2. Wu, C. F. J. and Hamada, M., Planning, Analysis and Parameter Design Optimization, John Wiley & Sons, New York, 2000.

3. Draper, N. R. and Smith, H., Applied Regression Analysis, 3rd edition, John Wiley & Sons, New York, 1998.

4. Sen, A. and Srivastava, M., Regression Analysis: Theory, Methods, and Applications, SpringerVerlag, New York, 1990, 234–238.

5. Hamada, M. and Wu, C. F. J., Analysis of designed experiments with complex aliasing, Journal of Quality Technology, 24, 130, 1992.

6. Li, W., Cheng, S., Hu, S. J., and Shriver, J., Statistical investigation of resistance spot welding quality using a two-stage, sliding-level experiment, Transaction of ASME—Journal of Manufacturing Science and Engineering, 123, 513, 2001.

7. Box, G. E. P. and Meyer, R. D., Finding the active factors in fractionated screening experiments, Journal of Quality Technology, 25, 94–105, 1993.

8. Myers, R. H. and Montgomery, D. C., Response Surface Methodology: Process and Product in Optimization Using Designed Experiments, John Wiley & Sons, New York, 1995.

9. Zhou, M., Hu, S. J., and Zhang, H., Critical specimen sizes for tensile-shear testing of steel sheets, Welding Journal, 78, 305-s, 1999.

10. Cheng, S., Zhang, H., and Hu, S. J., Statistics in welding research design and analysis, in Proceedings of Sheet Metal Welding Conference IX, Sterling Heights, MI, Paper No. 5-5, 2000.

11. Taguchi, G. and Konishi, S., Orthogonal Arrays and Linear Graphs, ASI Press, Dearborn, MI, 1987.

12. Zhang, H., Hu, J. S., Senkara, J., and Cheng, S., Statistical analysis of expulsion limits in resistance spot

welding, Transaction of ASME—Journal of Manufacturing Science and Engineering, 122, 501, 2000.

13. Atkinson, A. C. and Haines, L. M., Designs for nonlinear and generalized linear models, Handbook of Statistics, 13, 437, 1996.

14. Sitter, R. R. and Forbes, B., Optimal two-stage designs for binary response experiments, Statistica Sinica, 7, 941, 1997.

15. Sitter, R. R. and Wu, C. F. J., Two stage design of quantal response studies, Biometrics, 55, 396, 1999.

16. Agresti, A., Categorical Data Analysis, John Wiley & Sons, New York, 1990.

17. Hosmer, D. W. and Lemeshow, S., Applied Logistic Regression, 2nd edition, John Wiley & Sons, New York, 2000.

18. McCullagh, P. and Nelder, J. A., Generalized linear models, 2nd edition, Chapman & Hall, London, UK, 21–135, 1989.

19. Sacks, J., Welch, W. J., Mitchell, T. J., and Wynn, H. P., Design and analysis of computer experiments, Statistical Science, 4, 409, 1989.

20. Koehler, J. R. and Owen, A. B., Computer experiments, Handbook of Statistics, 13, 261, 1996.

21. Owen, A. B., Orthogonal arrays for computer experiments, integration and visualization, Statistica Sinica, 2, 439, 1992.

22. Tang, B., Orthogonal array-based Latin hypercubes, Journal of the American Statistical Association, 88, 1392, 1993.

23. Iman, R. L. and Conover, W. J., A distribution-free approach to inducing rank correlation among input variables, Communications in Statistics, Part B—Simulation and Computation, 11, 311, 1982.

24. Owen, A. B., Controlling correlations in Latin hypercube samples, Journal of the American Statistical Association, 89, 1517, 1994.

25. Tang, B., Selecting Latin hypercubes using correlation

criteria, Statistica Sinica, 8, 965, 1998.

26. Ye, K. Q., Orthogonal column Latin hypercubes and their application in computer experiments, Journal of the American Statistical Association, 93, 1430, 1998.

27. Park, J.-S., Optimal Latin-hypercube designs for computer experiments, Journal of Statistical Planning and Inference, 39, 95, 1994.

28. Morris, M. and Mitchell, T., Exploratory design for computer experiments, Journal of Statistical Planning and Inference, 43, 381, 1995.

29. Zhou, M., Hu, S. J., and Zhang, H., Relationships between quality and attributes of spot welds, Welding Journal, 82, 72, 2003.

FIGURE 1.28

Composition pro

les of electrode surfaces after 60 welds using schedules of (a) F = 4.5 kN, τ = 60 ms; (b) F = 4.5 kN,

τ = 180 ms; (c) F = 9.0 kN, τ = 60 ms; and (d) F = 9.0 kN, τ = 180 ms. Red line is for Cu, green is for Al, and blue

is for Mg.

FIGURE 1.34

Liquid metal embrittlement cracking in a Zn-coated HSLA steel spot weldment (a), and x-ray maps of Cu (b) and

Zn (c) of area outlined in (a). (From AET_Service_Capability.pdf. Available online at http://www.aet-int.com/

capability/AET_Service_Capability.pdf. Accessed in Nov. 2010. With permission.)

FIGURE 2.10

Electrode wear in welding steel.

FIGURE 2.11

Crater formation and growth on electrode surface as a function of number of welds. 22 (a) Alloy layer after 100

welds (11 μm); (b) crater depth after 300 welds (87 μm); (c) crater depth after 400 welds (101 μm); (d) crater depth

after 500 welds (140 μm).

FIGURE 2.13

Electrode surfaces after making 60 welds on sheets of different surface conditions: (a) chemically cleaned,

(b) degreased, (c) electric arc cleaned, and (d) untreated.

FIGURE 2.12

Electrode wear in aluminum welding.

FIGURE 4.26

A new impact tester.

FIGURE 2.15

Electrode surface morphology after life tests using (a) chemical cleaning, (b) degreasing, (c) electric arc cleaning

methods, and (d) untreated aluminum sheets. Electrodes on left side are from the lower arm of welder (nega

tive), and those on right side are from the upper arm (positive). F I G U R E 6 . 8 I n ﬂ u e n c e o f d i m e n s i o n a n d m e c h a n i c a l p r o p e r t i e s o f n u g g e t a n d H A Z .

FIGURE 6.10

von Mises stresses distribution at weldment.

FIGURE 6.24

Formation of a B-scan image of a spot weld.

FIGURE 6.26

Schematic diagram of probe setup.

FIGURE 6.27

B-scan image of a good weld.

FIGURE 6.34

B-scan and faying surface of a cold weld (current = 5000 A).

FIGURE 6.35

B-scan and faying surface of a cold weld (current = 5500 A).

FIGURE 6.36

B-scan and faying surface of a cold weld (current = 6500 A).

FIGURE 6.37

B-scan and faying surface of a peeled weld (current = 8000 A).

FIGURE 8.12

Signals obtained for a typical welding cycle using DAQ system.

FIGURE 6.39

B-scan and a peeled weld (current = 9500 A).

FIGURE 6.38

B-scan and faying surface of a peeled weld (current = 9000 A).

FIGURE 8.25

Effect of moving mass on electrode force.

FIGURE 9.12

Hardness gradients predicted in weldment. 25

FIGURE 9.14

Simulation results of nugget formation using conditioned electrodes.

FIGURE 9.15

Nugget growth simulation using uncoupled and coupled electrical–thermal–mechanical algorithms.

FIGURE 9.18

Temperature distribution after second cycle.

FIGURE 9.19

Temperature distribution after 5.5th cycle.

FIGURE 9.21

Temperature distribution after 8 cycles with perfectly aligned electrodes.

FIGURE 9.20

Temperature distribution after 8 cycles.